ENHANCED PHOTODEGRADATION OF DYE MIXTURES (METHYL ORANGE AND METHYL GREEN) AND REAL TEXTILE WASTEWATER BY ZnO MICRO/NANOFLOWERS

KEE MING WEI

UNIVERSITI TUNKU ABDUL RAHMAN

ENHANCED PHOTODEGRADATION OF DYE MIXTURES (METHYL ORANGE AND METHYL GREEN) AND REAL TEXTILE WASTEWATER BY ZnO MICRO/NANOFLOWERS

KEE MING WEI

**A project report submitted in partial fulfilment of
the requirements for the award of the degree of
Bachelor of Engineering (Hons) Environmental Engineering**

**Faculty of Engineering and Green Technology
Universiti Tunku Abdul Rahman**

May 2017

DECLARATION

I hereby declare that this project report is based on my original work except for citations and quotations which have been duly acknowledged. I also declare that it has not been previously and concurrently submitted for any other degree or award at UTAR or other institutions.

Signature : _____

Name : _____

ID No. : _____

Date : _____

APPROVAL FOR SUBMISSION

I certify that this project report entitled **"ENHANCED PHOTODEGRADATION OF DYE MIXTURES (METHYL ORANGE AND METHYL GREEN) AND REAL TEXTILE WASTEWATER BY ZnO MICRO/NANOFLOWERS"** was prepared by **KEE MING WEI** has met the required standard for submission in partial fulfilment of the requirements for the award of Bachelor of Engineering (Hons) Environmental Engineering at Universiti Tunku Abdul Rahman.

Approved by,

Signature : _____

Supervisor : Dr. Lam Sze Mun

Date   : _____

The copyright of this report belongs to the author under the terms of the copyright Act 1987 as qualified by Intellectual Property Policy of University Tunku Abdul Rahman. Due acknowledgement shall always be made of the use of any material contained in, or derived from, this report.

Specially dedicated to

my beloved grandfather, grandmother,

father, mother, sister and brother

ACKNOWLEDGEMENT

This thesis would not have come to fruition without the help of various people in many ways. Foremost, I would like to express my sincere gratitude to my advisor Dr. Lam Sze Mun for her continuous support of my final year project study and related research, for her patience, motivation, enthusiasm and immense knowledge. Her guidance helped me in all the time of research and writing of this thesis. I could not have imagined having a better advisor and mentor for my final year project study. My sincere thank also goes to my co-supervisor, Dr. Sin Jin Chung for his support and guidance.

My heartfelt thankfulness also goes towards Universiti Tunku Abdul Rahman (UTAR), Kampar, specifically the Faculty of Engineering and Green Technology (FEGT) for the provision of sufficient and adequate facilities to undertake this research project. Moreover, I would like to convey my truthful appreciation towards the ever helpful laboratory officers who tirelessly cater to my every request in the laboratory. This goes out especially to Ms. Ng Suk Ting, Ms. Noor Hazreena binti Noor Izahar, Mr. Voon Kah Loon, Ms. Mirohsha a/p Mohan and lastly Mr. Chin Kah Seng.

Furthermore, I would like to thank my fellow labmate, Quek Jian Ai who spend countless of hours of discussion together with me on the subject of final year project. I also would like to thank my seniors, Luk Mei Kwan and Christina Previtha for their useful advices on my final year project work. Last but not the least, I would like to thank my family and coursemates for their unwavering physical and mental support throughout the course of this project.

ENHANCED PHOTODEGRADATION OF DYE MIXTURES (METHYL ORANGE AND METHYL GREEN) AND REAL TEXTILE WASTEWATER BY ZnO MICRO/NANOFLOWERS

ABSTRACT

Textile industry is the largest contribution of the dye pollutants towards the environment and its persistent nature due to their complex molecular structure poses severe environmental hazards. Among numerous proposed treatments, heterogeneous photocatalysis using zinc oxide (ZnO) has emerged as an effective mean for the degradation of dyes. In this study, ZnO micro/nanoflowers were fabricated via a PVP-assisted co-precipitation method. As-synthesized ZnO micro/nanoflowers were characterized by XRD, FESEM, EDX, FTIR and PL analyses. The as-prepared ZnO was of the hexagonal wurzite phase with high crystallinity and it was observed to be a micro/nanoflower structure with an average diameters ranging from 890 nm to 1.261 μm. A possible formation mechanism of ZnO micro/nanoflowers was also suggested. The as-synthesized ZnO was also indicated to be ZnO with ample amount of –OH groups on the surface of ZnO and low radiative recombination. The photocatalytic activity of ZnO micro/nanoflowers were tested in the degradation of methyl orange (MO) and methyl green (MG) mixtures under UV-vis light irradiation. Comparison studies were performed using commercial ZnO and as-synthesized ZnO and as-synthesized ZnO manifested superior photocatalytic performance. Moreover, sedimentation test was conducted and as-prepared ZnO showed better sedimentation performance due to high density of as-prepared ZnO. The optimal synthesis parameter was investigated to be ZnO PVP-12.5, whereas the best process parameters were determined to be 2.5 mg/L of MO and 5 mg/L of MG and solution pH of 6.5. 93.83 % of MO and 100 % of MG were

degraded with 94.14 % of COD degradation efficiency within 240 minutes of irradiation. The degradation of real textile dye wastewater was also determined to be 75 % of COD degradation using as-synthesized ZnO micro/nanoflowers after 240 minutes of illumination.

TABLE OF CONTENTS

CHAPTER

LIST OF TABLES

Textile Wastewater using ZnO PVP-12.5.

LIST OF FIGURES

LIST OF SYMBOLS / ABBREVIATIONS

ΔE	Band Gap Energy
$\bullet OH$	Hydroxyl Radicals
3-D	Three Dimensional
A	Absorbance At A Certain Wavelength (Abs)
AN	Ammoniacal Nitrogen
AOP	Advanced Oxidation Process
b	Path Length (cm)
BG	Band Gap
BOD	Biochemical Oxygen Demand
C	Molar Concentration (mg/L)
CB	Conduction Band
CFL	Compact Fluorescent Lamp
C_o	Initial Concentration of Mixture of Dye Solution after 30 Minutes in Dark Condition (mg/L)
CO_2	Carbon Dioxide
COD	Chemical Oxygen Demand
C_t	Concentration of Mixture of Dye Solution at Reaction Time, t (min) (mg/L)
CWPO	Catalytic Wet Peroxide Oxidation
DO_0	Initial DO (mg/L)
DO_5	Final DO after 5 Days Incubation (mg/L)
ε	Molar Absorptivity Coefficient (mg/L/cm)
e^-	Electron
EDX	Energy Dispersive X-Ray Spectroscopy

FESEM	Field Emission Scanning Electron Microscope
FTIR	Fourier Transform Infrared Spectroscopy
h^+	Hole
H_2O	Water
H_2O_2	Hydtogen Peroxide
H_2O_2	Hydrogen Peroxide
HNO_3	Nitric Acid
$HO_2\bullet$	Perhydroxyl Radicals
HP	Heterogeneous Photocatalysis
MG	Methyl Green
MO	Methyl Orange
NaOH	Sodium Hydroxide
O_2	Oxygen
$O_2^-\bullet$	Superoxide Anion Radicals
O_3	Ozone
PL	Photoluminescence
PVP	Polyvinylpyrrolidone
RHEED	Reflection High-Energy Electron Diffraction
SDS	Sodium Dodecyl Sulfate
TEM	Transmission Electron Microscopy
TiO_2	Titanium Dioxide
TSS	Total Suspended Solid
UV	Ultraviolet
UV-vis	Ultraviolet-Visible
VB	Valence Band
XRD	X-Ray Diffraction
ZnO	Zinc Oxide

LIST OF APPENDICES

CHAPTER 1

INTRODUCTION

1.1 Dyestuff Industry and Advanced Oxidation Process (AOP)

Over the past decade, dye has been extensively used in industries including fabric, woven, leather, textile, pulp and paper production, tanneries, cosmetic, pharmaceuticals and food processing due to the increased demand (Ghowsi *et al.*, 2014). It is approximated about 700 kilotons of dyestuffs are produced worldwide (Zengin *et al.*, 2012). Among these, textile industry accounted for two-thirds of its market, making it the largest consumer of these dyes (Pereira & Alves, 2012). An estimated 7×10^5 tons is commercially produced worldwide. The increasing demand on dyestuff industry causes the wastewater produced from them to be increased as well. Wastewaters produced from dye industry are significant as they posed a high chemical oxygen demand (COD), salinity, total suspended solid (TSS), biochemical oxygen demand (BOD) and color (Carmen & Daniela, 2012).

Due to the severe pollution problems caused by dye-containing wastewater worldwide, it should be treated prior discharge to the environment. Numerous conventional treatments have been adopted to solve this crisis, such as biological treatments, physical means, chemical methods, and advanced oxidation processes. Nevertheless, each of the methods has various degree of effectiveness. AOPs provide promising technological solutions for wastewater treatment as they effectively oxidize a wide spectrum of contaminants to relatively non-toxic end products, carbon dioxide (CO_2) and water (H_2O), thereby improving the overall secondary effluent quality status. The examples of source of AOPs are ultraviolet (UV) radiation, ozone

(O$_3$), hydrogen peroxide (H$_2$O$_2$), and oxygen (O$_2$) (Sharma, Ruparelia & Patel, 2011). AOPs can be classified into homogenous and heterogeneous catalysis depending on the phase of the catalysts and the reactants. Some examples of homogenous catalysis are Fenton processes, wet peroxide oxidation, ozone based processes and wet oxidation, while some examples of heterogeneous catalysis are heterogeneous photocatalysis (HP), catalytic wet peroxide oxidation (CWPO), heterogeneous Fenton-like processes and catalytic ozonation (Ribeiro *et al.*, 2015).

Among AOPs, HP is widely adopted in wastewater treatment as it is cost-effective, non-toxic, capability of extended use without substantial loss of photocatalytic activity, potential to reduce toxicity and complete mineralization of organics, rapid reaction rates and small footprint (Zhang *et al.*, 2013; Lam *et al.*, 2012; Sharma, Ruparelia & Patel, 2011). HP adopts semiconductor photocatalysts for example zinc oxide (ZnO) or titanium dioxide (TiO$_2$) under light irradiation at ambient condition. This process is directed by the combined action of an energetic radiation source, a semiconductor photocatalyst and an oxidizing agent (Ahmed *et al.*, 2011). HP has been successfully implemented as it is capable of degrading wide range of organic contaminants such as pesticides and dyes (Umar & Aziz, 2013). Among various photocatalysts, TiO$_2$ emerges as an efficient catalyst as achievement of degradation rate of methyl orange was up to 75% using TiO$_2$ modified with 3 wt% alkali ions (Na, K and Pb) (Yang *et al.*, 2013). TiO$_2$/ ZnO/ chitosan were used as photocatalysts for degradation of methyl orange solution under irradiation of visible light (Zhu *et al.*, 2013). Most of the research papers are only deal with single dyes, though in real life applications, dyes exist as mixtures. Simultaneous treatment of dyes mixtures should be proposed to cope with real life application.

1.2   Problem Statement

Textile dyes mixture in reality contains not only dyes, but also pesticides, residual dyestuffs, metals (copper, chromium, lead, cobalt, nickel and cadmium), dye intermediates, huge numbers of organic compounds and unreacted raw materials such as inorganic sodium salts and aromatic amines (Kotelevtsev, Tonkopii & Hänninen, 2009; Lam *et al.*, 2012). In literatures, studies on degradation of textile dyes were mainly focused on synthetic solutions of single dyes, which may barely reflect the real condition (Saratale *et al.*, 2011). Dyes manifesting similar spectra may act differently during treatment even with the adequate spectrum of textile dyes being produced, leading to the limitations of transferability of the experimental data to real dye mixtures of wastewaters. Therefore, there is still a research demand on real textile effluent (Popli & Patel, 2015; Tomei, Pascual & Angelucci, 2016).

The HP can be driven by ultraviolet-visible (UV-vis) sunlight. In countries like Malaysia has ample amount of irradiation throughout the year. The sun produces 0.2-0.3 mole photons $m^{-2}h^{-1}$ in the range of 300-400 nm with a typical UV flux of 20-30 Wm^{-2} (Ahmed *et al.*, 2011). In fact, this approach has several merits, for examples, it is abundant, cheap and pollutant free. It is feasible to use sunlight as an economically and ecologically light source. In other word, if dye-containing wastewater can be treated under UV fluorescent light which contain wavelength of 200 nm to 800 nm, it can be extensively applied under sun irradiation in Malaysia.

Furthermore, TiO_2 has been widely used as photocatalyst over the recent years. Despite the chemical stability, it actually has some limitations such as the location of its band gap, which is in the UV region and fast electron-hole pairing in HP process (Pournuroz *et al.*, 2015). Hence, other promising catalyst such as ZnO is explored to replace TiO_2 owing to its low cost, high surface area, robustness and abundance (Hernández, *et al.*, 2015; Yang *et al.*, 2010; Xie and Wu, 2010). ZnO is also a competitive and attractive semiconductor in various application including light emitting diodes, gas sensors and photocatalysts (Kanjwal *et al.*, 2010). It can be synthesized into various structures, including nanorods, nanowires, nanotubes, nanoparticles and nanoflowers. Each of them has their own advantages. Growth of nanowires could be well aligned on most substrates whereas nanoparticles offer high

performance due to its larger surface area to volume ratio (Zhang *et al.*, 2012). On the other hand, nanoflowers exhibit high photocatalytic activity due to strong visible light absorbance as compared to the former (Safa *et al.*, 2014). Nanostructures emerge as an extended used technology because of their excellent physical and chemical properties (Amin, 2012; Guo *et al.*, 2010). In this study, ZnO micro/nanoflowers will be synthesized and used to treat mixture of Methyl Green (MG) and Methyl Orange (MO) and real textile dye wastewater under UV-vis light irradiation.

1.3 Objectives of Study

The specific objectives of study are:

1. To synthesize three dimensional (3-D) ZnO micro/nanoflowers using a polyvinylpyrrolidone (PVP)-assisted co-precipitation method.
2. To characterize the chemical and physical properties of as-synthesized ZnO micro/nanoflowers using various characterization techniques.
3. To examine the effects of synthesis parameter including PVP concentration and process parameters including initial dye concentration and solution pH on the degradation of a mixture of MO and MG dye solutions under UV-vis light.
4. To evaluate the real textile dye effluent using the as-synthesized ZnO micro/nanoflowers under UV-vis light.

1.4   Scope of Study

The present study covers the synthesis of ZnO micro/nanoflowers, characterization of as-synthesized ZnO micro/nanoflowers, synthesis parameter study, process parameters study, and real textile dye wastewater studies. Synthesis of ZnO micro/nanoflowers will be carried out using a PVP-assisted co-precipitation method. The as-prepared ZnO micro/nanoflowers will be then characterized by means of X-ray diffraction (XRD), field emission scanning electron microscopy with energy dispersive X-ray spectroscopy (FESEM-EDX), fourier transform infrared spectroscopy (FTIR) and photoluminescence (PL) analyses. Simultaneous degradation of a mixture of MG and MO will be tested under UV-vis light irradiation. Photoactivity of the as-synthesized ZnO micro/nanoflowers will be evaluated in different synthesis variable such as PVP concentration and process variables such as solution pH and initial substrate concentration. Each variable was selected based on reports in literature and through the process of trial and error. The concentration change and degree of mineralization for dye will be monitored by the UV-vis spectrophotometer and COD analyzer, respectively (Joseph & Thiripuranthagan, 2015). Furthermore, real textile dye mixtures will be also studied using the as-fabricated ZnO micro/nanoflowers under UV-vis light.

CHAPTER 2

LITERATURE REVIEW

2.1   Dyes

Dyes are complex aromatic molecular structures that are stable and relatively resistant to degradation (Nor *et al.*, 2015). In order to achieve better treatment on the dyes-containing effluent, the structures of dyes must be first understood. A dye can typically refer as a coloured substance as it absorbs a certain wavelength in the visible spectrum range. Table 2.1 shows the different colours of the visible spectrum when a certain wavelength is being absorbed. The major structure elements in dye molecules are chromophore and auxochromes groups. Chromophore group is a delocalized electron system with conjugated double or simple bonds, which is also known as colour-bearing group. Typical chromophores include azo ($-N=N-$), carbon ($=C=C=$), nitro ($-NO_2$ or $NO-OH$), carbon-nitrogen ($>C=NH$ or $-CH=N-$), carbonyl ($=C=O$), nitroso ($-NO$ or $N-OH$) and sulphur ($C=S$) (Satyanarayana, Johri, and Prakash, 2012). Auxochromes are electron donors that are complement to the electron accepter action aimed to enhance the colour (Malik and Grohmann, 2011). Usual auxochromes include amino ($-NH_3$), carboxylic acid ($-COOH$), sulfonic acid ($-SO_3H$) and hydroxyl group ($-OH$) (Teo and Khoh, 2014). Dyes can be also classified by their Colour Index (CI) based on its application, colour and chemical structure (Pereira and Alves, 2012; Sharma, 2015; Suresh and Sundaramoorthy, 2014; Malik and Grohmann, 2011). Generic name is first given to the dyes depending on their application and colour and five arabical CI numbers are then assigned based on their chemical structure, for examples, Acid Red 14 (14720), Basic Blue 41 (11105) and Reactive Orange 16 (17757), as shown in Figure 2.1 (Khataee and Kasiri, 2010).

Table 2.1: Different Colours of the Visible Spectrum and their Corresponding Wavelength and Frequency Intervals (Pereira and Alves, 2012).

Colour	Wavelength interval (nm)	Frequency interval (THz)
Red	~700-635	~430-480
Orange	~635-590	~480-510
Yellow	~590-560	~510-540
Green	~560-490	~540-610
Blue	~490-450	~610-670
Violet	~450-400	~670-750

Acid Red 14 (14720)

Basic Blue 41 (11105)

Reactive Orange 16 (17757)
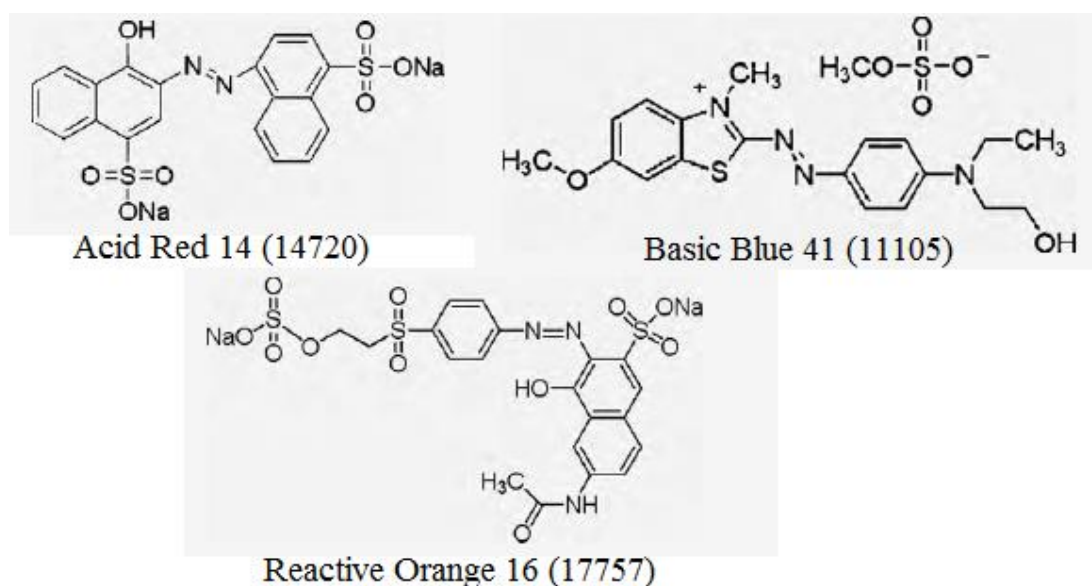
Figure 2.1: Examples of Dyes. Their Colour Indexes (CI) Are Given Based on Their Generic Name and Five Arabical CI Numbers (in parentheses) (Khataee and Kasiri, 2010).

The CI distinguishes them into different classes: basic, mordant, direct, reactive, metallic, pigment, solvent, acid, sulphur, disperse and vat dyes (Malik and Grohmann, 2011; Carmen and Daniela, 2012). Basic dyes are cationic; acid, reactive and direct dyes are water-soluble anionic dyes; and disperse, solvent and pigment dyes are non-ionic. Disperse dyes are sparingly soluble in water for application in hydrophobic fibres from an aqueous dispersion, usually of anthraquinone and

sulphide structure, with many –NH–, –C=O and aromatic groups. Mordant dyes are mainly anionic; with small portion exist as cationic. Moreover, vat dyes are water-insoluble; nonetheless, they can be converted into a 'leuco' form, which is soluble in alkaline aqueous solutions. Metallic dyes possess higher light and wash fastness due to the transition metals, such as chromium, copper, nickel or cobalt that modify the surface chemistry between the dye molecule and the fabric (Pereira and Alves, 2012).

Wijannarong *et al.* (2013) and Gupta *et al.* (2014) stated that 93 % of the intake water is discharged as coloured wastewater in textile industries due to high concentration of organic compounds and heavy metals containing in dyes. The stable and persistent nature of dyes of textile industries poses a severe environmental hazard. An approximately 200,000 tons of dyestuff is released into the global environment annually (Chequer *et al.*, 2013). High concentrations of textile dyes in water bodies prevent the re-oxygenation capacity of the receiving water and the penetration of sunlight into the water body, thereby disrupting the biological activity of the aquatic ecology system and hinder the photosynthesis process of aquatic plants such as algae (Chequer *et al.*, 2013).

The colour in water body, even in a trace amount (<1 ppm) are highly visible and can cause visual impact to the public due to aesthetic merits. The contaminants in dyes are toxic because they are carcinogenetic and mutagenic. These contaminants may also accumulate in the food chain through bioconcentration and bioaccumulation. The bioconcentration factor is a measure to estimate the bioaccumulation potential of dyes in fish. The effect of the toxicity can even be magnified throughout the food chain (Carmen and Daniela, 2012). Hence, it is primitive to remove the colour presence in dye-containing wastewater.

In present study, MO and MG were chosen as model pollutants for ZnO mediated photocatalytic activity under UV-vis irradiation due to their escalated demand on the textile industry. The structures and characteristics of these dyes are summarized in Table 2.2. MO and MG result in harmful health effects such as eye irritation and skin irritation upon contact, respiratory tract irritation upon inhalation and digestive tract irritation upon consumption (Acros Organics, 2008).

Table 2.2: Molecular Structure and Properties of MO and MG.

	Methyl Orange	**Methyl Green**
Alternate name	Helianthine	Ethyl Green
Abbreviation	MO	MG
Empirical formula	$C_{14}H_{14}N_3NaO_3S$	$C_{27}H_{35}N_3BrCl \cdot ZnCl_2$
Molar mass	327.33 g/mol	653.24 g/mol
C.I number	13025	42590
Colour	Orange	Blue-Green
λ_{max}	465 nm	631 nm
References	Merck Millipore, 2016	Geethakrishnan and Palanisamy, 2006
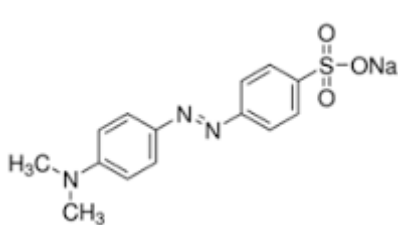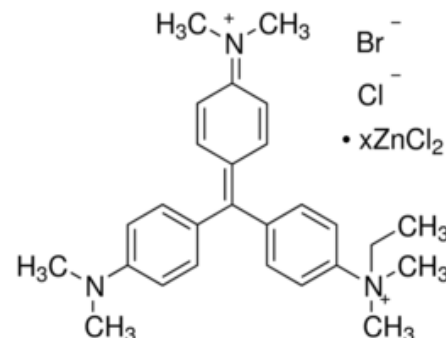
Government legislation regarding the removal of dyes from industrial effluents is becoming increasingly stringent. In developed countries such as United States of America (US), Canada, Australia and the nations of the Europe (EU) have enforce the law to ensure the textile and other dye-utilizing industries to keep their dye-containing effluent below the desired standards (Pereira and Alves, 2012). The principal quality indicators of the wastewater that pollute the environment are the

COD, BOD, heavy metals, salt content, TSS, colour of the textile effluent and other potential hazardous organic pollutants. In Malaysia, fifth schedule and seventh schedule of the Environmental Quality (Industrial Effluent) Regulations 2009 is used as the standard that must be complied by dye-containing industries. Table 2.3 represents the fifth schedule of the Environmental Quality (Industrial Effluent) Regulations 2009 enforced in Malaysia whereas Table 2.4 shows the seventh schedule of the Environmental Quality (Industrial Effluent) Regulations 2009 stipulated in Malaysia.

2.2 Conventional Treatment Methods for Dye Removal

To comply with the legislations enforced by the Malaysia Government, dye-containing effluent must be treated prior discharge to the watercourse. It is not only aimed at colour removal, nevertheless it also targets the decomposition and mineralization of the dye compounds. In the past decade, a wide variety of conventional technologies has been established for the treatment of dyes in wastewaters to reduce their ramifications to the environment, including chemical, physical and biological methods. Physical methods include membrane filtration and sorption techniques, chemical methods comprise coagulation and flocculation combined with flotation and filtration, precipitation and electrochemical processes and biological methods involve aerobic and anaerobic microbial degradation (Pereira and Alves, 2012). Each of them has various degree of effectiveness in treating the dye-containing wastewater based on the literatures reported by other researchers (Shah, 2014; Dawood and Sen, 2013; Carmen and Daniela, 2012).

Table 2.3: Discharge Limit of Industrial Effluent for Standards A and B (Environmental Quality (Industrial Effluents) Regulations 2009).

Fifth Schedule

[Paragraph 11(1) (a)]

Parameter	Unit	Standard	
		A	B
Temperature	℃	40	40
pH value	-	6.0 – 9.0	5.5 – 9.0
BOD$_5$	mg/L	20	40
Suspended Solids	mg/L	50	100
Mercury	mg/L	0.005	0.05
Cadmium	mg/L	0.01	0.02
Chromium, Hexavalent	mg/L	0.05	0.05
Chromium, Trivalent	mg/L	0.20	1.0
Arsenic	mg/L	0.05	0.10
Cyanide	mg/L	0.05	0.10
Lead	mg/L	0.10	0.5
Copper	mg/L	0.20	1.0
Manganese	mg/L	0.20	1.0
Nickel	mg/L	0.20	1.0
Tin	mg/L	0.20	1.0
Zinc	mg/L	2.0	2.0
Boron	mg/L	1.0	4.0
Iron (Fe)	mg/L	1.0	5.0
Silver	mg/L	0.1	1.0
Aluminium	mg/L	10	15
Selenium	mg/L	0.02	0.5
Barium	mg/L	1.0	2.0
Fluoride	mg/L	2.0	5.0
Formaldehyde	mg/L	1.0	2.0
Phenol	mg/L	0.001	1.0
Free Chlorine	mg/L	1.0	2.0

Fifth Schedule

[Paragraph 11(1) (a)]

Parameter	Unit	Standard	
		A	**B**
Sulphide	mg/L	0.50	0.50
Oil and Grease	mg/L	1.0	10
Ammoniacal Nitrogen	mg/L	10	20
Colour	ADMI*	100	200

Notes:

*: American Dye Manufactures Institute

Table 2.4: Discharge Limits of Industrial Effluent Containing COD for Specific Trade or Industry Sector (Environmental Quality (Industrial Effluents) Regulations 2009).

Seventh Schedule

(Regulation 12)

Trade/ Industry	Unit	Standard	
		A	**B**
(a) Pulp and paper industry			
(i) Pulp mill	mg/L	80	350
(ii) Paper mill (recycled)	mg/L	80	250
(iii)Pulp and paper mill	mg/L	80	300
(b) Textile industry	mg/L	80	250
(c) Fermentation and distillery industry	mg/L	400	400
(d) Other industries	mg/L	80	200

For a biological treatment, Ong *et al.* (2011) reviewed that the degradation efficiencies of Mordant Blue-9 and Direct Red-80 separately and in a mixture by immobilized *Phanerochaete chryosporium* in a batch-operated rotating biological contactor reactor could go up to 94 – 100 % and 77 – 97 % respectively. Carmen and Daniela (2012) stated that the degradation efficiency of azo dyes (Acid Red 151,

Basic Red 46 and 16, Basic Blue 41, Basic Yellow 28 and 19) in an aerobic biofilm system attained 80%. Carmen and Daniela (2012) also demonstrated that some aerobic bacterial are responsible for the reduction of azo compounds and production of aromatic amines in the presence of specific oxygen-catalysed enzymes called azo reductases. In another study, Gupta *et al.* (2014) indicated that the microorganisms such as fungi, bacteria, algae, yeast and enzymes can be used to degrade a wide spectrum of dyes through aerobic, anaerobic and sequential anaerobic-aerobic treatment processes. Table 2.5 presents the bacterial degradation of mixture of dyes and their respective removal efficiency.

Table 2.5: Bacterial Biodegradation of Mixture of Dyes (Gupta *et al.*, 2014).

Dyes	Degradation (%)
Diazo Evans blue (EB) and triphenylmethane brilliant green (BG)	88.9
Brown 3REL (B3REL), SRR, Remazol Red (RR), Direct Red 2B (DR2B) and Malachite Green (MG)	100
Sulphonated Azo dyes, Acid Orange 7 (AO7) and Acid Red 88 (AR88)	~100
Yellow P3R, Blue H5R, Orange P3R, Violet P3R, Black V3R, Brown P5R, Orange P2R	47.24
Remazol Red, Rubine GFL, Brown 3REL, Scarlet RR, Golden Yellow HER, Methly Red, Brilliant Blue GL	87
Bordeaux, Ranocid Fast Blue, Congo Red and Blue BCC	50-60

Using a physical method, Wang *et al.* (2011) stated that the membrane separation process such as reverse osmosis, ultrafiltration, nanofiltration and microfiltration are implemented in dye-containing effluent due to their high separation efficiencies and ease of operation. Reverse osmosis can achieve a 90 % or more retention rate for most types of ionic compounds which is commonly found in the dye wastewater. Gupta *et al.* (2014) demonstrated 87 % to 90 % colour removal efficiency was obtained after 96 hours and 60 hours using a biosorbent *Portulaca grandiflora*. Ong *et al.* (2011) reviewed that the batch adsorption method was

adopted in the removal of Methyl Orange by calcined Lapindo volcanic mud. The investigated results showed a maximum adsorption capacity of 333.3 mg/g.

Using a chemical method, Carmen and Daniela (2012) indicated that the coagulation-flocculation and precipitation methods can be employed to treat the dye-containing discharge with ferric chloride and a commercial organic coagulant aid at pH of 6.7-8.3 or with alum at pH of 8.2. The formal one achieves colour removal of more than 80 % and the latter attains colour removal in the range of $54 - 81$ %. If electrocoagulation treatment is carried out under optimum condition, it can have a degradation of $90 - 95$ % and a COD removal of $30 - 36\%$.

Despite the wide application of conventional method, each of them has their respective limitations. Chemical methods only convert the pollutants in the discharge from one phase to other without elimination. The accumulation of concentrated sludge also require proper disposal (Pereira and Alves, 2012). On the other hand, biological treatments are usually ineffective in degrading complex structured dye (Pajootan *et al.*, 2011). Physical methods can effectively eliminate colour, nevertheless, the dyes are not completely mineralized, and through the process, it concentrate and will pose disposal problem. Table 2.6 summarizes the treatment processes and their advantages and limitations (Carmen and Daniela, 2012).

2.3   Advanced Oxidation Process

AOP is an oxidative degradation process driven by the in-situ formation of non-selective and highly reactive species including hydroxyl radicals ($\bullet$OH), superoxide anion radicals ($O_2^-\bullet$) and hydrogen peroxide (H_2O_2) (Lam *et al.*, 2012). Among AOPs, HP has been attracted global attention owing to its effectiveness in decomposing and mineralizing the recalcitrant organic compounds as well as the possibility of utilizing the solar UV and visible light spectrum (Ahmed *et al.*, 2011). HP has been first discovered to be used for photo-activated water splitting process using TiO_2 by Fujishima and Honda in 1972. Intensive studies on HP have been carried out after some of the semiconductors were found to be able to completely

Table 2.6: Different Types of Dyes-Containing Industrial Wastewater Treatment Processes and Their Advantages and Limitations (Carmen and Daniela, 2012).

Treatment processes	Advantages	Limitations
Chemical methods		
Coagulation-flocculation, precipitation	Low capital costs and short detention time. Relatively good elimination efficiencies.	Agglomerates separation and treatment. Selected operating condition.
Biological methods		
Aerobic process	Partial or complete degradation for all dye classes	Costly treatment
Anaerobic process	Resistant to wide range of complex coloured compounds.	Longer adaptation phase.
Physical treatments		
Membrane filtration	Eradicates all dye types, recovery and reuse of chemicals and water	High operation cost, concentrated sludge production.
Activated carbon	Economically attractive. Good elimination efficiency of wide variety of dyes.	Very expensive, excessive sludge production.

mineralize various organic and inorganic pollutants.

In contrast with other conventional methods as stated in section 2.2, HP is performed at ambient conditions and the inputs are non-hazardous and economical. HP enables complete mineralization of dyes to simple and non-hazardous substances (CO_2 and H_2O) in short detention time through redox reaction. Therefore, no sludge is produced and no secondary pollutant is produced. No secondary treatment is

required to process the sludge and this prevents the disposal problem. It is an environmentally friendly approach and thus it can be applied worldwide. In addition, the catalyst remains unchanged throughout the process and thus can be reuse; leading to a significant reduction in overall operating cost (Kaan *et al*, 2012).

HP is initiated by the absorption of light and electron-hole ($e^- – h^+$) pairs are generated, which subsequently undergo a series of reaction to produce •OH radicals (Ibhadon and Fitzpatrick, 2013). •OH radicals are strong oxidizing agent with a standard oxidation potential of 2.8 eV, which is right after the fluorine gas that having the highest electronegative oxidation potential. The oxidation potential of certain species is shown in Table 2.7. Fluorine is not used in water or wastewater treatment because of its high toxicity. On the other hand, •OH radical is powerful, non-selective oxidizing agent that can rapidly reach with most organic compounds and non-hazardous. Hence, HP is emerged as an effective and cheap alternative to the conventional methods (Goi, 2005).

Table 2.7: Relative Oxidation Power of Some Oxidizing Species (Goi, 2005).

Oxidation species	Oxidation potential (eV)
Fluorine	3.06
Hypochlorous Acid	1.49
Chlorine	1.36
Hydrogen peroxide	1.78
Ozone	2.07
Perhydroxyl radical	1.70
Hydroxyl radical	**2.80**
Atomic oxygen	2.42

2.3.1 Basic Principle of Photocatalysis

The fundamental of the mechanism and reaction of HP must be fully understood before apply into the dye-containing effluent treatment. In the photocatalytic system, organic compounds are degraded in the presence of a semiconductor photocatalysts,

a light source and an oxidizing agent. Valence band (VB) electrons are excited when photons absorb energies higher than the band gap energy (ΔE). On the other hand, the absorption of photons with energy less than ΔE results in energy dissipation in forms of heat. When the photocatalytic surface is irradiated with sufficient energy, positive hole (h^+) is formed in the VB and an electron (e^-) is formed in the conduction band (CB). h^+ is responsible in the oxidation of either pollutant directly or formation of •OH radicals, while the excited electron in the CB is responsible for the reduction of oxygen adsorbed on the photocatalyst. The activation of photocatalyst by light energy can be represented by the following Eqs. (2.1 − 2.2) (Ahmed *et al.*, 2011; Lam *et al.*, 2012; Fox and Dulay, 1993).

$$Photocatalyst + hv \rightarrow h^+ + e^- \tag{2.1}$$

$$e^- + O_2 \rightarrow O_2^-• \tag{2.2}$$

In this reaction, h^+ and e^- are strong oxidizing and reductive agents, respectively. The oxidation and reduction processes are shown in Eqs. (2.3 − 2.5) (Ahmed *et al.*, 2011).

Oxidation reaction:

$$h^+ + Dyes \rightarrow Degradation\ compounds \tag{2.3}$$

$$h^+ + H_2O \rightarrow •OH + H^+ \tag{2.4}$$

Reductive reaction:

$$•OH + Dyes \rightarrow Degradation\ compounds \tag{2.5}$$

•OH is produced from the oxidation of adsorbed water and the presence of oxygen prevents the recombination of an $e^- − h^+$ pair. In HP, when the redox reactions do not progress simultaneously, the e^- accumulates in the CB, leading to the rise in the rate of recombination of h^+ and e^-. Therefore, it is extremely important to prevent e^- accumulation in HP (Ahmed *et al.*, 2011). The perhydroxyl radicals ($HO_2•$) can also be formed from the reaction between $O_2^-•$ and H^+. Formation of H_2O_2 can be resulted from the reaction between $HO_2•$ species. The reactions are shown in Eqs. (2.6 – 2.7) (Barrat, 2011).

$$O_2^-\bullet + H^+ \rightarrow HO_2\bullet \qquad (2.6)$$

$$2HO_2\bullet \rightarrow H_2O_2 + O_2 \qquad (2.7)$$
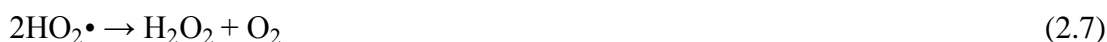
The formation of H_2O_2 inhibits the $e^- - h^+$ recombination by providing electron acceptor (O_2). Nonetheless, it can also become scavenger of VB holes. Various reaction of H_2O_2 is shown in Eqs. (2.8 – 2.10) (Barrat, 2011).

$$H_2O_2 + 2h^+ \rightarrow O_2 + 2H^+ \qquad (2.8)$$

$$H_2O_2 + \bullet OH \rightarrow H_2O + O_2 \qquad (2.9)$$

$$H_2O_2 + e^- \rightarrow OH^- + \bullet OH \qquad (2.10)$$
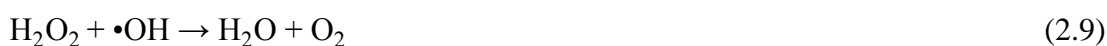
Figure 2.2 illustrates the schematic presentation of the semiconductor excited by the band gap illumination, leading to the $e^- - h^+$ formation in CB and VB, respectively (Ibhadon and Fitzpatrick, 2013).
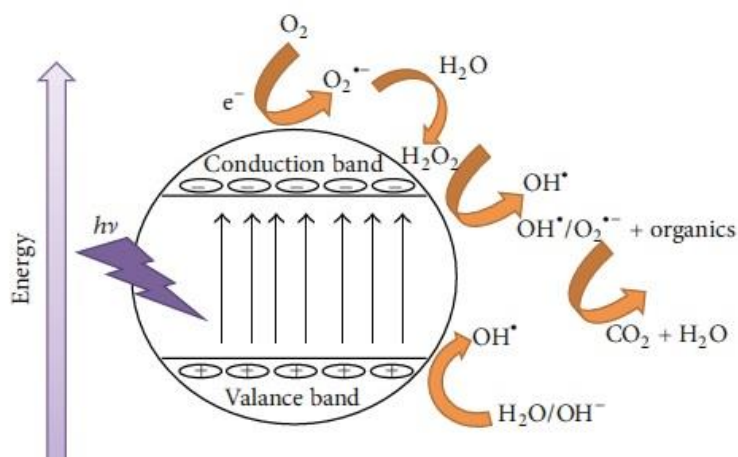
Figure 2.2: Schematic Presentation on the Photocatalytic Mechanism and Degradation Process (Muhd Julkapli, Bagheri and Bee Abd Hamid, 2014).

2.3.2   ZnO as a Photocatalyst

ZnO is a semiconductor that has attracted considerable attention worldwide due to its wide range of applications. For instance, its high refractive index which is 1.95-2.10,

was useful in pigment applications (Moezzi, McDonagh and Cortie, 2012). It has high thermal stability that can withstand temperature of at least 1800 ℃ (Moezzi, McDonagh and Cortie, 2012). ZnO is also applied in optoelectronics and in transparent conducting films (Moezzi, McDonagh and Cortie, 2012).

Three crystal structures of ZnO are available, including cubic rock-salt, cubic zinc-blende structure and hexagonal wurtzite. Wurtzite form is the most thermodynamically stable structure, whereas zinc-blende structure is metastable and the cubic rock-salt structure is generally only stable under extreme pressure, which is approximately 2 GPa. Figure 2.3 demonstrated the ZnO crystal structures using stick-and-ball representation. The tetrahedral coordination of ZnO results in non-centrosymmetric structure.
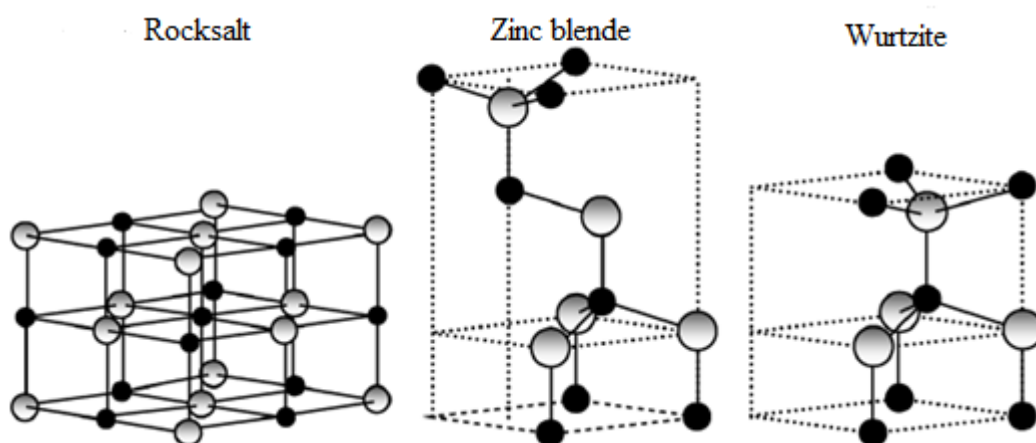
Figure 2.3: Stick-And-Ball Representation of ZnO Crystal Structures: (a) Cubic Rocksalt, (b) Cubic Zinc Blende and (c) Hexagonal Wurtzite. Shaded and Black Spheres Indicate Zn and O Atoms, Respectively (Morkoc and Ozgur, 2009).

The exciton binding energy is 60 meV at 300 K and is one of the reasons why ZnO is so attractive for optoelectronic device applications. Morkoc and Ozgur (2009) stated that the lattice constant of ZnO wurtzite range from 3.2475 to 3.2501 Å and 5.2042 to 5.2075 Å for the α-parameter and *c*-parameter, respectively. For the zinc blende structure of ZnO, the lattice constants are anticipated to be 4.60 and 4.619 Å, 4.463 Å, 4.37 Å and 4.47 Å using modern *ab initio* technique, spacing of reflection high-energy electron diffraction (RHEED) pattern, albeit spotty, comparison of the

XRD peak position, and examination of the transmission electron microscopy (TEM) images, respectively (Morkoc and Ozgur, 2009).

ZnO can be used as substitute semiconductor to TiO_2 due to its similar band gap (BG) energy of 3.2 eV and relatively lower cost of production. ZnO is better performed in the removal of several organic contaminants in both acidic and basic medium (Muruganandham and Wu, 2008; Lee *et al.*, 2009; Gupta, Saurav and Bhattacharya, 2015). It is also cheap, and contains large initial rates of activities and many sites with high surface reactivity. Nonetheless, it also suffers from the fast $e^- - h^+$ recombination. Hence, to overcome this shortfall, modification of morphology of ZnO has been proposed in attempt to increase the photocatalytic activity owing to the increase in surface area, porosity, crystallinity and lesser $e^- - h^+$ recombination (Zhang *et al.*, 2014).

2.3.3 Synthesis of ZnO Nanostructures

Nanomaterials are those having size of less than 100 nm with at least one dimension. Nanocatalysts has been used in vast applications, including water purification, biodiesel production, fuel cell application, and photocatalytic degradation (Likodimos *et al.*, 2013; Feyzi, Hassankhani and Rafiee, 2013; Kung *et al.*, 2014; Sathishkumar *et al.*, 2013). For photocatalytic applications, the ZnO nanostructures have a large surface-to-volume ratio and comprise more active sites on the surface, thereby enhancing the degradation efficiency (Umar *et al.*, 2011). Therefore, they are effective to use as catalyst (Chaturvedi, Dave and Shah, 2012).

The morphology of photocatalyst is the determinant of the enhancement of the degradation efficiency (Bandekar *et al.*, 2014; Patrocinio *et al.*, 2015). The adsorption of reactants and the desorption of product are improved due to the increase in surface-volume ratio. The short charge-transfer distance toward adsorbed species reduces the $e^- - h^+$ recombination (Lam *et al.*, 2012; Altavilla and Ciliberto, 2010). Owing to these merits, many researchers have recently attempted various synthesis methods and succeeded in fabricating various morphologies of different

sizes of ZnO such as nanorods, nanoplates, nanosheets, nanoboxes, hexagonal prisms, nanowires, nanobelts, nanorings, nanoneedles, nanotubes, and nanoflowers (Liu *et al.*, 2016; Phuruangrat, Thongtem and Thongtem, 2016; Khan *et al.*, 2016; Yathisha, Nayaka and Vidyasagar, 2016). Figure 2.4 depicts the morphologies of various ZnO nanostructures that have been reported in literatures. The morphology of ZnO is depending on the various synthesis techniques, process conditions, precursors, pH of the system or concentration of the reactants (Milea, Bogatu and Duta, 2011).

Synthesis of various ZnO nanostructures have been reported by a large variety of methods, such as mechanochemical process, chemical process, sol-gel and emulsion as shown in Table 2.8. Kołodziejczak-Radzimska and Jesionowski (2014) stated that mechanochemical process is a relatively inexpensive and simple method to produce nanostructures in large scale. The obtained nanostructures are also small in particle sizes and have little tendency to agglomerate. Moreover, the advantages of this method include the high homogeneousness of the crystalline structure and morphology. Sol-gel method is simple, low cost, reliable, repeatable and requires relatively mild conditions of synthesis. It also enables the surface alteration of ZnO with selected organic compounds (Kołodziejczak-Radzimska and Jesionowski, 2014). On the other hand, hydrothermal method provides simple and environmentally friendly technique, as well as producing a high degree of crystallinity and high purity of the products (Kołodziejczak-Radzimska and Jesionowski, 2014).

In this current study, the co-precipitation method was selected as the synthesis route to produce ZnO. The advantages of using a co-precipitation method include low costing, produces large quantity of particles with high purity, easily controlled reaction conditions and the preparation process is performed in aqueous phase (Yan *et al.*, 2015). Moreover, it only requires short preparation time and is capable to yield excellent polycrystalline samples (Bargougui *et al.*, 2014). Furthermore, it enables control over the chemical composition of the synthesized product (Milenova *et al.*, 2013). In this study, capping agent such as PVP was used to provide a structured photocatalyst as it greatly affect the nucleation and particle growth (Kołodziejczak-Radzimska and Jesionowski, 2014). Shahmiri *et al.* (2013) demonstrated the synthesis of copper oxide (CuO) nansheets using co-precipitation with the aid of PVP and the results showed that the increasing PVP concentration

formed well-defined nanosheets on the surface of CuO. Furthermore, Karami, Bigdeli and Matini (2016) synthesized ZnO nanoparticles using pulsed galvonostatic method with the assistance of PVP and sodium dodecyl sulfate (SDS). The results confirmed that PVP achieved finer and more uniform ZnO nanoparticles than SDS. According to Miao *et al.* (2016), flower-like ZnO architectures assembled with nanosheets was successfully fabricated by the addition of SDS.
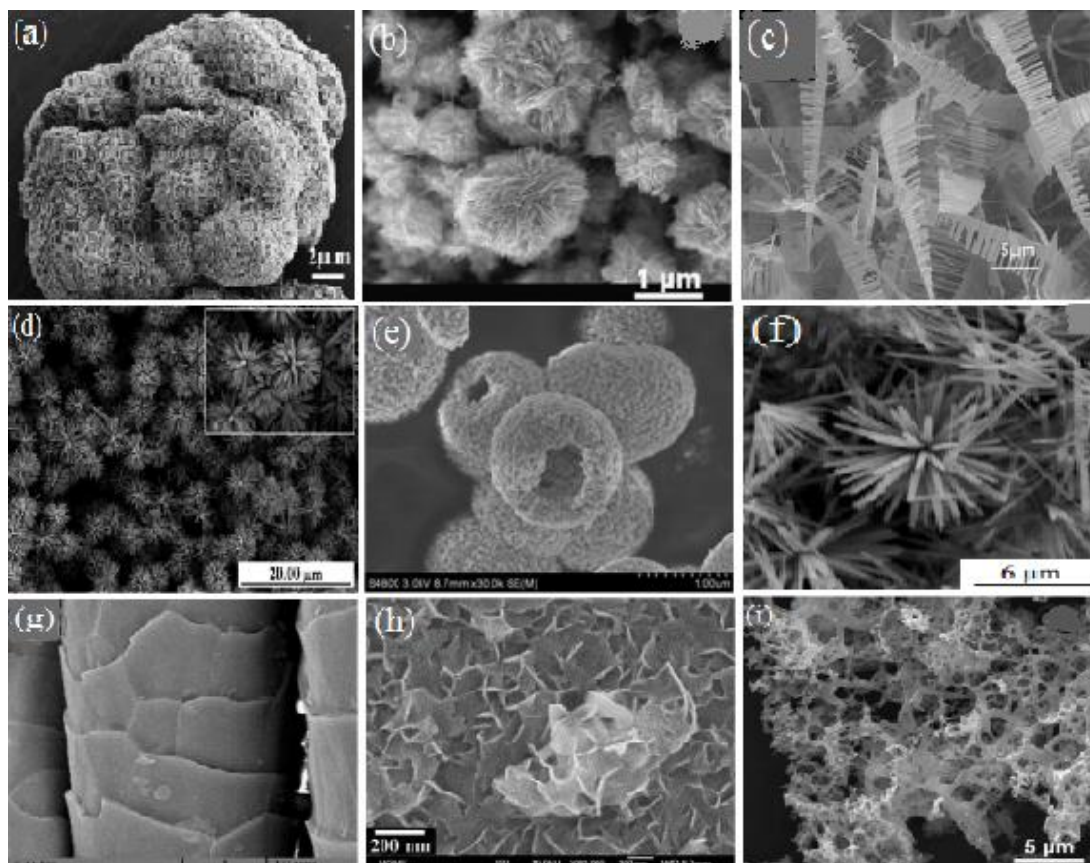
Figure 2.4: Various ZnO Nanostructures Morphologies. (a) Caddice Clew-Like ZnO Nanostructures (Luo *et al.*, 2014), (b) ZnO Balls Made Of Fluffy Nanosheets (Umar *et al.*, 2011), (c) Comb-Like ZnO Nanostructures (Zhang *et al.*, 2014), (d) Urchin-Like ZnO Nanostructures (Yang *et al.*, 2016), (e) Broken ZnO Hollow Microspheres (Bao, Wang and Ma, 2016), (f) Flower-Like ZnO Nanostructures (Yang *et al.*, 2015), (g) Honeycomb-Like ZnO Nanostructures (Behzadnia, Montazer and Rad, 2015), (h) Lotus Leaf-Like ZnO Nanostructures (Qi, Zhao and Yuan, 2013) and (i) Coral-Like ZnO Nanostructures (Cai *et al.*, 2014) .

Table 2.8: Summary of Preparation Method of ZnO.

ZnO nanostructure	Method	Precursors	Synthesis conditions	Particle size (nm)	Surface area (m^2/g)	References
NA	Mechanochemical process	$ZnCl_2$, Na_2CO_3, NaCl	400 – 800 °C	18 – 35	47	Stankovic *et al.* (2011)
Spherical	Precipitation process	$Zn(NO_3)_2$, NaOH	Synthesis: 2 h; drying: 2 h, 100 °C	40	NA	Lanje *et al.* (2013)
NA	Precipitation process	$Zn(CH_3COO)_2$, KOH	Precipitation temperature: 20 – 80 °C; drying : 120 °C	160 – 500	4 – 16	Kolodziejczak-Radzimska, Jesionowski and Krysztafkiewicz (2010)
Flower-like	Precipitation process	Micro-sized ZnO powder, NH_4HCO_3	Reaction: ~ 2 h, 25 °C; drying: 80 °C; calcination: 1 h, 350 °C	15 – 25	50 – 70	Khoshhesab, Sarfaraz and Houshyar (2012)
NA	Precipitation process	$ZnSO_4$, NH_4HCO_3, ethanol	Drying: overnight, 100 °C,	12	30 – 74	Wang *et al.* (2010)

ZnO nanostructure	Method	Precursors	Synthesis conditions	Particle size (nm)	Surface area (m^2/g)	References
			calcination: 300 – 500 ℃			
Spherical	Sol-gel	Zn(CH$_3$COO)$_2$, oxalic acid (C$_2$H$_2$O$_4$), ethanol	Reaction: 50 ℃, 60 min; dried of gel: 80 ℃, 20 h; calcination: under flowing air for 4 h at 650 ℃	NA	NA	Benhebal *et al*. (2013)
Rod	Emulsion	Zn(CH$_3$COO)$_2$, NaOH and KOH, cyclohexane, non-ionic surfactants	Reaction: ambient temperature; drying: 24 h, 120 ℃	396 – 825	12	Kolodziejczak-Radzimska, Markiewicz and Jesionowski (2012)
Flake	Emulsion	Zn(CH$_3$COO)$_2$, NaOH and KOH, cyclohexane, non-ionic surfactants	Reaction: ambient temperature; drying: 24 h, 120 ℃	220 – 712	20	Kolodziejczak-Radzimska, Markiewicz and Jesionowski (2012)

2.4 Operating Parameter Study

HP is governed by numerous parameters such as solution pH, substrate concentration, light intensity and photocatalytic loading. In this study, some operating parameters such as solution pH and initial dye concentration are focused due to their significant on the photocatalytic reactions.

2.4.1 Initial Dye Concentration

The initial dye concentration is one of the significant parameters in photocatalytic degradation efficiency. The degradation efficiency of dyes decreased with the increasing initial dye concentration. When initial dye concentration increases, more dye molecules are adsorbed onto the photocatalyst surface but they are not degraded immediately because the light intensity and photocatalyst loading is constant. In addition, the path length of the photons striking the surface of the photocatalyst is reduced as the intensity of solution increases. Thus, the generation of •OH is limited and subsequently reduce the photocatalytic degradation (Gupta *et al.*, 2012). Table 2.9 shows the summary of photocatalytic degradation of various dyes under the influence of initial dye concentration (Ahmed *et al.*, 2011).

Daneshvar *et al.* (2007) demonstrated that the photo-degradation of acid orange 7 by ZnO under UV irradiation in the range of initial dye concentration of 0.003 mM to 0.009 mM. The optimum concentration was found to be 0.003 mM with a degradation percentage of 88%. Furthermore, according to Tariq *et al.* (2008), 90% of degradation efficiency of acid blue 45 was achieved using TiO_2 under UV illumination at an optimum initial dye concentration of 0.3 mM. Sobana and Swaminathan (2007) indicated the complete degradation (100%) of acid red 18 using ZnO under UV radiation at 0.2 mM. It was observed that the degradation efficiency decreased with the escalating of initial dye concentration. The above results could be well explained by the low absorption of light at high initial dye concentration with a fixed photocatalyst loading, thereby decreasing the photocatalytic degradation efficiency.

Table 2.9: Effect of Initial Dye Concentration on the Photo-Degradation of Various Dyes.

Pollutant type	Light source	Photocatalyst	Range of initial dye concentration (mM)	Optimum concentration (mM)	Degradation (%)	References
Acid orange 7	UV	ZnO	0.003-0.009	0.003	88	Daneshvar *et al*. (2007)
Reactive Orange 4	UV	F-TiO$_2$	0.015-0.035	0.3	85	Vijayabalan *et al*. (2009)
Acid Blue 45	UV	TiO$_2$	0.3-0.6	0.3	90	Tariq *et al*. (2008)
Acridine Orange	UV	TiO$_2$	0.1-0.5	0.25	82	Faisal *et al*. (2007)
Ethidium bromide	UV	TiO$_2$	0.1-0.4	0.1	99	Faisal *et al*. (2007)
Fast Green FCF	UV	TiO$_2$	0.031-0.125	0.031	93	Saquib *et al*. (2008)
Acid Red 18	UV	ZnO	0.2-1.0	0.2	100	Sobana and Swaminathan (2007)

2.4.2   Solution pH

Solution pH of watercourse is a parameter that can affect the photo-degradation of organic pollutants as it governs the surface charge of the photocatalyst and the size of aggregates it forms. In addition, organic compounds in dye-containing wastewater vary based on the solubility in water, speciation behaviour and hydrophobicity. An organic compound is referred to as a neutral species at pH below its pKa value whereas it possesses a negative charge above this pKa value. Some organic compounds can even present in the forms of positive, neutral and negative in aqueous solution. This variation in pH values can considerably govern their photocatalytic behaviour. Table 2.10 demonstrated a summary of photocatalytic degradation of dyes under various solution pH (Ahmed *et al.*, 2011).

Vijayabalan *et al.* (2009) examined the effect of solution pH in the range of 1– 9 on the photocatalytic degradation of reactive orange 4 using $F-TiO_2$ under UV light source. The authors stated that 98% of degradation efficiency was attained at optimum pH of 3.0. The surface of $F-TiO_2$ was positively charged at pH 3.0, attracting reactive orange 4 onto the surface of $F-TiO_2$ and increasing the degradation efficiency Furthermore, Ananandan *et al.* (2008) achieved complete degradation of acid red 88 using $Ag-TiO_2$ under visible light source at the optimum pH of 1.8 due to the maximal adsorption of acid red 88 to the protonated $Ag-TiO_2$. Additionally, Pare *et al.* (2008) demonstrated that with an optimum pH of 7.1, the degradation efficiency of acridine orange could achieve 90 % using ZnO under visible illumination. This could be well attributed to the amphoteric nature of ZnO that it could form corresponding salt at acidic condition and produce complexes at alkaline condition.

Table 2.10: Effect of Solution pH on the Photo-Degradation of Various Dyes.

Pollutant type	Light source	Photocatalyst	pH range	Optimum pH	Degradation (%)	References
Reactive Orange 4	UV	$F\text{-}TiO_2$	1.0-9.0	3.0	98	Vijayabalan *et al*. (2009)
Acid Red 88	Visible	$Ag\text{-}TiO_2$	0.2-1.8	1.8	100	Ananandan *et al* (2008)
Disperse Blue 1	UV	TiO_2	3-11	3.0	80	Saquib *et al*. (2008)
Methyl Orange	UV	$Pt\text{-}TiO_2$	2.5-11.0	2.5	100	Huang *et al*. (2008)
Acid Blue 45	UV	TiO_2	2.05-10.05	5.8	100	Tariq *et al*. (2008)
Acridine Orange	Visible	ZnO	2.9-7.1	7.1	90	Pare *et al*. (2008)
Fast Green FCF	UV	TiO_2	3.0-11.0	4.4	100	Saquib *et al*. (2008)
Acid Blue 80	Solar	TiO_2	2.0-10.0	10.0	99	Su *et al*. (2008)
Reactive Blue 4	UV	$Nd\text{-}ZnO$	3.0-13.0	11	100	Zhou *et al*. (2009)
Methylene Blue	Visible	$La^{3+}\text{-}TiO_2$	2-10	10	95	Parida *et al*. (2008)

2.4.3 Dye Mixtures and Real Textile Dye Wastewater

Real textile dye wastewater in reality comprises of a wide range of pollutants such as organic compounds and inorganic sodium salts (Lam, *et al.*, 2012). Therefore, there is an increase in research demand on real textile dye effluent (Popli and Paterl, 2015; Tomei, Pascual and Angelucci, 2016). The efficiency of the treatment of real textile dye wastewater can be investigated by assessing the characteristics of real textile dye wastewater including COD, BOD_5, TSS, AN, colour, turbidity and pH. Sahoo, Gupta and Sasidharan (2012) indicated that the 98 % of photodegradation of real textile wastewater under UV irradiation was obtained using 1 g/L of $Ag-TiO_2$ after 420 minutes of UV irradiation, demonstrating an excellent destruction of refractory organic pollutants from textile industry discharge. In addition, Saravanan, *et al.* (2013) stated that the degradation of textile wastewater using ZnO/CuO composite under visible light illumination presented more than 90%, proving ZnO/CuO mineralize the organic contaminants present in the textile wastewater. Hussein (2013) investigated the photocatalytic degradation of real and simulated textile wastewater using ZnO. The chemical properties of textile wastewater are indicated in Table 2.11. As demonstrated in the table, the mineralization of real textile wastewater was always lower than the simulated wastewater due to the presence of recalcitrant organic compounds and chloride ions that might inhibit the photocatalytic reaction. This situation eventually complicated the degradation mechanism of the photocatalyst.

Table 2.11: Parameters of Treated Wastewater by ZnO (Hussein, 2013).

Parameter	Type of textile wastewater							
	Real		Simulated Vat Yellow		Simulated Reactive Black		Simulated Reactive Blue	
	Untreated	Treated	Untreated	Treated	Untreated	Treated	Untreated	Treated
Total hardness (ppm)	237.00	50.60	246.62	48.66	76.58	16.86	98.25	25.60
Total alkalinity (ppm)	73.68	61.61	76.66	62.24	37.54	36.20	40.36	38.44
COD (ppm)	225.08	98.60	160.32	60.42	182.32	59.55	142.70	70.12
BOD$_5$ (ppm)	149.30	68.61	103.18	45.61	118.34	52.88	94.56	48.60
*TOC (%)	100	78	100	88	100	84	100	84
pH	12.90	7.01	9.40	7.02	10.50	6.98	8.41	7.20
CI (ppm)	63.91	9.12	68.49	10.12	28.57	ND	32.08	ND
Na (ppm)	697.60	696.88	4.524	4.496	18.730	18.276	5.116	4.984
K (ppm)	44.831	44.654	0.328	0.298	0.335	0.321	0.214	0.221

Notes:

ND: Not determined

*: Measured after 10 hours of irradiation.

2.5   Summary of Literature Review

The properties and structures of dyes have been discussed in literature review and various spectrums of conventional methods have been used to remove the dye-containing wastewater. Each of them has different degrees of effectiveness in degrading the dyes as each of them has their own limitations. Principle and mechanism of HP was then conferred to enhance the understanding toward the process. Among photocatalyst used in HP, ZnO is an extensively used catalyst owing to its low cost of production, high initial rates of activities and many sites with high surface reactivity. Various synthesis methods of ZnO nanostructures have been also discussed in this work. Morphological modification on ZnO was chosen in this study due to their large surface-to-volume ratio and high active sites on the surface. In addition, the effect of several process parameters such as initial dye concentration and solution pH have been described as they could significantly influence the efficiency of degradation of dyes.

A lot of photocatalytic studies have been conducted based on single dye removal as stated in the literature reports. However, in real textile dye effluents, the dyes are present in a mixture, this study begin with simultaneous treatment of dye mixtures using ZnO nanostructure. Thus, this challenge is attempted to overcome the limitations as observed in the literature reports. There is a scarce report highlighted on the ZnO on simultaneous removal in the literatures. The MO and MG dyes will be chosen in the simultaneous treatment using ZnO nanostructure. This was followed by real textile dye treatment via the as-synthesized ZnO nanostructure.

CHAPTER 3

METHODOLOGY

This chapter discussed the methodology of the experimental works in this research work. The experimental set-up and methodology of this study was illustrated in the Figure 3.1.

3.1 Materials and Chemicals

Materials and chemicals used in this study are listed in Table 3.1. All chemicals were in analytical grade and used as-purchased without further purification.
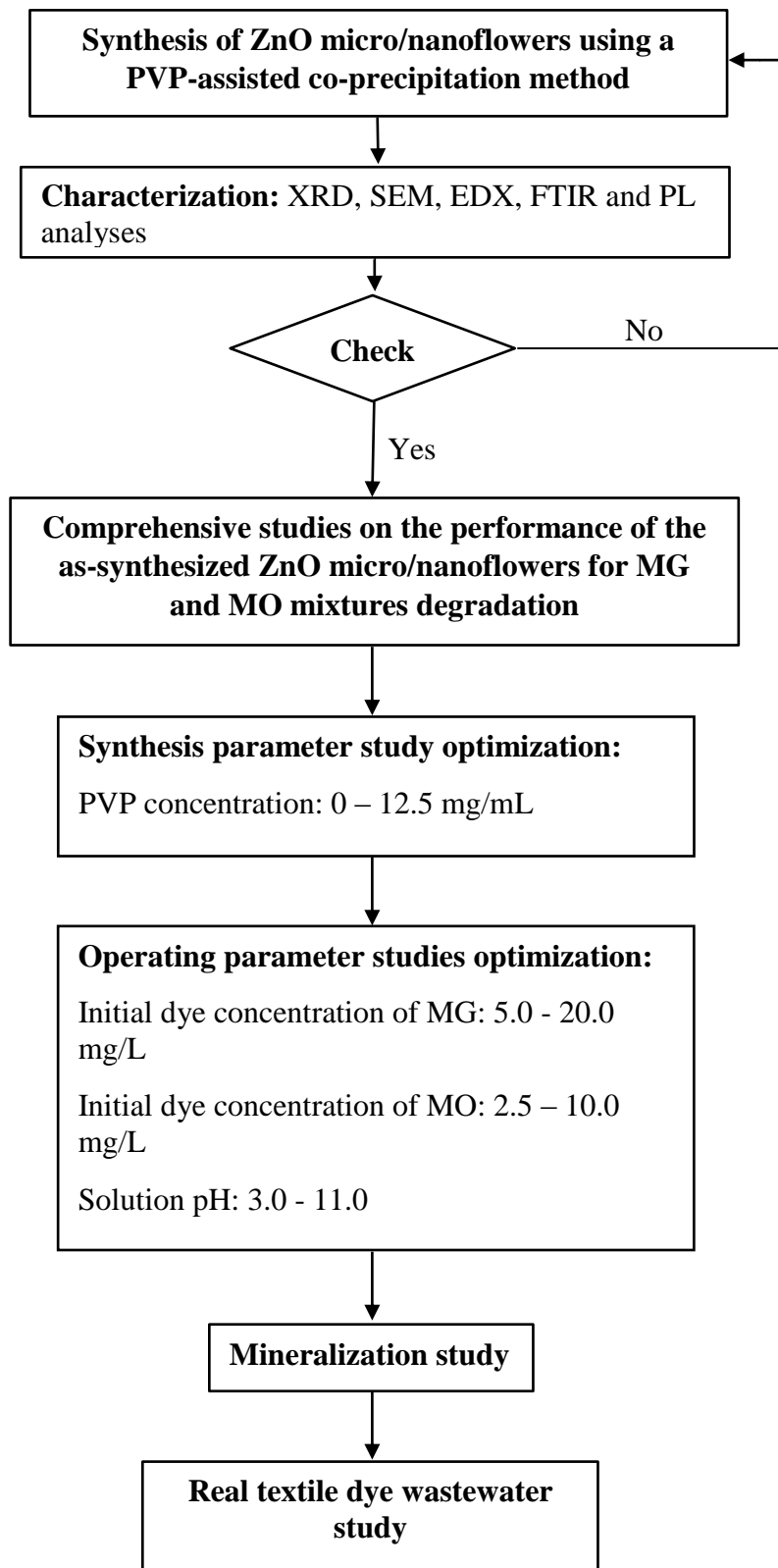
Figure 3.1: Flowchart Of Experimental Work Involved In This Study.

Table 3.1: List of Materials and Chemicals Used.

Chemical/Reagent	Purity	Supplier	Purpose of use
Zinc nitrate hexahydrate ($Zn(NO_3)_2 \cdot 6H_2O$)	> 98.5 %	QReC	Used as precursor in ZnO synthesis
PVP	Not applicable (N/A)	Acros Organics	Used as capping agent in ZnO synthesis
Sodium hydroxide (NaOH)	> 99.0 %	R&M Chemicals	Used as precursor in ZnO synthesis and for pH adjustment
Nitric acid (HNO_3)	> 99.0 %	QReC	Used for pH adjustment
Distilled water (0.30M $\Omega \cdot cm$)	N/A	Favorit	For preparation of different aqueous solutions, for cleaning of apparatus, and as a "control"
MG	83 %	Sigma Aldrich	Used as model organic dye pollutant
MO	85 %	Sigma Aldrich	Used as model organic dye pollutant

3.2 Apparatus

3.2.1 Fluorescent Light Experimental Apparatus

The schematic diagram of the experimental apparatus was indicated in Figure 3.2 whereas the actual experimental apparatus was set-up as illustrated in Figure 3.3. Photodegradation of mixture of model organic pollutants were carried out in an acrylic black box which was used to prevent the solution from exposure to other light sources except the compact fluorescent lamp (CFL). A CFL was used as a light source in this experiment for photodegradation of mixture of MG and MO. It is light powered and has light intensity striking the surface of the reaction solution about 6.50×10^3 lux as measured by a digital lux meter (LX-101, EθSUN).

The CFL had been found to give an irradiation in both UV and visible spectrum (Nawi, et al., 2011; NEMA, 2014). It should be noted that the content of UV light from the fluorescent lamp was very low and its contribution of UV was much lower in comparison to that of sunlight, because fluorescent lamp mainly emits visible light (Nakata & Fujishima, 2012). A mixture of MG and MO solution was poured into a 250 mL glass beaker in this fluorescent light irradiation experiment.

The beaker was positioned in a way such that the distance between the surface of the solution and CFL was 12 cm in vertical direction. Two cooling fans were used to regulate the increased temperature induced by the heat generation from the CFL. Furthermore, air pump was used for the provision of air source to the solution throughout the experiment. The flow rate of 3 L/min was maintained by a rotameter which is connected to the air pump. Magnetic stirrer was used to ensure well mixing between mixture of dyes and ZnO micro/nanoflowers.
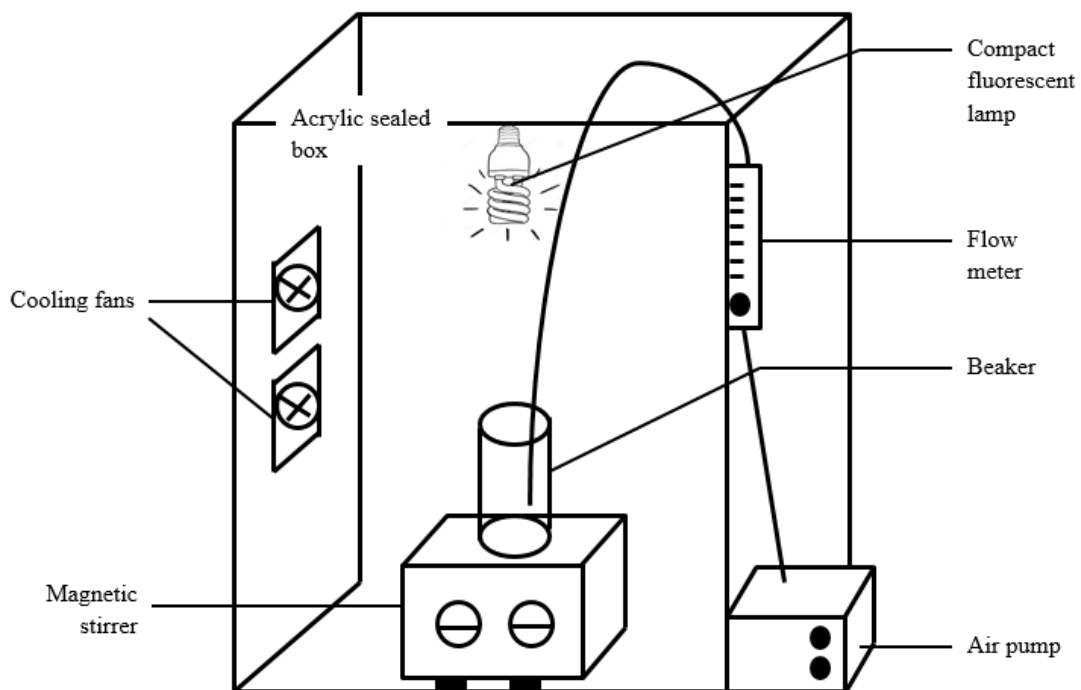
Figure 3.2: Schematic Diagram of Fluorescent Light Experiment Set-Up.
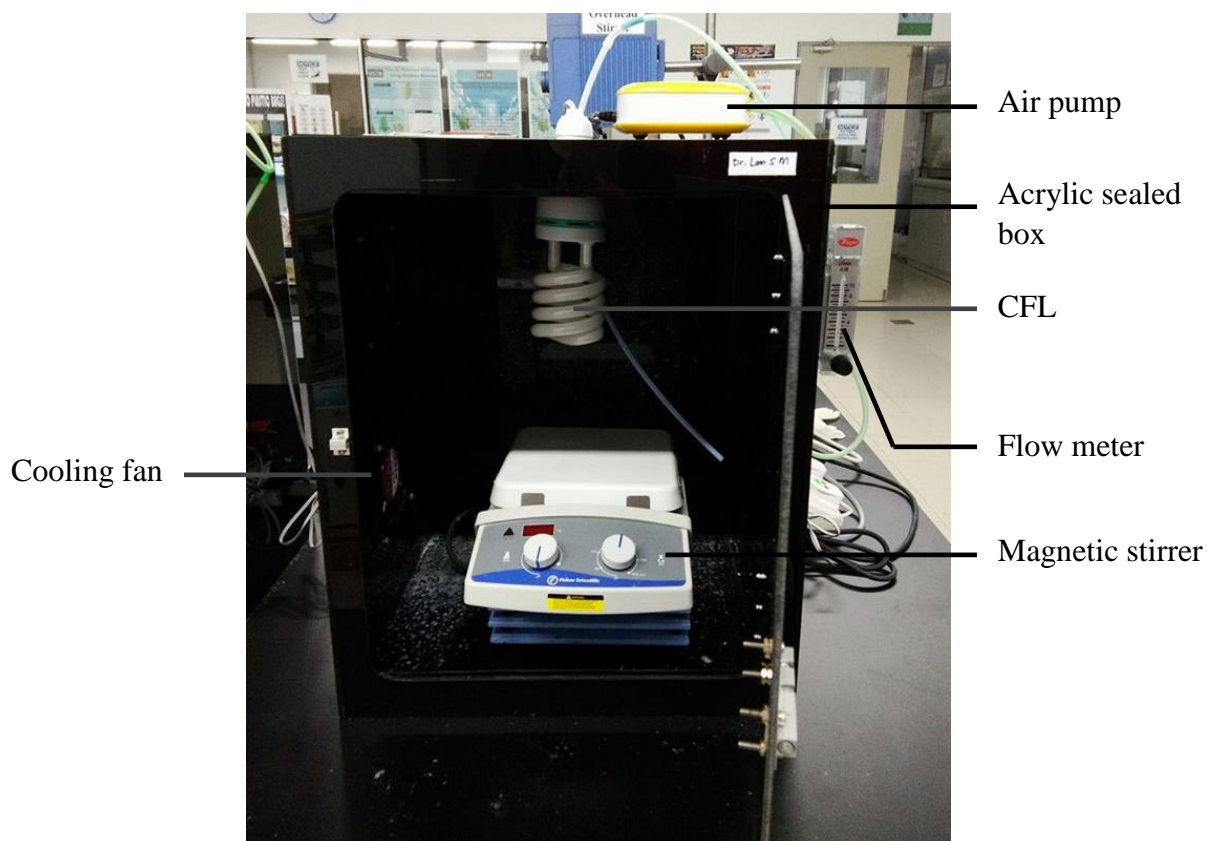
Figure 3.3: Actual Fluorescent Light Experimental Set-Up in the Laboratory.

3.3 Analytical Procedures

3.3.1 UV-Vis Spectrophotometer

The concentration changes of dye were measured using a *HACH DR6000* UV-Vis spectrophotometer. Dye samples were poured into cuvette and UV-Vis adsorption measurement was made at particular wavelength. In the analysis, a fraction of the light energy will be absorbed by the organic molecules which incur the promotion of electrons from lower energy level to higher energy level (Kalsi, 2007). The intensity of light passing through the dye solution will eventually be reduced. Hence, the degree of absorption by mixture of dyes was recorded. As demonstrated by Beer-Lambert law, the absorbance is directly proportional to concentration of sample solution, as given in the Eq. (3.1) (Valente, Tzompantzi and Prince, 2011).

$$A = \varepsilon bC \qquad\qquad (3.1)$$

where A is the absorbance at a certain wavelength (Abs), ε is the molar absorptivity coefficient (mg/L/cm), b is the path length (cm), and C is molar concentration (mg/L). Therefore, the absorbance increases with the concentration as there is linear relationship between them.

MG and MO dyes were first screened to obtain their maximum absorbances wavelength (nm). The measured wavelength was 632 nm and 464 nm, respectively (Lamia, *et al.*, 2016; Sanroman, *et al.*, 2004; Zucca, 2012; Hadjltaief, *et al.*, 2016; An *et al.*, 2015; Marchena, *et al.*, 2016; Wang, *et al.*, 2013, Sun, *et al.*, 2014). Calibration curves of these dyes were also performed and the data is shown in Appendix A1 and A2.

3.3.2   Chemical Oxygen Demand Analyzer

A COD analyzer was used to assess the degree of mineralization of sample present in the solution. The COD measurement was conducted according to HACH Reactor Digestion Method 8000 in Hach Water Analysis Handbook using a *HACH DRB 200* COD Reactor (HACH, 2014). The COD reactor was preheated to 150 ℃ before the dye samples analysis. For dye samples preparation, 2 mL distilled water as blank sample and 2 mL dye sample was pipette into different HR COD digestion reagent vial and mixed gently. Then, the vials were cooled to room temperature and preceded for testing with *HACH DR6000* UV-Vis spectrophotometer. The blank sample was set as zero and the COD value of the dye samples were obtained in mg/L. The results were duplicated to obtain an average reading.

3.4   Preparation of Photocatalysts

3.4.1   Preparation of ZnO Micro/Nanoflowers

The synthesis of ZnO micro/nanoflowers was carried out via a PVP-assisted co-precipitation method reported by Chamjangali and Boroumand (2013). First, 25 mL of distilled water was heated in a beaker to reach a constant temperature of 60 ℃. Next, 250 mL of aqueous appropriate amount of PVP solution and subsequently 25 mL of zinc nitrate (0.10 M) were added at 60 ℃ under constant stirring for about 1 min. 25.0 mL of NaOH (0.50 M) was added and stirred at 60 ℃ for 1 h. The resultant precipitate was centrifuged and washed with ethanol and distilled water for three times. After being washed, the precipitate was then dried in an oven for 2 h at 80˚C. Finally, the precipitate was calcined in a furnace for 2 h at 550˚C. The synthesis of ZnO micro/nanoflowers was repeated with varying the concentration of PVP between the ranges of 0 to 12.5 mg/mL. The flow of the PVP-assisted co-precipitation method was illustrated in the following Figure 3.4.

```
┌─────────────────────────────────────────────┐
│     25 mL of DI water was heated to 60 ℃      │
└─────────────────────────────────────────────┘

┌───────────────────────┐        ┌───────────────────────────┐
│  250 mL of appropriate │        │   25 mL Zn(NO₃)₂ (0.1 M)   │
│     amount of PVP      │        │                           │
└───────────────────────┘        └───────────────────────────┘

          ┌───────────────────────────────┐
          │     Stirring for about 1 min   │
          └───────────────────────────────┘

┌─────────────────────────────────────────────────────┐
│ 25.0 mL NaOH (0.50 M) was added and stirred at 60 ℃ for 1 h │
└─────────────────────────────────────────────────────┘

┌─────────────────────────────────────────────────────┐
│   Centrifuged and washed using distilled water and ethanol  │
└─────────────────────────────────────────────────────┘

          ┌───────────────────────────────┐
          │   Dried in an oven for 2 h at 80˚C │
          └───────────────────────────────┘

          ┌───────────────────────────────┐
          │ Calcined in a furnace for 2 h at 550˚C │
          └───────────────────────────────┘
```
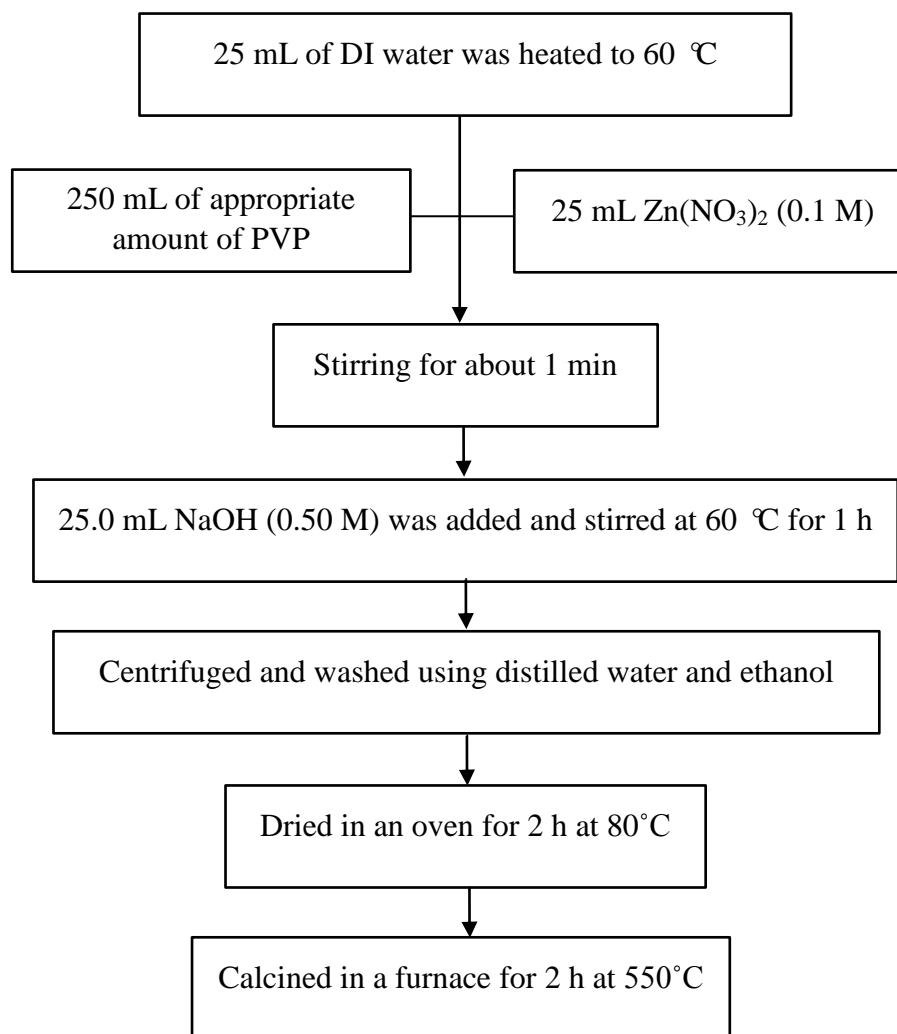
Figure 3.4: Flowchart of ZnO Micro/Nanoflowers Preparation.

3.5   Characterization of Photocatalysts

3.5.1   Crystal Phase Analysis

XRD is analysis used to identify crystal structure/ crystal phase of ZnO samples. This analysis was performed using a *Philips PW1820* diffractometer equipped with Cu Kα radiation at scanning rate of 2° min^{-1} in the range of 2θ, which was set to 20 – 70 °. The analysis was carried out at Universiti Tunku Abdul Rahman (UTAR).

3.5.2   Surface Morphology and Elemental Composition Analysis

FESEM is a method used to detect the morphology of sample. This analysis was conducted using a *Jeol JSM-6701F* FESEM. Prior to the analysis, the solid sample was taped with double-sided tape on aluminium tube and then vacuumed for 5 minutes. The solid sample was also fine coated with a layer of platinum using *Jeol JFC-1600* auto fine coater. The analysis was carried out at UTAR.

EDX analysis was also undertaken to determine the elemental composition of the as-synthesized ZnO micro/nanoflowers. It was also carried out on the same equipment as FESEM at UTAR.

3.5.3   Functional Group Analysis

FTIR analysis is an analysis used to identify the functional group of sample. It was used to detect the chemical bonds present in the sample by forming an infrared adsorption spectrum. The method was performed using a *Spectrum RX 1* FTIR Spectrometer. Prior to analysis, FTIR accessories kit including FTIR sample holder, evacuable die set and grinder was cleaned with absolute ethanol to remove the impurities. The analysis was performed at UTAR.

3.5.4   Electronic Property Analysis

PL spectroscopy is a characterization method to examine the electronic property of sample. It was used to compare the recombination rate band gap determination of different photocatalyst systems. Light is directed onto the sample, which it is absorbed and imparts excess energy into the material in a process known as photo-excitation, leading to the promotion of electrons to permissible excited states. These electrons return to their equilibrium states with the release of excess energy, either a radiative process (the emission of light) or a non-radiative process (Barron, 2012).

The PL spectra were carried out using a *Perkin Elmer Lambda S55* spectrofluorometer using a Xe lamp with an excitation λ of 325 nm at School of Chemical Sciences, Universiti Sains Malaysia (USM). The PL emission data were then recorded after the sample holder was run in the instrument. Prior to the instrument measurement, the sample was ground in an agate mortar. The sample was then transferred into a sample holder which had glass at one side and subsequently screwed cover by the sample holder lid to give a uniform surface of the sample.

3.6 Photocatalytic Activity of Photocatalysts

3.6.1 Photocatalytic Activity of ZnO Micro/Nanoflowers under Fluorescent Light Irradiation

The photocatalytic performances of as-developed ZnO micro/nanoflowers were carried out in the presence of fluorescent light irradiation. In a typical experiment, 100 mL mixture of dye solution and 10 mg/L ZnO micro/nanoflowers were prepared and fed into a beaker. An air was bubbled into the solution at constant 3 L/min flow rate throughout the experiment. The suspensions were continuously agitated with the aid of a hot plate stirrer. Prior to the experiment, the heterogeneous mixture was premixed in the dark for 30 minutes before it was exposed for the irradiation of light. After the elapse of a period of time, 5 mL of the solution was withdrawn from the system, centrifuged and filtered with 0.45 μm PTFE filters before being subjected to analysis. This was to screen any suspended solid present in the samples that will affect the accuracy of the results obtained from UV-Vis spectrophotometer. All the experiments were duplicated to increase the accuracy of the experimental works. In addition, the photocatalytic activity of the as-developed ZnO micro/nanoflowers and the commercially available ZnO were compared. The photocatalytic degradation of mixture of dye solution was calculated as shown in Eq. (3.2).

$$\text{Degradation efficiency} = \frac{C_0 - C_t}{C_0} \times 100\ \%$$
(3.2)

where degradation efficiency is expressed in terms of percentage (%), C_o is the initial concentration of mixture of dye solution after 30 minutes in dark condition (mg/L) and C_t is the concentration of mixture of dye solution at reaction time, t (min) (mg/L).

3.7 Process Parameters Studies

The effect of the process parameters including initial dye concentration and solution pH were investigated in this study. These process parameters were varied at a time while other process parameters remain constant.

3.7.1 Effect of Initial Dye Concentration

The effect of initial dye concentration on the photocatalytic degradation of MG and MO dyes was studied using 100 mL of mixture of dye. The initial dye concentration of MO and MG was on the range of 2.5 to 10.0 mg/L and 5.0 mg/L to 20.0 mg/L respectively. The selection of initial substrate concentration range was based on the research conducted by Chamjangali *et al.* (2015). The experiments were conducted at a fixed catalyst loading of 1 g/L and natural pH of the solution (pH 6.5 for MO and MG dye mixtures) (Li *et al.*, 2005; Zhang *et al.*, 2009; Hadjltaief *et al.*, 2016).

3.7.2 Effect of Solution pH

The effect of solution pH on the photocatalytic degradation of mixture of MG and MO dyes was investigated on the pH range of 3.0 to 11.0 over the synthesized ZnO photocatalysts (Bel Hadjltaief *et al.*, 2015; Huang *et al.*, 2008; Liu, Yang & Choy, 2006). Four different pH of solutions were adjusted by the addition of dilute 1.0 M HNO$_3$ or 1.0 M NaOH before the light was turned on. The values of solution pH were chosen based on the different conditions such as acidic, natural, neutral, and

alkaline media. The experiment was monitored using a *HANNA Instruments HI2550 pH/ORP & EC/TDS/NaCl Meter*. The experiments were carried out with optimum initial dye concentration.

3.8   Real Textile Dye Wastewater

Real textile dyes mixture was collected from Penfabric Sdn Bhd at Butterworth, Malaysia. The collected volume was 1.5 L and it was stored in 4 °C freezer. The real textile dyes mixture was pre-characterized. Some significant parameters which include ammoniacal nitrogen (AN), TSS, BOD_5, colour, turbidity, pH and COD of the real textile dyes mixture were examined and characterized. The dilution ratio of 1:10, 1:50 and 1:100 had been made prior to pre-characterization. Table 3.2 shows the characteristics of real textile dye wastewater.

Table 3.2: Characteristics of Real Textile Dye Wastewater.

Parameter	Value
COD (mg/L)	2515
BOD_5 (mg/L)	340.5
BOD/COD	0.14
Turbidity (NTU)	136
Colour (Pt-Co)	884
TSS (mg/L)	920
AN (mg/L)	5.35
pH	11.7

3.8.1 Biochemical Oxygen Demand

BOD_5 was measured to determine the extent to which oxygen in the sample can support microorganism according to dilution method (APHA, 2005). The sample was diluted with a dilution factor and then poured into the 300 mL BOD bottle. The initial DO (DO_0) was measured using the *EUTECH DO 2700* dissolved oxygen meter. After the measurement, the BOD bottle was sealed immediately with parafilm to prevent air from entering the bottle and affect the accuracy of the result. Then, it was stored in the *VELP SCIENTIFICA FOC 225E* BOD incubator at 20 ℃ for 5 days. Lastly, the final dissolved oxygen (DO_5) was measured after 5 days incubation. The results were duplicated to obtain an average reading. The BOD_5 was calculated based on Eq. (3.3):

$$BOD_5 = \frac{DO_0\text{-}DO_5}{\text{Dilution Fraction}} \tag{3.3}$$

where DO_0 is the initial DO (mg/L) and DO_5 is the final DO after 5 days incubation (mg/L).

3.8.2 Ammoniacal Nitrogen

NH_3-N was used to measure the NH_4^+ concentration present in real textile dyes mixture by ammoniacal nitrogen reagents according to Nessler method in APHA 2005 (Jeong, *et al.*, 2013). Those reagents include the mineral stabilizer, polyvinyl alcohol dispersing agent and Nessler reagent. 25 mL of diluted samples were prepared. The diluted sample was then added with three drops of mineral stabilizer and mixed gently. Next, three drops of polyvinyl alcohol dispersing agent were also dripped into the diluted sample and mixed gently. Then, 1 mL of Nessler reagent was dropped into the diluted sample and a homogenous mixing was made prior to the measurement. The blank sample was first set as zero and the diluted sample was measured using a *HACH DR6000* UV-vis spectrophotometer at 425 nm wavelength under *380 Nitrogen Ammonia Nessler* program. The results were expressed in terms

of mg/L. The results were duplicated to obtain an average reading.

3.8.3   Colour

Colour testing was used to evaluate the pollution levels in real textile dyes mixture according to method 8025 Platinum-Cobalt (Pt-Co) standard method by Hach Company. Adequate dilution was required for the sample before the measurement to ensure that the resulting reading was within the stipulated range of the spectrophotometer. Two empty glass vials were filled with the sample and distilled water, respectively. The measurement was performed using a *HACH DR6000* UV-Vis spectrophotometer at the 465 nm wavelength. Blank sample was set as zero and the tested colour value was obtained in Platinum-Cobalt scale, PtCo. The readings were repeated to obtain an average reading.

3.8.4   Turbidity

Turbidity of the sample was measured directly without the need of dilution using a *Lovibond Turbicheck* turbidity meter. The meter was required for calibration beforehand with the provided standard standard solutions accordingly. Then, the samples were filled into the sample cell until marked line and wiped with clean towel before the measurement. The sample was measured for turbidity in Nephelometric Turbidity Units (NTU). The results were repeated to obtain an average reading.

3.8.5 Suspended Solid

The suspended solid measurement was used to measure the amount of solid that is suspended in the sample according to an 8006 Photometric Method (HACH, 2014). One blank sample with distilled water was needed for zeroing purpose prior to the

measurement. Direct measurement could be taken from glass vial containing sample using a *HACH DR6000* UV-Vis spectrophotometer and the result obtained was in mg/L. The results were duplicated to obtain an average reading.

CHAPTER 4

RESULTS AND DISCUSSION

This chapter discussed the results of the experiment in this research work. First section of this chapter presented the characterization studies of ZnO micro/nanoflowers. In second section, the simultaneous photocatalytic degradation of MO and MG using ZnO under UV-vis light irradiation was demonstrated. The third section consisted of photocatalytic degradation study under synthesis parameter such as PVP concentration. Consequently, the photocatalytic performance of ZnO was studied at various process parameters including initial dye concentration and solution pH. The fifth section comprised of a mineralization study of the mixture of MO and MG at optimized condition. Lastly, the photocatalytic degradation of real textile dye wastewater was investigated using ZnO under UV-vis light irradiation.

4.1 Characterization of ZnO Micro/Nanoflowers

Characterization of the as-synthesized ZnO micro/nanoflowers were performed in order to assess its photocatalytic degradation performance in terms of its structure and crystal phase, surface morphology, chemical composition and optical properties. The structure and crystal phase of ZnO was evaluated via the XRD analysis whereas the surface morphology of ZnO was confirmed through the FESEM technique. The elemental composition and the functional group of ZnO were determined through EDX and FTIR analyses, respectively. Lastly, the electronic property was assessed by PL measurement.

4.1.1 Crystal Phase Analysis

Figure 4.1 presents the XRD patterns of as-prepared ZnO micro/nanoflowers. The major diffraction peaks observed at the angles of $2\theta = 31.9°$, $34.4°$, $36.2°$, $47.5°$, $56.7°$, $62.7°$, $68.1°$, $68.8°$ and $69.2°$ were corresponded to (100), (002), (101), (102), (110), (103), (200), (112) and (201) crystal planes, respectively. These crystal planes could be perfectly indexed to the hexagonal wurtzite phase of ZnO with lattice constants $a = 3.249$ and $c = 5.206$ according to the ZnO standard JCPDS (card No. 36-1451). No diffraction peak due to any other impurities such as $Zn(OH)_2$ were detected, indicating high purity of as-prepared ZnO. The strong and sharp diffraction peaks proposed that the product was highly crystallized. The results obtained were also in accordance with other literatures (Luo et al., 2014; Peng et al., 2016; Rai et al., 2010).

Furthermore, it was also observed that the peak broadness of the as-synthesized ZnO increased with the concentration of PVP added. With comparing the broadness of the peaks, it can be clearly showed that ZnO synthesized with 12.5 mg/L PVP concentration had the broadest peaks, indicating that ZnO sample was the smallest size. As the result of high crystallinity and small size of ZnO micro/nanoflowers, it was believed that the photocatalytic performance of ZnO micro/nanoflowers would be improved by reducing the $e^- - h^+$ recombination, generating more free photocarriers to be involved in the photocatalytic activity (Khan et al., 2015; Lin et al., 2015).

4.1.2 Surface Morphology Analysis

Figures 4.2a and b illustrate the representative FESEM images of the as-synthesized ZnO PVP-12.5 micro/nanoflowers. As shown in Figures 4.2a and b, it was exhibited that the as-synthesized ZnO was consisted of numerous well-defined flower-like 3-D micro/nanostructures with regular shape and size. The average diameter of the ZnO micro/nanoflowers was ranging from 890 nm to 1.261 μm, which were assembled by numerous petals that grow on a certain direction.
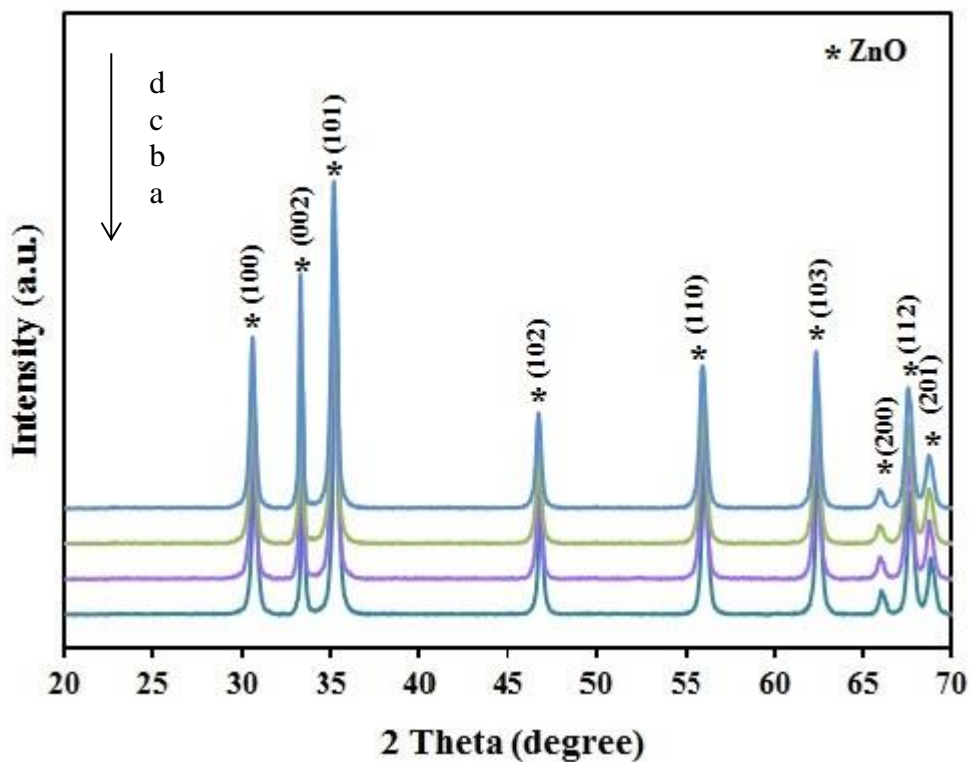
Figure 4.1: XRD patterns of the As-Synthesized ZnO Micro/Nanoflowers Synthesized with or without PVP (d) without PVP (c) PVP-2.5 (b) PVP-6.5 and (a) PVP-12.5.
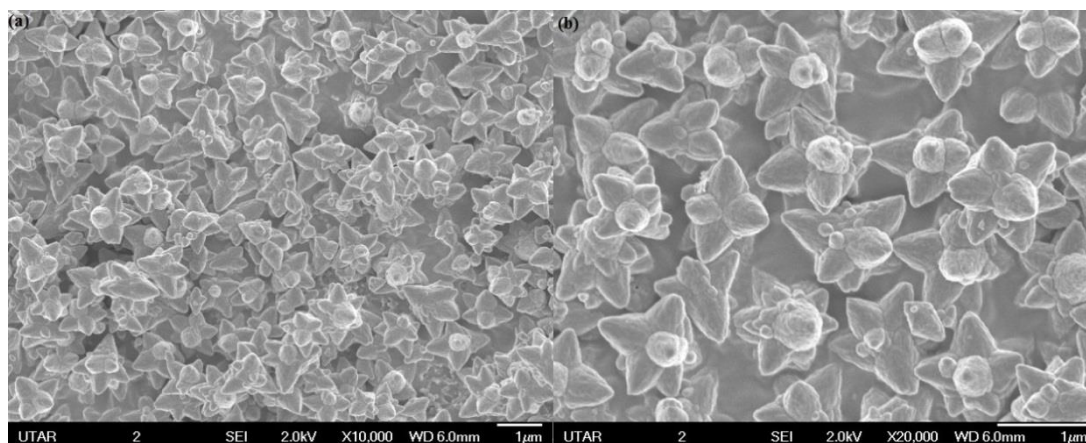
Figure 4.2: FESEM Images with (a) Low Magnification and (b) High Magnification of the As-Prepared ZnO PVP-12.5 Micro/Nanoflowers.

It was suggested that the growth of crystals was not only governed by the intrinsic structure but also the external conditions. The concentration of capping agent used in the synthesis of ZnO is crucial in the reduction of the particle size and enhancement of the uniformity and regularity of the structure. Therefore, PVP was varied at three different concentrations and control synthesis in the absence of PVP was carried out to understand the formation mechanism of flower-like micro/nanostructures as displayed in Figure 4.3. As presented in the figure, it was obvious that the micro/nanoflowers prepared without PVP surfactant were irregular in shapes and agglomerated. However, when the PVP concentration increased, the micro/nanoflowers demonstrated more regular and uniform flower-like ZnO micro/nanostructures. The capping agent, PVP was used to control the growth of morphology by preventing the nanoparticles agglomeration and producing a uniform growth of ZnO micro/nanoflowers as each particle on nucleation grow evenly on all direction (Ansari, Bazarganipour and Salavati-Niasari, 2016; Wang et al., 2013). From the obtained FESEM images, ZnO PVP-12.5 exhibited the most well-defined, regular and uniform flower-like micro/nanostructures. Furthermore, sizes of ZnO micro/nanoflowers were also measured and the results were found to reduce from 1.850 μm to 1.261 μm as increasing the PVP concentration from 0 to 12.5 mg/mL. Similar results were reported by Joshi (2012) and Kamari *et al.* (2017), in which the sizes of the ZnO nanoparticles decreased with the increasing concentration of PVP.

According to the FESEM observations, a formation mechanism was proposed for the evolution of the 3-D flower-like hierarchical ZnO micro/nanostructures as presented in Figure 4.4. During the initial stage of the synthesis, the formation of ZnO could occur as a consequence of the dehydration of $Zn(OH)_4^{2-}$ ions which acted as the nucleation sites for the growth of ZnO spherical particles as shown in the following Eqs. (4.1 – 4.3) (Peng et al., 2016).

$$Zn^{2+} + 2OH^- \rightarrow Zn(OH)_2 \tag{4.1}$$

$$Zn(OH)_2 + 2OH^- \rightarrow Zn(OH)_4^{2-} \tag{4.2}$$

$$Zn(OH)_4^{2-} \rightarrow ZnO + H_2O + 2OH^- \tag{4.3}$$
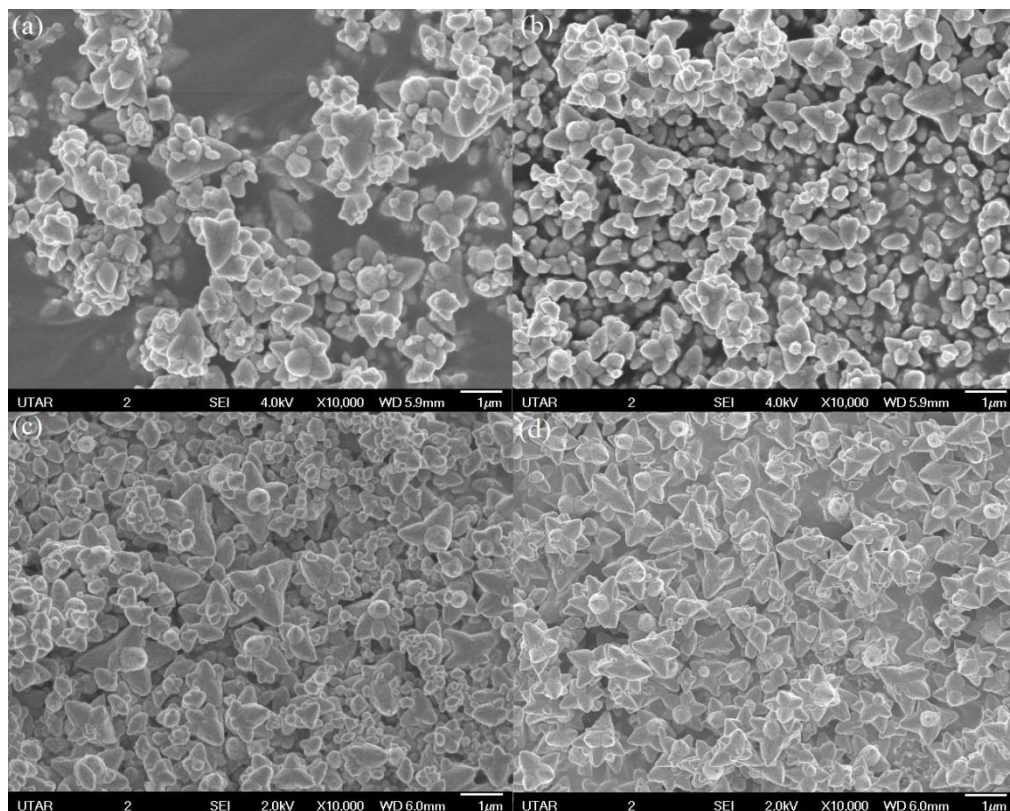
Figure 4.3: FESEM Images of ZnO Micro/Nanoflowers. (a) without PVP, (b) PVP-2.5, (c) PVP-6.5 and (d) PVP-12.5.
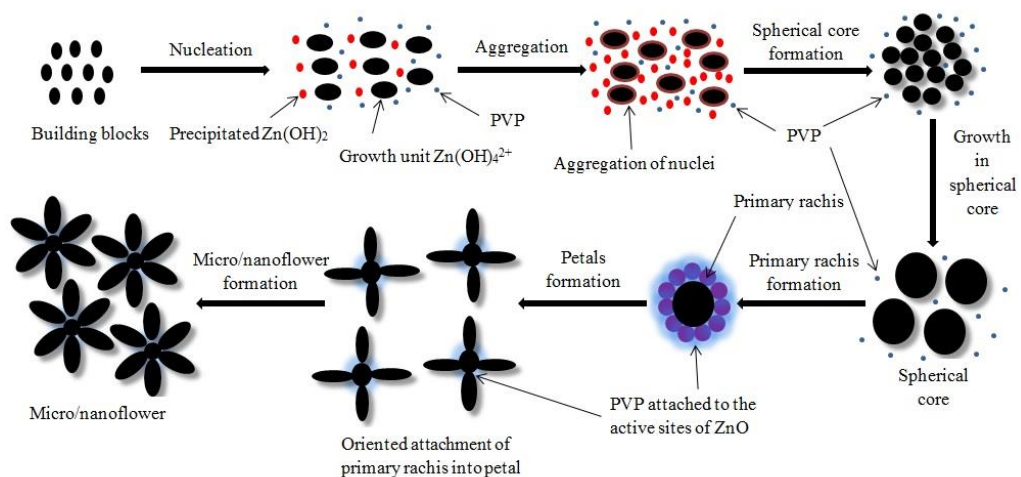
Figure 4.4: Schematic Illustration of Formation Mechanism of As-Prepared ZnO Micro/Nanoflowers.

Subsequently, a huge quantity of ZnO nuclei were formed and aggregated when the degree of saturation exceeds its critical value (Peng et al., 2016). ZnO is a polar crystal with the positive polar plane rich in Zn and the negative polar plane rich in O and it has the anisotropic growth habit because various crystal facets have different growth rates (Hu, Zhu and Wang, 2004). ZnO crystallite usually grows along <0001> direction (*c*-axis) based on the surface energy minimization. The growing ZnO nanocrystals may attract to each other to self-assembly as a flower-like structure to minimize the interfacial energy. The spherical molecules were formed as growth unit, which continued growing to produce big core spheres in such a way that providing a proper surface energy for the attachment of active molecules of ZnO. These active molecules were primary rachis which attached on the core cells of the ZnO micro/nanoflowers. The formation of flower rachis followed by the arrangement of small petals on the surface of core cells and grew in linear direction. Owing to the presence of PVP in the solution system, the oriented attachment of ZnO particles onto the primary rachises proceeded continuously from these active sites on the surface of the primary rachises. The primary rachises formed in initial stage had many crystalline boundaries that had more defects. This caused other region to be thermodynamically unstable and these boundary regions rearranged their surface to reduce their surface energy, which promoted secondary heterogenous growth of ZnO micro/nanoflowers, leading to the continuous formation of the ZnO micro/nanoflowers (Wahab, Kim and Shin, 2011). In the research, the ZnO micro/nanoflowers were fabricated successfully by a facile PVP-assisted solution route.

4.1.3   Elemental Composition Analysis

Figure 4.5 shows the elemental composition of the as-synthesized ZnO micro/nanoflowers as determined from EDX spectrum. The spectrum confirmed that the as-synthesized ZnO PVP-12.5 was composed of Zn and O elements. The obtained results also determined that there were no other impurities found in the as-synthesized ZnO, signifying the presence of high purity of ZnO.
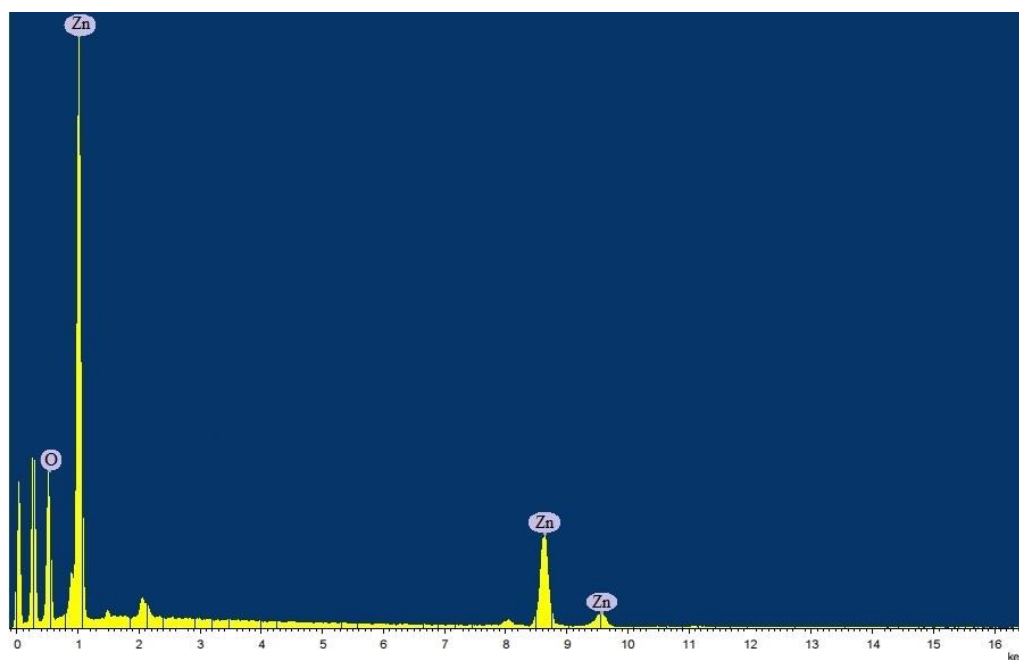
Figure 4.5: EDX Spectrum of As-Synthesized ZnO PVP-12.5 Micro/Nanoflowers.

4.1.4 Functional Group Analysis

Figure 4.6 displays the FTIR spectra of as-synthesized ZnO micro/nanoflowers with different PVP concentrations. The peaks found at 3428 cm^{-1} and 1637 cm^{-1} were assigned to the –OH stretching vibration of adsorbed water and the surface OH^{-} groups on the surface of the ZnO micro/nanoflowers, respectively. Based on the FTIR analysis, it was demonstrated that the PVP-12.5 exhibited the strongest peak at 3428 cm^{-1} among the four samples, deducing that more –OH groups might be present on the surface of ZnO micro/nanoflowers due to the large surface area offered by unique 3-D structure of micro/nanoflowers. In the photocatalytic reaction, the activity was closely related to the amount of –OH groups available on the surface of ZnO micro/nanoflowers as –OH groups could capture the photo-generated hole and transformed to reactive •OH radicals.

Another peak found at 1521 cm^{-1} was ascribed to the C=O stretching vibration from PVP (Safa et al., 2015). In addition, the peak observed at 1325 cm^{-1} was assigned to the C–H bond of PVP (Gutul et al., 2014). The peaks at 550 cm^{-1}
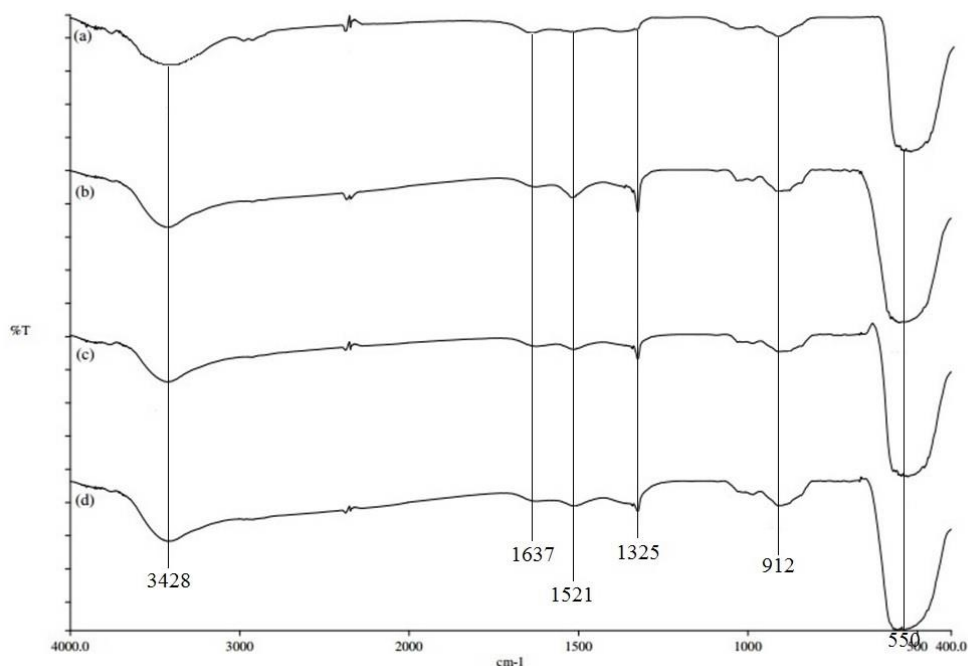
Figure 4.6: FTIR Spectra of As-Prepared ZnO Micro/Nanoflowers (a) without PVP, (b) PVP-2.5, (c) PVP-6.5 and (d) PVP-12.5.

were corresponded to the stretching vibration of the Zn-O bond (Safa et al., 2015). Similar results were reported in study of Gutul et al. (2014) where the peaks found were matched with the results obtained in this research.

4.1.5 Electronic Property Analysis

The PL spectra are crucial for discovering the efficiency of charge carrier trapping, immigration and transfer and for understanding the fate of electron hole pairs in semiconductor since PL emission results from the recombination of free carriers. Figure 4.7 depicts the PL spectra of ZnO micro/nanoflowers. It was notable that the intensities of visible emission of ZnO micro/nanoflowers were weaker as the concentration of PVP used for synthesis of ZnO micro/nanoflowers increased, denoting that the radiative recombination was lower when the concentration of PVP used increased. This was well-accredited to the small particle size of ZnO micro/nanoflowers as the smaller size of ZnO micro/nanoflowers allowed the
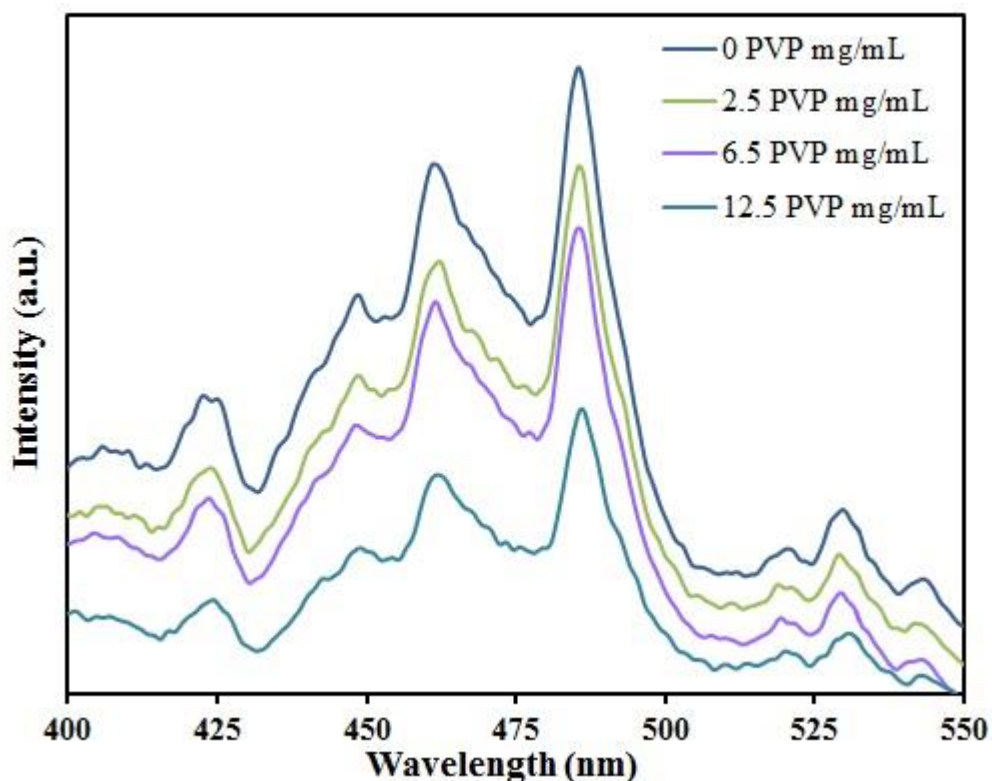
Figure 4.7: PL Spectra of As-Synthesized ZnO Micro/Nanoflowers.

irradiation of light energy to be reached into the active site faster, enhancing the $e^- - h^+$ separation. This gave rise to the increase of the participation of $e^- - h^+$ in the reaction and accordingly improved the photocatalytic performance (Sin and Lam, 2016). Hence, the lowest PL intensity was manifested by ZnO PVP-12.5 mirco/nanoflowers which had the smallest particle size, suggesting that it had the lowest $e^- - h^+$ recombination rate, increasing the lifetime of $e^- - h^+$ and forming more amounts of reactive species in the photocatalytic reaction (Lam et al., 2014).

4.2 Simultaneous Photocatalytic Degradation of MO and MG using ZnO Micro/Nanoflowers under UV-Vis Light Irradiation

Figure 4.8 illustrates the photocatalytic activities of the as-synthesized ZnO PVP-12.5 micro/nanoflowers in the degradation of MO and MG mixtures under various conditions. The photolysis test resulted in 2.55 % degradation of MO and 84.96 %
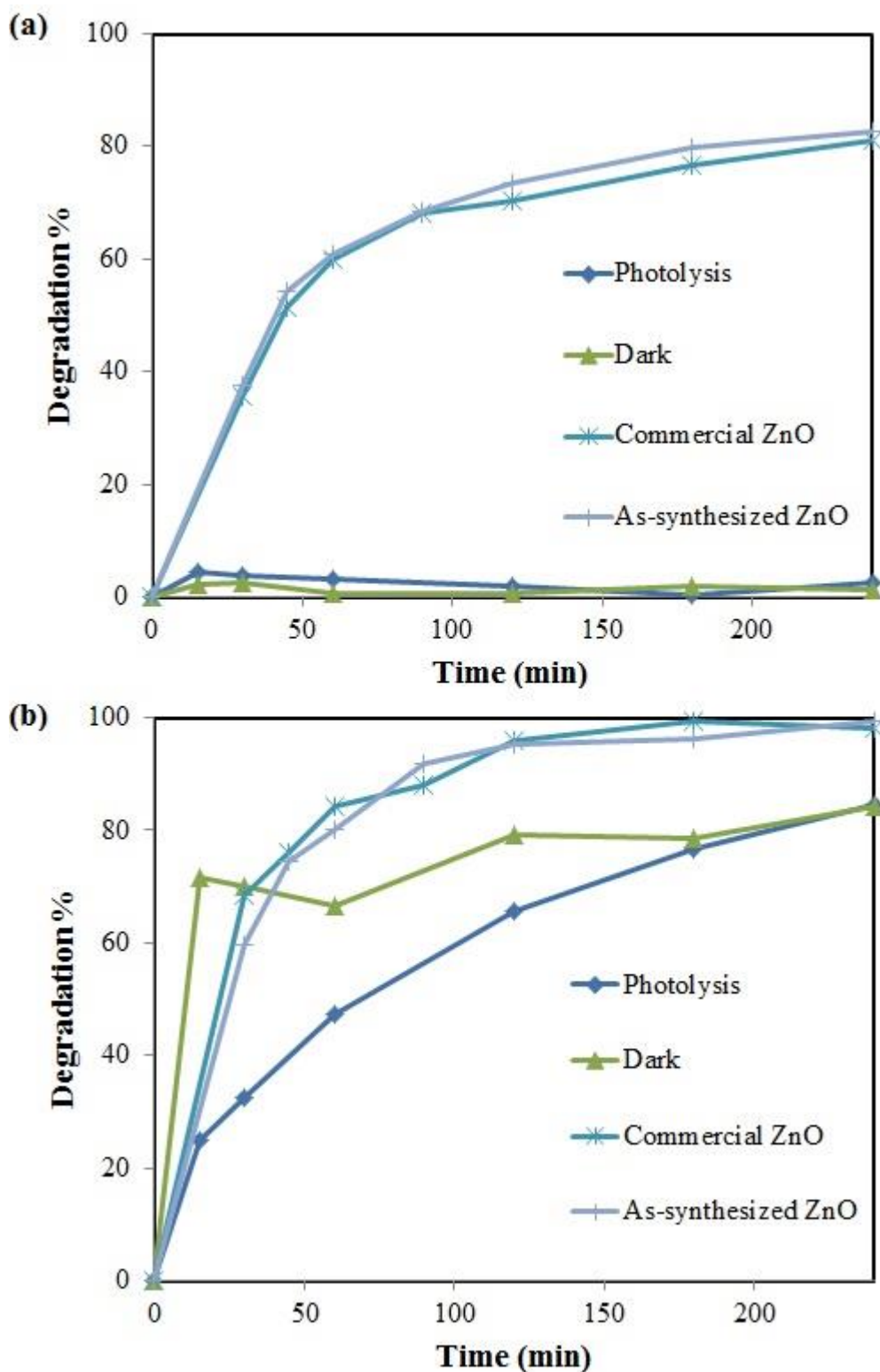
Figure 4.8: Photocatalytic Experiments of MO (a) and MG (b) in their Mixture ([MO] = 5 mg/L; [MG] = 10 mg/L; ZnO Loading = 1 g/L; Solution pH = 6.5).

degradation of MG within 240 minutes of irradiation, respectively. During the dark experiment without the irradiation of fluorescent light, it was observed that the degradation of MO and MG were 1.23 % and 84.40 %, correspondingly. Under the similar irradiation time, the photocatalytic degradation of MO and MG using commercial ZnO achieved respective 80.95 % and 98.01 %, whereas, the photocatalytic performance of the as-synthesized ZnO PVP-12.5 micro/nanoflowers in the degradation of MO and MG exhibited corresponding 82.75 % and 99.80 % degradation. The results showed that the as-synthesized ZnO PVP-12.5 micro/nanoflowers had the maximal degradation efficiency of MO and MG.

The control experiment suggested that only little amount of MO was degraded by direct photolysis owing to the fact that MO was stable in the presence of UV-vis light irradiation. The result was in accordance with Chamjangali et al. (2015). It was suggested that the photolysis could be ignored as there was only little degradation after irradiation of 60 minutes. From the dark experiment, it was confirmed that there was no detectable changes of MO concentration occurred. This indicated that the presence of both photocatalyst and light were essential for the acceleration of photocatalysis.

Nonetheless, MG was substantially degraded by photolysis. According to a research conducted by Bousnoubra et al (2016), it was indicated that the significant degradation of MG could be well attributed towards the characteristic of good absorbance of light in photolysis. The noticeable degradation of MG in the dark was owing to the direct adsorption of MG onto the surface of the as-synthesized ZnO samples. This was in agreement with studies carried out by Chen et al. (2015) and Xu et al. (2015). In a research performed by Chen et al. (2015), it was observed that 93.8 % of RhB degradation after 40 minutes in the dark, while Xu et al. (2015) achieved approximately 25 % of MB degradation after 30 minutes of dark adsorption. The results elucidated that the degradation of both MO and MG dyes in the dark was constant after 30 minutes, signifying that the adsorption of two dyes on the surface of the ZnO had achieved an equilibrium state after 30 minutes. This recommended that the binary solution was continuously stirred for 30 minutes in the dark prior to the photocatalytic activity.

As compared to commercial ZnO, the as-synthesized ZnO PVP-12.5 micro/nanoflowers established exceptional photocatalytic degradation of MG and MO mixtures. This could be well ascribed towards the high crystallinity, 3-D morphology and huge amount of functional group (–OH) of the micro/nanoflowers. As stated in XRD analysis, high crystallinity enabled efficient $e^- - h^+$ separation, increasing the number of charge carriers in the photocatalytic degradation. Moreover, the morphology of micro/nanoflowers was critical in the enhancement of photocatalytic degradation as well. Large surface area offered an ample amount of active sites available for the photocatalytic reaction. The result was in accordance to the results obtained in FESEM analysis. As mentioned in FTIR analysis, huge amount of –OH was available for the photocatalytic reaction, thereby increasing the number of •OH to participate the photocatalytic degradation.

The quantification of the intervention of one dye with others due to overlapping of absorption spectra or any interactions is very crucial in the multi-dye photo-degradation system. Figure 4.9 shows the UV-vis spectrum of MO and MG dyes. It was evident that the λ_{max} values of both MO and MG did not shift upon mixing; however, two distinguish peaks were detected for MO and MG. Hence, the photo-degradation of MO and MG in the mixture solution can be investigated separately at their respective λ_{max} of 464 nm and 632 nm. The observed maximum absorption peaks at 464 nm and 632 nm were on account of the azo group that produce strong orange and blue-green colour correspondingly (Karnan & Selvakumar, 2016; Bel Hadjltaief et al., 2015). Figure 4.10a presents the UV-vis absorption spectra of MO and MG during different time intervals of the photocatalytic activity performed in the presence of as-synthesized ZnO micro/nanoflowers under fluorescent light irradiation. It was obvious that the maximum absorption peaks of MO and MG disappear almost completely upon 240 minutes of irradiation. The reduction in the absorption band intensities of the two dyes and the absence of new peak formation indicates that the dyes had been photodegraded by as-synthesized ZnO PVP-12.5 micro/nanoflowers. The green colour of MO and MG mixtures was gradually turned into colourless, as illustrated in Figure 4.10b. This confirmed the destruction of the azo bonds of the dye structure and photodegradation of organic dye (Zyoud et al., 2015).
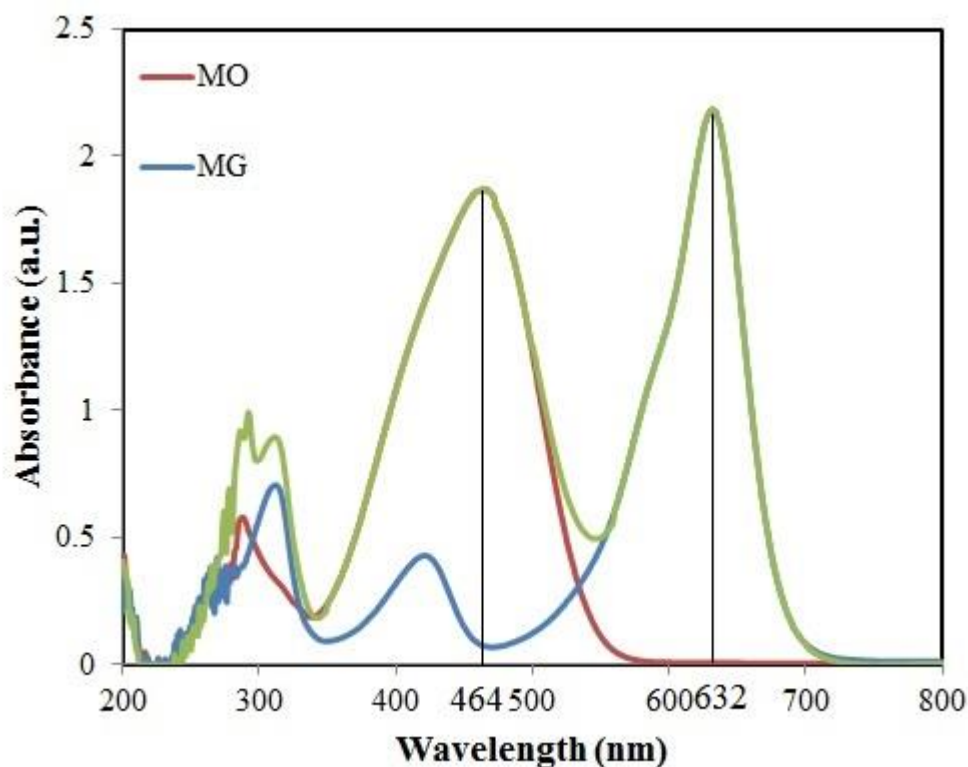
Figure 4.9: UV-vis Spectrum of MO and MG ([MO] = 10 mg/L; [MG] = 20 mg/L).

A photocatalyst was economical if it could be easily separated and recovered from the reaction system upon completion of the photocatalytic reaction. Sedimentation test of as-synthesized ZnO PVP-12.5 micro/nanoflowers and commercial ZnO was carried out to compare their performances in this study. The solutions were left untouched for 30 minutes after their photocatalytic activities. Figures 4.11a and b demonstrates the sedimentation performance of commercial ZnO and as-synthesized ZnO respectively. It was notable that the solution containing as-synthesized ZnO PVP-12.5 micro/nanoflowers was relatively less turbid with a visible layer of photocatalyst settled at the bottom of the beaker, whereas commercial ZnO showed a more turbid mixture with no visible separation layer of deposited photocatalyst. This could probably due to the different densities of both as-synthesized and commercial ZnO, in which a higher density of as-synthesized ZnO PVP-12.5 micro/nanoflowers favoured the higher sedimentation performance compared to spherical-shaped commercial ZnO. This could facilitate the recovery of
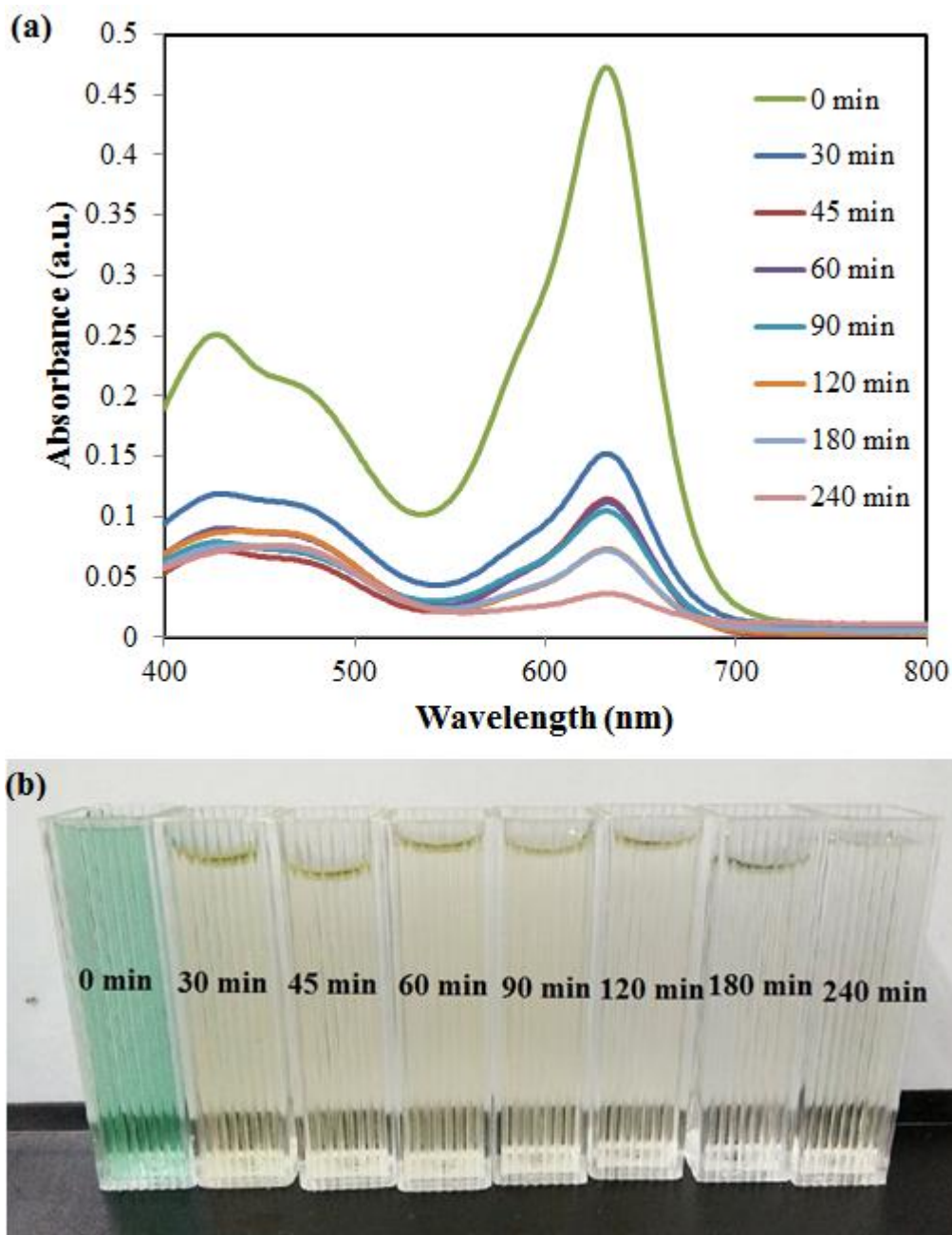
Figure 4.10: (a) Evolution of UV-vis Spectra of MO and MG Solution with ZnO at Various Time Intervals ([MO] = 5 mg/L; [MG] = 10 mg/L; ZnO Loading = 1 g/L; pH = 6.5) and (b) Colour Change of MO and MG Mixtures at Various Time Intervals ([MO] = 5 mg/L; [MG] = 10 mg/L; ZnO Loading = 1 g/L; pH = 6.5).

the photocatalyst from the aqueous suspension for their recyclabilities in the wastewater treatment application.
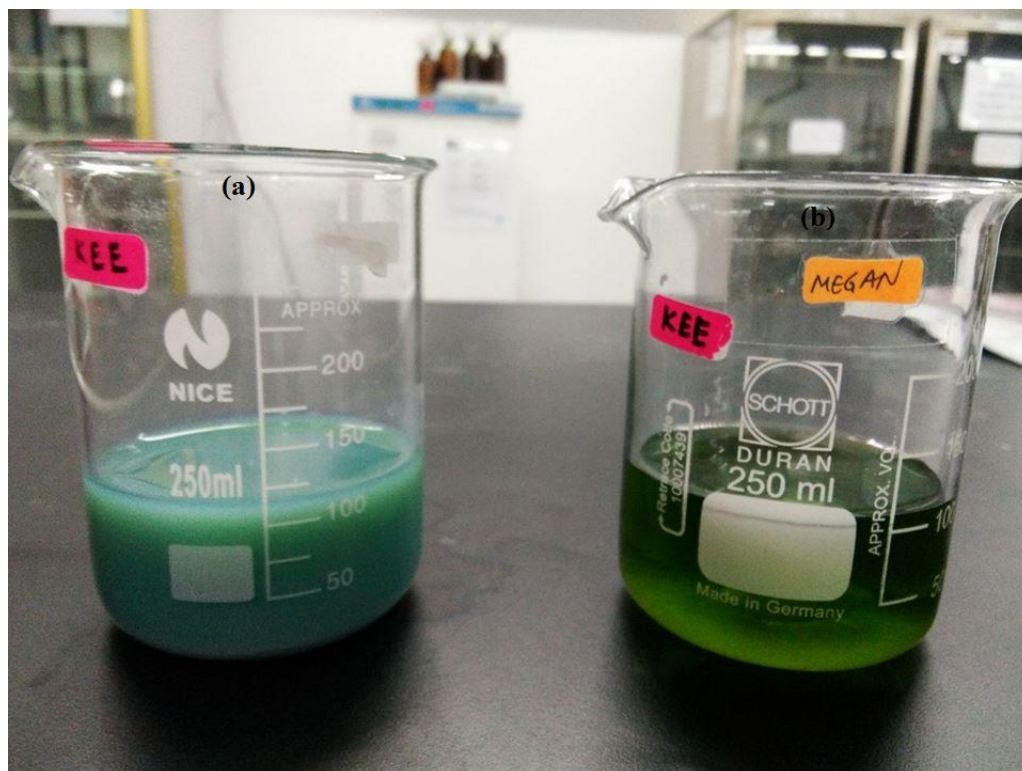
Figure 4.11: Sedimentation Test after 30 Minutes of MO and MG Photocatalytic Activity using (a) Commercial ZnO and (b) As-Synthesized ZnO PVP-12.5 Micro/Nanoflowers.

4.3 Synthesis Parameter Study

4.3.1 Effect of PVP Concentration

Figure 4.12 presents the effect of various PVP concentrations used in the synthesis of ZnO micro/nanoflowers on the degradation of MO and MG mixtures. The MO and MG dye mixtures was evaluated using ZnO micro/nanoflowers synthesized with or without PVP. From the figure, it was obvious that the degradation efficiency improved as the concentration of PVP used to synthesize ZnO micro/nanoflowers increased. Both MO and MG had maximal degradation efficiency of 82.63 % and 95.42 % respectively using ZnO 12.5-PVP micro/nanoflowers.

The influence of PVP concentration on the photocatalytic activity could be described by several factors including the size, crystallinity and amount of functional
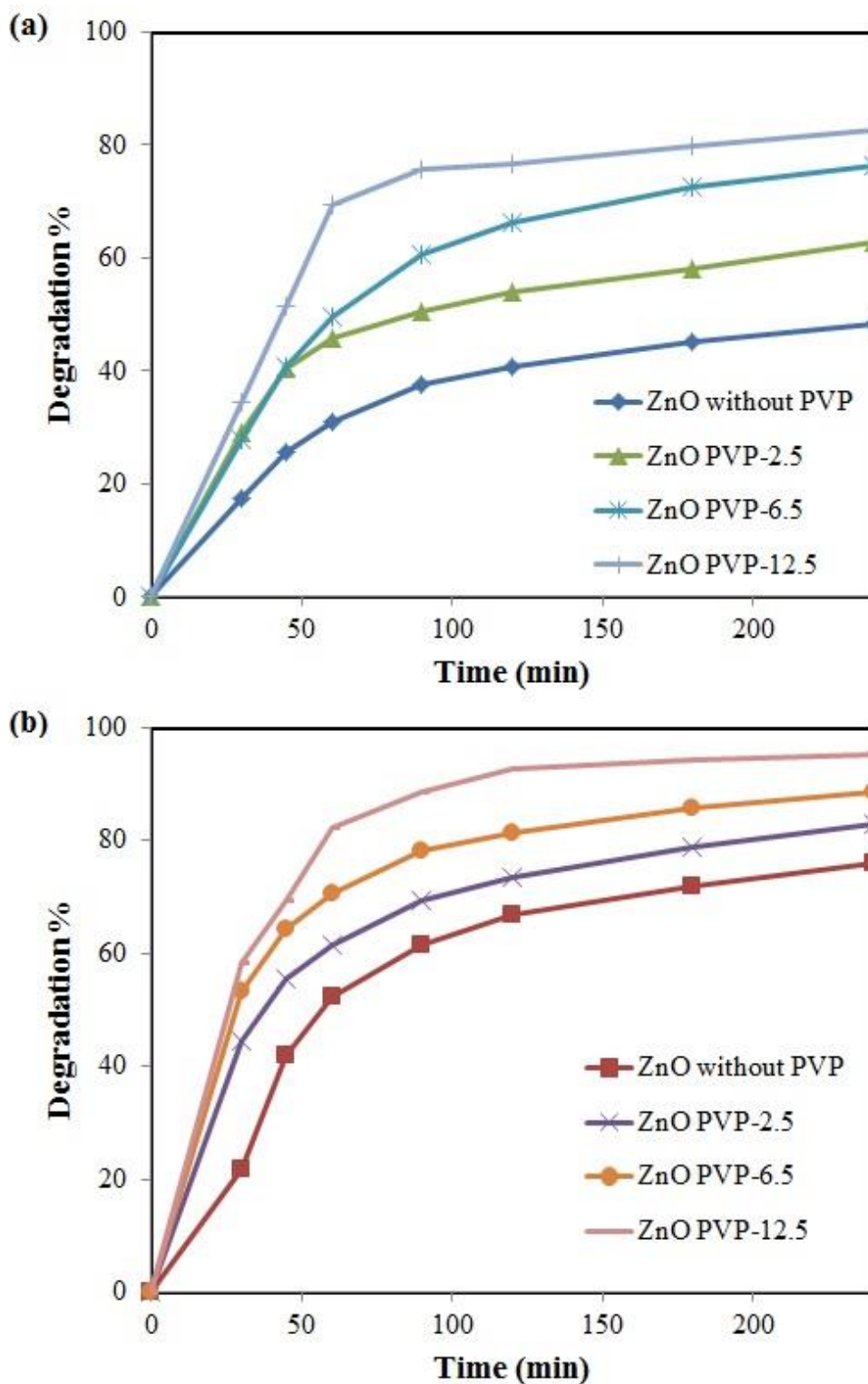
Figure 4.12: Effect of Various PVP Concentrations in the Synthesis of ZnO on the Degradation of MO (a) and MG (b) Mixtures. ([MO] = 5 mg/L; [MG] = 10 mg/L; ZnO loading = 1 g/L; solution pH = 6.5).

group available on the surface of the as-synthesized ZnO. As discussed in FESEM results, increasing PVP concentration would result in the smaller size of ZnO. This would increase the surface area of ZnO for favorable adsorption of MO and MG dyes on the surface of photocatalyst. In addition, high crystallinity of ZnO promoted the e^- $- h^+$ separation, enabling ample generation of reactive species to partake in the photocatalytic degradation system, which was in accordance to the results obtained in XRD analysis. Furthermore, as stated in FTIR results, the photocatalytic activity of ZnO micro/nanoflowers was also conceivably attributed to its huge amount of hydroxyl group present on the surface of ZnO as this improved the availability of •OH ready for the photocatalytic system. Lower radiative recombination of $e^- - h^+$ pairs was acquired with the increasing PVP concentration, producing huge amount of $e^- - h^+$ to participate the photocatalytic reaction, which was in agreement to the PL results. The results obtained were in accordance to research conducted by Naseri, Saion and Zadeh (2013). Naseri, Saion and Zadeh (2013) reported that the addition of PVP improved the crystallinity of nickel ferrite nanoparticles, leading to a high photocatalytic activity. Hence, ZnO PVP-12.5 micro/nanoflowers was chosen as the optimum photocatalyst for the photocatalysis study.

4.4   Process Parameter Studies

4.4.1   Effect of Initial Dye Concentration

The initial dye concentration plays an important role in affecting the degradation efficiency of photocatalytic reaction. The MO and MG dyes degradation was investigated in the concentration range of 2.5 to 10 mg/L for MO and 5.0 to 20.0 mg/L for MG, while the other parameters was kept constant. As illustrated in Figure 4.13, it was clear that the highest degradation efficiency was at 2.5 mg/L of MO and 5.0 mg/L of MG, which was 93.83 % for MO and 100 % for MG among four different varied concentrations for each dye.
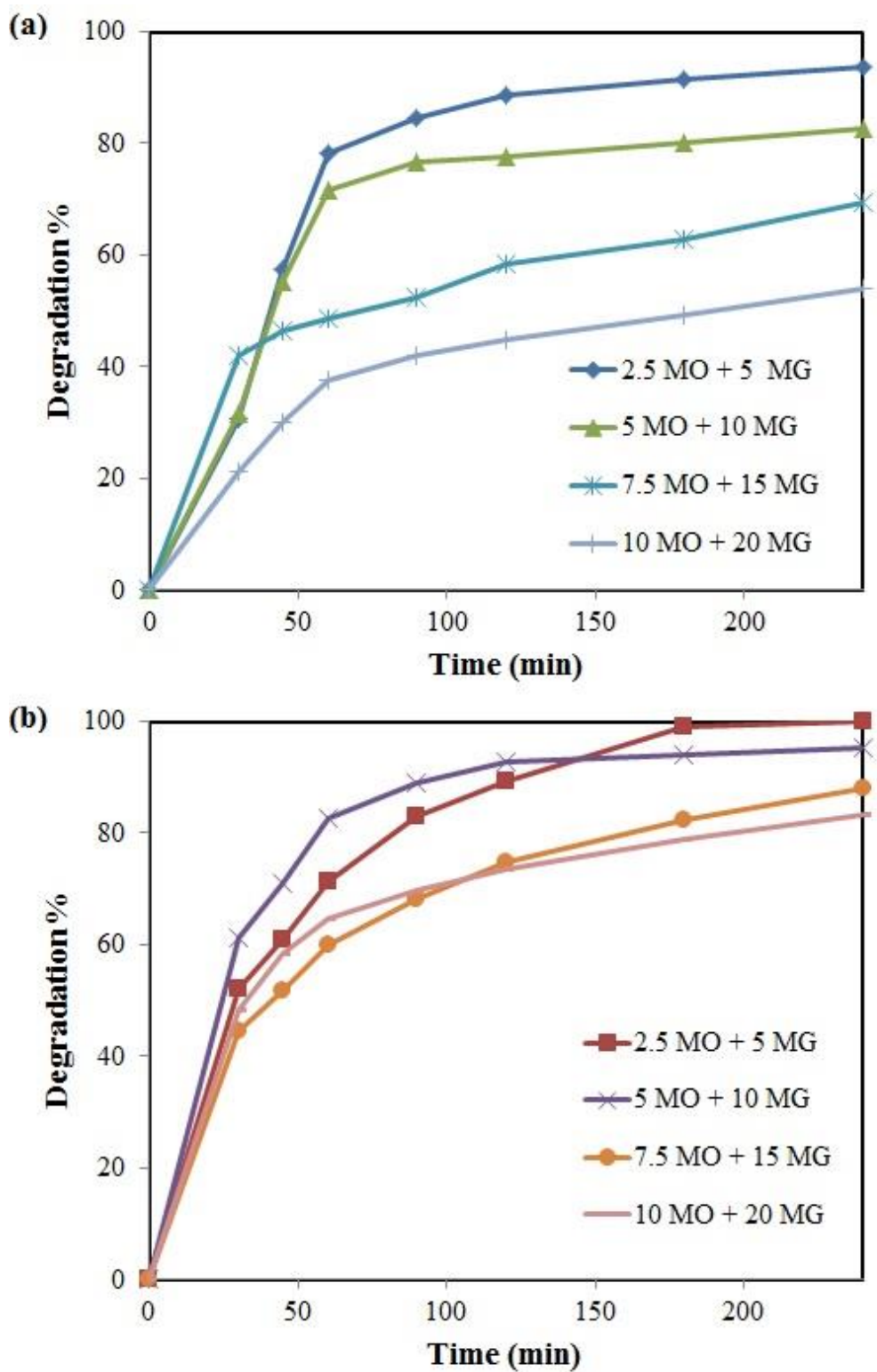
Figure 4.13: Effect of Initial Dye Concentration on the ZnO PVP-12.5 Photocatalytic Degradation of MO (a) and MG (b) in their Mixtures (ZnO loading = 1 g/L; Solution pH = 6.5).

The results suggested that the simultaneous degradation efficiency decreased with the increasing of the initial dye concentration of the two dyes in solution. This could be due to the increased consumption rate of •OH in the increasing initial dye concentration; however, the formation of hydroxyl radicals remained constant as the ZnO photocatalyst loading was kept constant, leading to low degradation efficiency (Admat, Qadri and Uddin, 2011; Saggioro et al., 2011). Some authors reported that the declination of photocatalytic degradation efficiency was attributed to lesser penetration of UV-vis light into the solution and reduction of light reaching the surface of ZnO photocatalyst (Saggioro et al, 2011; Chamjangali et al, 2015; Bandekar et al., 2014; Ram, Pareek and Singh, 2012). The increase in initial dye concentration reduced the number of photons or path length of photon, hindering the photon adsorption on the surface of ZnO. Low photons adsorption could lead to the promotion of the $e^- - h^+$ recombination, thereby inhibited the generation of •OH radicals, for the photocatalytic reaction (Gnanaprakasam, Sivakumar and Thirumarimurugan, 2015). Furthermore, the escalation of initial dye concentration also enhanced the concentration of intermediates. This was because huge amount of intermediates can be generated when the •OH destructed the dye molecules at high concentration. Consequently, competition between these intermediates with the parent molecules for the limited active sites on the photocatalyst surface can occur (Ahmed et al, 2010; Lam et al, 2012).

Similar results have been reported in researches conducted by several authors. Chamjangali et al. (2015) noted that the degradation efficiency of MO and MG was highest at 2.5 mg/L of MO and 5 mg/L of MB within 60 minutes of irradiation. It was also proven by Zyoud et al. (2015) that the degradation efficiency of MO decreased from 100 % to 45 % in the initial dye concentration range of 10 mg/L to 40 mg/L. In addition, Zhou et al. (2017) examined the effect of various initial dye concentrations in the range of 1 mg/L to 20 mg/L using ZnO nanowires under UV irradiation. The photocatalytic degradation of MO declined from 94.9 % to 46.0 % when the initial dye concentration increased from 1 mg/L to 20 mg/L. Thus, 2.5 mg/L of MO and 5 mg/L of MG was chosen as the optimum initial dye concentration for the simultaneous degradation of MO and MG.

4.4.2 Effect of Solution pH

Dye-containing wastewaters manifest huge variety of pH according to their source and the type of dye used (He et al., 2012). Thus, it is important to study the effect of pH on the photodegradation efficiency. The effect of solution pH on the degradation of binary mixture of MO and MG using ZnO photocatalyst was examined by varying the solution pH from pH 3 to pH 10, while all other parameters remained constant. Four different solutions pH were adjusted by the addition of dilute 1.0 M HNO_3 or 1.0 M NaOH. The natural pH for MG and MO mixtures was measured to be 6.5. Figure 4.14 depicts the effect of solution pH on the photocatalytic degradation of mixture of MO and MG. From the result obtained, it was evident that the degradation efficiency was highest at pH 6.5, with 93.83 % of MO and 100 % of MG degradation. The efficiency descended in an order of pH 6.5, pH 7.5, pH 3 and pH 10.

It can be deduced that the maximal degradation efficiency was reached under slightly neutral condition, rather than in acidic or alkaline conditions. This could be well associated to the surface charge of the photocatalyst and well described by the concept of point of zero charge (pzc). The pzc is defined as uncharged photocatalyst surface under certain pH (Nekouei et al., 2016). As the pH above or below this value, the surface of photocatalyst is either negatively or positively charged. The pH of pzc (pH_{pzc}) for ZnO is pH 9 (Lam et al., 2012). ZnO surface is positively charged under acidic condition and predominantly negatively charged under alkaline condition. Anionic MO was predominantly adsorbed to the ZnO surface under acidic condition whereas cationic MG is principally adsorbed to the ZnO surface under alkaline condition. At acidic pH 3, the positively charged ZnO surface favoured the adsorption of MO and hindered the adsorption of MG. Nonetheless, Tiwari et al. (2015) and Shanthi and Kuzhalosai (2012) stated that the scavenging of •OH by H^+ was dominant as a result of the presence of substantial amount of these molecules in acidic condition. It can be interpreted that the photocatalytic degradation efficiency dropped at pH 3.
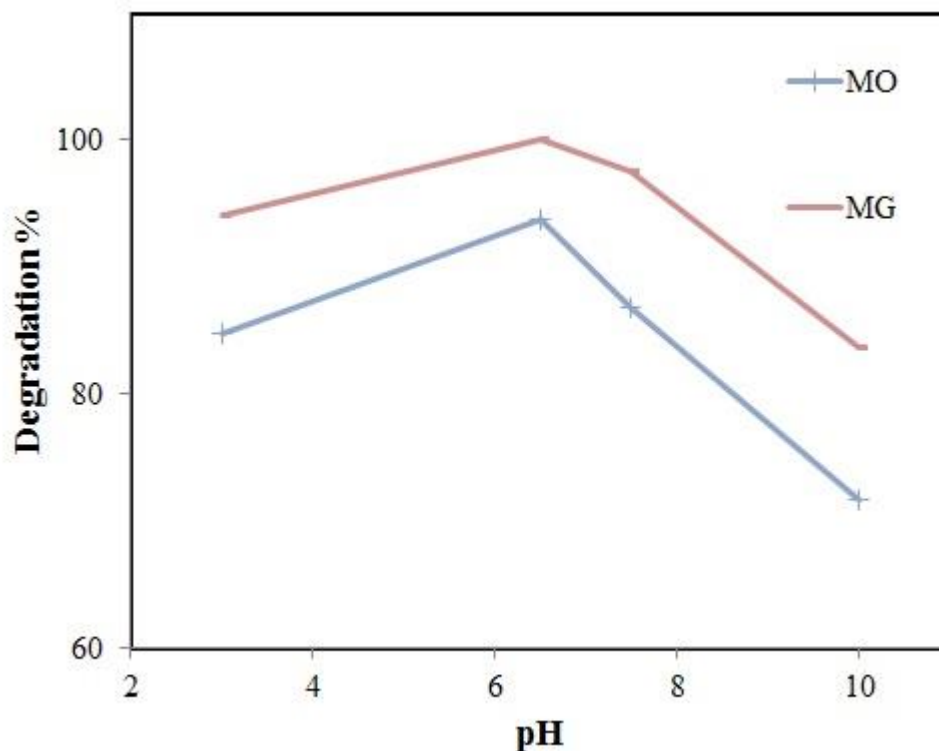
Figure 4.14: Effect of Various Solution pH on the Degradation of Binary Mixtures of MO and MG Dyes ([MO] = 2.5 mg/L; [MG] = 5 mg/L; ZnO Loading = 1 g/L).

On the other hand, significant photocatalytic degradation of MO and MG was proved to be at pH 6.5 and pH 7.5. The surface charge of ZnO was positively charged at pH lower than pH_{pzc}, encouraging the adsorption of MO onto the surface of ZnO. Nevertheless, the scavenging of •OH by H^+ was less significant as no pH adjustment was performed, signifying that no H^+ was added into the solution mixture. Additionally, a slightly alkaline medium promoted the generation of •OH as more OH^- were present in binary solution. On the contrary, at pH 10, the degradation efficiency declined the most as the pH higher than pH_{pzc}, producing negatively-charged ZnO surface. This could be well explained by the presence of Na^+ ions from NaOH can compete with dyes for the active site on ZnO surface. Moreover, the increase in pH escalated the OH^- concentration. Abundant amount of OH^- competed with dyes for the active sites on photocatalyst. The electrostatic repulsion was occurred between the negatively charged ZnO surface, OH^- and anionic MO (Abdollahi et al., 2011).

The findings from present study were also in agreement with other researchers. Hayat et al. (2010) and Tiwari et al. (2015) demonstrated that the degradation efficiency of alizarin yellow dye was maximal at 80 % and 90 % at pH near neutral pH, respectively. It was also confirmed by Chamjangali et al. (2015) that the highest degradation efficiency was occurred at pH 6.5. Furthermore, according to Hassan et al. (2015), it was proven that the photocatalytic degradation of MO was greatest at pH 7 within 240 minutes of irradiation. Zyoud et al. (2015) showed that the highest degradation efficiency of MO occurred at pH 5 and 7. Therefore, pH 6.5 was chosen as the optimum solution pH for the simultaneous degradation of MO and MG.

4.5 Mineralization Study of MO and MG Mixtures

It is important that not only degradation of dyes being achieved in the treatment of organic pollutants present in wastewater, but also the mineralization of the dye molecules. Figure 4.15 illustrates the variation of MO, MG and COD efficiency at various intervals in the presence of ZnO micro/nanoflowers. The results indicated that photocatalytic degradation of MG and MO was complete (100 %) and almost complete (92.92 %), respectively within 240 minutes of illumination whereas the maximal COD reduction observed after 240 minutes of irradiation was 94.14 %. The destruction of recalcitrant organic compounds from the mixtures of MO and MG and their intermediates resulted in the mineralization of MO and MG. Nevertheless, traces of COD were still remained after the treatment period, representing that the degradation can improve the aesthetic quality of water, rather than the total purification and detoxification of water. Therefore, prolonged irradiation time would be reasonable for complete mineralization.

Divya, Bansal and Jana (2013) suggested that the generation of •OH enabled the redox reaction of the azo bonds that held the colour of the dye. This promoted the cleavages of these bonds, thereby encourage the degradation of MO and MG. MO and MG might be attacked by active species, followed by oxidation of intermediates
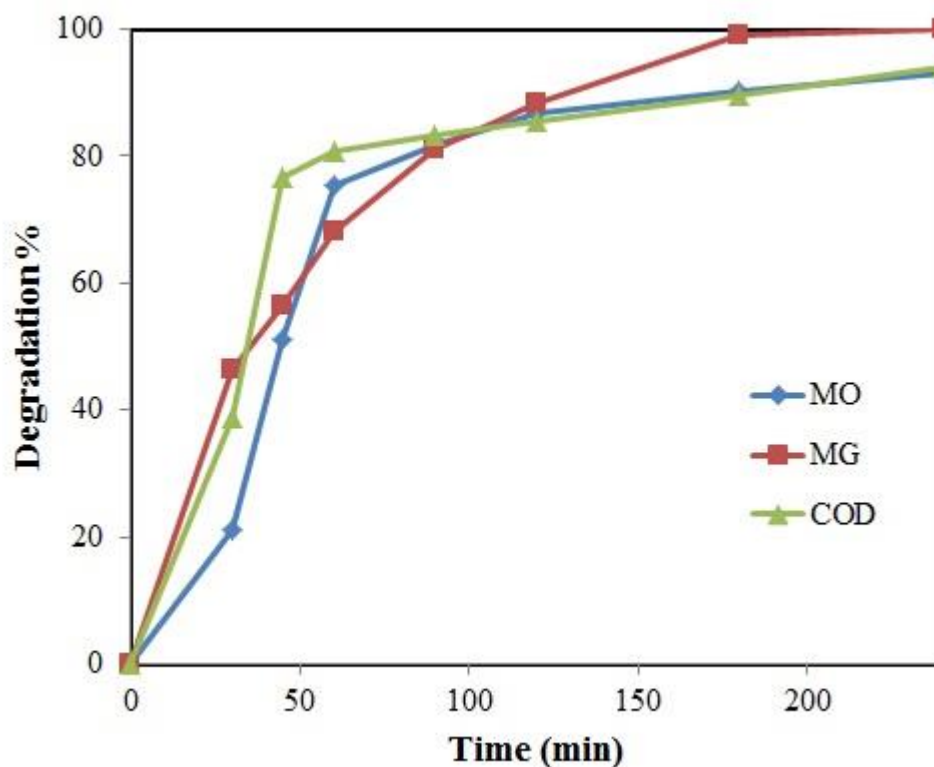
Figure 4.15: Variation of MO, MG and COD Efficiency at Various Intervals in the Presence of ZnO PVP-12.5 Micro/Nanoflowers ([MO] = 2.5 mg/L; [MG] = 5 mg/L; ZnO loading = 1 g/L; Solution pH = 6.5).

by the oxidants available in the photocatalytic system. It was suggested by Reddy, Sk and Ch (2014) that the azo group might be converted to amines, followed by organic acids and finally CO_2. Zyoud et al. (2015) reported that the azo group of MO was degraded to nitrogen gas as the adsorption spectrum in the range of 400 – 500 nm which responsible for the azo group had disappeared. More stable intermediates could be formed and eventually transformed into the harmless end-products (CO_2 and H_2O) when the azo groups were destroyed. According to Mai et al. (2008), it was indicated that 32 identified colourless intermediates of MG were formed within 12 hours of visible light irradiation.

Similar results have been obtained in other several studies experimented by Saikia et al. (2015), Kamani et al. (2015), Vignesh, Rajarajan and Suganthi (2014), Soltani et al. (2015) and Zhang et al. (2013). Saikia et al. reported that 100 % Malachite Green was degraded while achieving 90.8 % of COD removal within 100

minutes of UV light irradiation. Kamani et al. (2015) achieved 96 % of Sulphur Red while 90 % of COD was removed after 50 minutes of illumination. It was confirmed by Vignesh, Rajarajan and Suganthi (2014) that 93 % of MB degradation was obtained after 180 minutes of visible light irradiation. Consistent with Soltani et al. (2015), it was demonstrated that the COD efficiency was 81 %, whereas 100 % of MB was degraded. Additionally, Zhang et al. (2013) indicated that the COD removal was only 73.47 % when the 98 % of degradation was acquired within 8 hours of UV light irradiation.

4.6   Photocatalytic Degradation of Real Textile Dye Wastewater

4.6.1   Characterization of Raw Real Textile Dye Wastewater

Textile dyes mixture in reality contains not only dyes, but also pesticides, residual dyestuffs, metals (copper, chromium, lead, cobalt, nickel and cadmium), dye intermediates, huge numbers of organic compounds and unreacted raw materials such as inorganic sodium salts and aromatic amines (Kotelevtsev, Tonkopii & Hänninen, 2009; Lam *et al.*, 2012).Thus the textile dye wastewater must be characterized to understand well the composition of textile industry wastewater. Table 4.1 presents the characterization of the raw real textile dye wastewater. As shown in the table, it demonstrated a high COD, BOD_5, turbidity, colour, TSS, AN and pH. The concentration of COD, BOD_5, turbidity, colour, TSS, AN were 2515 mg/L, 340.5 mg/L, 136 NTU, 884 Pt-Co, 920 mg/L and 5.35 mg/L while the pH was 11.7.

Table 4.1: A Summary of Photocatalytic Degradation of Real Textile Wastewater using ZnO PVP-12.5.

Parameter	Pre-treatment	Post-treatment	Efficiency (%)
COD(mg/L)	2515	630	75
BOD_5 (mg/L)	340.5	82	76
BOD/COD	0.14	-	-
Turbidity (NTU)	136	26.2	81
Colour (Pt-Co)	884	220	75
TSS (mg/L)	920	210	77
AN (mg/L)	5.35	2.8	48
pH	11.7	6-7	-

High COD level confirmed the presence of a significant amount of organic matter resulting from the chemicals used in the textile dyeing process such as detergents, softeners, oxidants acids and bases, whereas high TSS level could be ascribed to the presence of suspended solid material in the wastewater (Souza et al., 2016). Furthermore, trace metals including chromium, arsenic and copper that contained in the textile wastewater contributed to the highly visible coloured textile wastewater. BOD_5/COD ratio, which is known as biodegradable index is a measure of the biodegradability of the wastewater. If the ratio is less than 0.3, the waste is hardly treated biologically and contains toxic material (Lee and Nikraz, 2014). In this study, the low BOD_5/COD ratio of 0.14 showed that the real textile dye wastewater was non-biodegradable and contained some toxic and recalcitrant compounds. Hence the photocatalysis could be applied to completely mineralize the pollutants found in real textile dye wastewater.

4.6.2   Monitoring of Real Textile Dye Wastewater

An adequate mineralization of real textile dye wastewater to carbon dioxide, water and mineral ions must be attained through photocatalysis to emerge as an applicable alternative for real textile dye wastewater treatment. Table 4.1 indicates the characteristic of real textile wastewater after the treatment of photocatalysis. As demonstrated, a substantial COD reduction of 75% was achieved using as-prepared ZnO micro/nanoflowers after 240 minutes of irradiation. Nonetheless, it was still lower than the attained efficiency with the synthetic dye mixtures as recorded in Figure 4.15. This could be due to the presence of some impurities including dissolved organic substances and chloride ions which retard the efficiency of the photocatalytic performance and the incapability of UV-vis light to penetrate into the solution. On the other hand, a considerable BOD reduction of 76 % was accomplished while a maximal turbidity removal of 81 % was achieved. The colour was significantly reduced by 75 % after 240 minutes of illumination. The reduction efficiency of TSS and AN was 77 % and 48 %, respectively. Lastly, the solution pH of the treated real textile wastewater also changed from 11.7 to 6.5, implying that real textile wastewater had changed from alkaline condition to neutral condition.

The results obtained were in accordance to the researches experimented by Souza et al. (2016), Mahdizadeh and Aber, 2015, Jorfi et al. (2016) and Saravanan et al. (2013). Souza et al. (2016) reduced the COD of the textile wastewater by 50 % using ZnO calcined at 500 °C after 300 minutes of irradiation, while Mahdizadeh and Aber (2015) yielded a greatest reduction efficiency of 72 % using CuO/ZnO nanoparticles immobolized on scoria rocks. According to Jorfi et al. (2016), the 98.3 % of COD removal was achieved through the sequence coagulation-UVA/MgO nanoparticles photocatalytic degradation after 300 minutes of illumination. In addition, Saravanan et al. (2013) stated that the reduction of COD of textile wastewater was more than 90 % using ZnO/CuO composite under 300 minutes of irradiation.

CHAPTER 5

CONCLUSION AND RECOMMENDATIONS

5.1 Conclusion

In the present study, 3-D ZnO micro/nanoflowers with enhanced photocatalytic activities were successfully fabricated by a PVP-assisted co-precipitation method for simultaneous degradation of MO and MG and real textile dye wastewater under UV-vis light irradiation. The as-prepared ZnO were characterized by XRD, FESEM, EDX, FTIR and PL analyses. The XRD analysis evidenced that the as-synthesized ZnO PVP-12.5 micro/nanoflowers was of the hexagonal wurzite phase with high crystallinity and small size. FESEM images revealed the surface morphology of the ZnO micro/nanoflowers and it was observed to be micro/nanoflower structure with regular shape and size with an average diameters ranging from 890 nm to 1.261 μm. The formation mechanism of the 3-D ZnO micro/nanoflowers was also suggested. Additionally, EDX analysis demonstrated that as-prepared ZnO PVP-12.5 micro/nanoflowers consisted of Zn and O elements with high purity. FTIR analysis discovered the presence of Zn-O bonding, proving the identity of as-synthesized ZnO micro/nanoflowers with the presence of –OH groups on the surface of as-synthesized ZnO micro/nanoflowers. PL analysis detected the low visible emission that resulted from the radiative recombination of a photogenerated hole and electron.

Subsequently, a comparison study was performed using commercial ZnO and as-synthesized ZnO micro/nanoflowers. It was found that the as-prepared ZnO micro/nanoflowers showed superior photocatalytic performance compared to commercial ZnO owing to the high crystallinity, 3D morphology and huge amount –

OH manifested by as-synthesized ZnO micro/nanoflowers. The photo-degradation efficiency of MO and MG using commercial ZnO was 80.95 % and 98.01 %, whereas for as-synthesized ZnO micro/nanoflowers, it was 82.75 % and 99.50 %, respectively. Sedimentation test was conducted and as-synthesized ZnO micro/nanoflowers settled quicker than commercial ZnO due to higher density of as-synthesized ZnO micro/nanoflowers, allowing easier recovery from aqueous suspension for their recyclablities in the wastewater treatment application.

Moreover, the effect of synthesis parameter including PVP concentration was investigated. The findings proved that ZnO PVP-12.5 micro/nanoflowers achieved the highest photo-degradation efficiency of 82.63 % and 95.42 % for MO and MG after 240 minutes of irradiation, respectively. The photocatalytic activity was enhanced by the small size, high crystallinity and high amount of –OH groups of the as-prepared ZnO micro/nanoflowers.

The effect of process parameters including initial dye concentration and solution pH were also studied. The outcomes verified that the maximal photocatalytic degradation efficiency was at the initial dye concentration of 2.5 mg/L of MO and 5 mg/L of MG, and solution pH of 6.5. Under these optimized conditions, the degradation efficiency was 93.83 % for MO and 100 % for MG after 240 minutes of irradiation, correspondingly. Mineralization study of MO and MG mixtures were evaluated in terms of COD degradation. The COD degradation efficiency achieved 94.14 % after 240 minutes of irradiation, indicating the destruction of recalcitrant organic compounds from MO and MG mixtures. Nonetheless, prolonged time would be required for mineralization than degradation to achieve complete mineralization.

Additionally, the degradation of real textile dye wastewater was evaluated by the ZnO photocatalysis. Significant COD degradation of 75 % was attained using ZnO micro/nanoflowers after 240 minutes of irradiation. Nevertheless, the efficiency was lower than that of synthetic dye mixtures owing to the presence of photocatalytic retardants such as dissolved organic substances and chloride ions and the incapability for the UV-vis light penetration to the solution. The other parameters were reduced considerably after the photocatalysis of real textile dye wastewater. As a conclusion,

this postulated a promising avenue for simultaneous photocatalytic degradation of dye mixtures and real textile dye wastewater by 3-D ZnO micro/nanoflowers.

5.2   Recommendations

Upon completion of the present study, the following fundamentals and engineering aspects were to be taken into considerations in the future research works.

i.   The effects of other process parameters that were not studied in this study such as photocatalyst loading, light intensity, presence of oxidizing agents, irradiation time and air flow rate could be investigated in the future studies to further improve the photocatalytic degradation efficiency.

ii. The photocatalytic performance of the as-prepared photocatalyst is suggested to evaluate under the solar light irradiation as it is cheap, clean and abundant, making it as an economically and ecologically light source.

iii. HPLC and GC could be utilized to further identify the intermediates and monitor the reaction details during the photocatalytic degradation in order to understand the photocatalytic degradation mechanism.

iv. Toxicity analysis of the ZnO photocatalyst should be conducted to understand its effect on the human health and environment especially water bodies.

REFERENCES

Abdollahi, Y., Abdullah, A.H., Zainal, Z. and Yusof, N.A., 2011. Photocatalytic degradation of p-Cresol by zinc oxide under UV irradiation. *International Journal of Molecular Sciences*, 13, pp. 302-315.

Acros Organics, 2008. Material Safety Data Sheet: Methyl Orange. [online] Available at: https://www.ch.ntu.edu.tw/~genchem99/msds/exp8/methyl%20orange.pdf [Accessed 28 Mar. 2017].

Ahmed, S., Rasul, M.G., Martens, W.N., Brown, R., and Hashib, M.A., 2011. Advances in heterogeneous photocatalytic degradation of phenols and dyes in wastewater: a review. *Water, Air, & Soil Pollution*, 215, pp.3-29.

Altavilla, C. and Ciliberto, E. eds., 2010. *Inorganic nanoparticles: synthesis, applications, and perspectives*. CRC Press.

Amin, G., 2012. ZnO and CuO nanostructures: low temperature growth, characterization, their optoelectronic and sensing applications.

Anandan, S., Kumar, P.S., Pugazhenthiran, N., Madhavan, J. and Maruthamuthu, P., 2008. Effect of loaded silver nanoparticles on TiO_2 for photocatalytic degradation of Acid Red 88. *Solar Energy Materials and Solar Cells*, 92, pp. 929-937.

Ansari, F., Bazarganipour, M. and Salavati-Niasari, M., 2016. $NiTiO_3$/$NiFe_2O_4$ nanocomposites: Simple sol–gel auto-combustion synthesis and characterization by utilizing onion extract as a novel fuel and green capping agent. *Materials Science in Semiconductor Processing*, 43, pp. 34-40.

An, X., Gao, C., Liao, J., Wu, X. and Xie, X., 2015. Synthesis of mesoporous N-doped TiO_2/ZnAl-layered double oxides nanocomposite for efficient photodegradation of methyl orange. *Materials Science in Semiconductor Processing*, 34, pp. 162-169.

APHA, 2005. Standard Methods for the Examination of Water and Wastewater, 6th edition. American Public Health Association, Washington DC, USA, p. 2005.

Azmat, R., Qadri, M. and Uddin, F., 2011. Spectrokinetics study of probable effects of diverse inorganic ions on bleaching of dye. *Frontiers of Chemical Science and Engineering*, 5, pp. 131-138.

Bandekar, G., Rajurkar, N.S., Mulla, I.S., Mulik, U.P., Amalnerkar, D.P. and Adhyapak, P.V., 2014. Synthesis, characterization and photocatalytic activity of PVP stabilized ZnO and modified ZnO nanostructures. *Applied Nanoscience*, 4, pp. 199-208.

Bargougui, R., Oueslati, A., Schmerber, G., Ulhaq-Bouillet, C., Colis, S., Hlel, F., Ammar, S. and Dinia, A., 2014. Structural, optical and electrical properties of Zn-doped SnO_2 nanoparticles synthesized by the co-precipitation technique. *Journal of Materials Science: Materials in Electronics*, 25, pp. 2066-2071.

Barrat, C.F., 2012. Analytical methodologies based on chemometrics to optimize the photodegradation of dyes: doctoral thesis (Doctoral dissertation, Universitat Rovirai Virgili).

Barron, A.R., 2012. Physical methods in chemistry and nano science. *Houston, Texas: Connexions, Rice University*, pp. 535-619.

Bao, Y., Wang, C. and Ma, J.Z., 2016. A two-step hydrothermal route for synthesis hollow urchin-like ZnO microspheres. *Ceramics International*, 42, pp. 10289-10296.

Bedi, P.S. and Kaur, A., 2015. An overview on uses of zinc oxide nanoparticles. *World Journal of Pharmacy and Pharmaceutical Sciences*, 4, pp. 1177-1196.

Behnajady, M.A., Moghaddam, S.G., Modirshahla, N. and Shokri, M., 2009. Investigation of the effect of heat attachment method parameters at photocatalytic activity of immobilized ZnO nanoparticles on glass plate.*Desalination*, 249, pp. 1371-1376.

Behzadnia, A., Montazer, M. and Rad, M.M., 2015. In situ photo sonosynthesis and characterize nonmetal/metal dual doped honeycomb-like ZnO nanocomposites on wool fabric. *Ultrasonics sonochemistry*, 27, pp. 200-209.

Bel Hadjltaief, H., Omri, A., Ben Zina, M., Da Costa, P. and Galvez, M.E., 2015. Titanium dioxide supported on different porous materials as photocatalyst for the degradation of methyl green in wastewaters. *Advances in Materials Science and Engineering*, 2015, pp. 1-10.

Benhebal, H., Chaib, M., Salmon, T., Geens, J., Léonard, A., Lambert, S.D., Crine, M. and Heinrichs, B., 2013. Photocatalytic degradation of phenol and benzoic acid using zinc oxide powders prepared by the sol–gel process. *Alexandria Engineering Journal*, 52, pp. 517-523.

Bousnoubra, I., Djebbar, K., Abdessemed, A. and Sehili, T., 2016. Decolorization of methyl green and bromocresol purple in mono and binary systems by photochemical processes: direct UV photolysis, Acetone/UV and H_2O_2/UV. A comparative study. *Desalination and Water Treatment*, 57, pp. 27710-27725.

Cai, X., Hu, D., Deng, S., Han, B., Wang, Y., Wu, J. and Wang, Y., 2014. Isopropanol sensing properties of coral-like ZnO–CdO composites by flash

preparation via self-sustained decomposition of metal–organic complexes. *Sensors and Actuators B: Chemical*, 198, pp. 402-410.

Carmen, Z. and Daniela, S., 2012. Textile organic dyes–characteristics, polluting effects and separation/elimination procedures from industrial effluents–a critical overview. In *Organic Pollutants Ten Years After the Stockholm Convention-Environmental and Analytical Update*, pp. 55-81. InTech: Croatia.

Chamjangali, M.A. and Boroumand, S., 2013. Synthesis of flower-like Ag-ZnO nanostructure and its application in the photodegradation of methyl orange. *Journal of the Brazilian Chemical Society*, 24, pp.1329-1338.

Chamjangali, M.A., Bagherian, G., Javid, A., Boroumand, S. and Farzaneh, N., 2015. Synthesis of Ag–ZnO with multiple rods (multipods) morphology and its application in the simultaneous photo-catalytic degradation of methyl orange and methylene blue. *Spectrochimica Acta Part A: Molecular and Biomolecular Spectroscopy*, 150, pp. 230-237.

Chaturvedi, S., Dave, P.N. and Shah, N.K., 2012. Applications of nano-catalyst in new era. *Journal of Saudi Chemical Society*, 16, pp. 307-325.

Chen, C.C. and Lu, C.S., 2007. Mechanistic studies of the photocatalytic degradation of methyl green: an investigation of products of the decomposition processes. *Environmental science & technology*, 41, pp. 4389-4396.

Chen, C., Cao, S., Yu, W., Xie, X., Liu, Q., Tsang, Y. and Xiao, Y., 2015. Adsorption, photocatalytic and sunlight-driven antibacterial activity of Bi_2WO_6/graphene oxide nanoflakes. *Vacuum*, 116, pp. 48-53.

Chequer, F.M.D., de Oliveira, D.P., Ferraz, E.R.A., de Oliveira, G.A.R., Cardoso, J.C. and Zanoni, M.V.B., 2013. Textile dyes: dyeing process and environmental impact, pp. 151-176. INTECH Open Access Publisher.

Chiou, C.H., Wu, C.Y. and Juang, R.S., 2008. Influence of operating parameters on photocatalytic degradation of phenol in UV/TiO_2 process.*Chemical Engineering Journal*, 139, pp. 322-329.

Coleman, V.A. and Jagadish, C., 2006. Basic properties and applications of ZnO. *Zinc Oxide Bulk, Thin Films and Nanostructures: Processing, Properties, and Applications*, pp. 1-20.

Daneshvar, N., Rasoulifard, M.H., Khataee, A.R. and Hosseinzadeh, F., 2007. Removal of CI Acid Orange 7 from aqueous solution by UV irradiation in the presence of ZnO nanopowder. *Journal of Hazardous Materials*, 143, pp. 95-101.

Daneshvar, N., Salari, D. and Khataee, A.R., 2003. Photocatalytic degradation of azo dye acid red 14 in water on ZnO as an alternative catalyst to TiO_2. *Journal of Photochemistry and Photobiology A: Chemistry*, 157, pp. 111-116.

Das, R., 2014. Application Photocatalysis for Treatment of Industrial Waste Water— A Short Review. *Open Access Library Journal*, 1, pp. 1-10.

Dave, R.S. and Patel, A.R., 2010. Photochemical and photocatalytic studies of Cypermethrin under UV irradiation. *Der pharma chemica*, 2, pp. 152-158.

Dawood, S. and Sen, T.K., 2013. Review on dye removal from its aqueous solution into alternative cost effective and non-conventional adsorbents.*Journal of Chemical and Process Engineering*, 1, pp. 1-19.

Department of Environment, 2010. Environmental Requirements: A Guide For Investors. 11th ed. [online] Available at: http://www.doe.gov.my/eia/wp-content/uploads/2012/03/A-Guide-For-Investors1.pdf [Accessed 28 Mar. 2017].

Di Paola, A., García-López, E., Marcì, G. and Palmisano, L., 2012. A survey of photocatalytic materials for environmental remediation. *Journal of hazardous materials*, 211, pp. 3-29.

Divya, N., Bansal, A. and Jana, A., 2013. Photocatalytic degradation of azo orange II in aqueous solutions using copper-impregnated titania. *International Journal of Environmental Science and Technology*, 10, pp. 1265-1274.

DOE, 2014. Malaysia Environmental Quality Report 2014. Department of Environment, Ministry of Natural Resources and Environment Malaysia, Kuala Lumpur, pp. 156-164.

Faisal, M., Tariq, M.A. and Muneer, M., 2007. Photocatalysed degradation of two selected dyes in UV-irradiated aqueous suspensions of titania. *Dyes and Pigments*, 72, pp. 233-239.

Feyzi, M., Hassankhani, A. and Rafiee, H.R., 2013. Preparation and characterization of Cs/Al/Fe_3O_4 nanocatalysts for biodiesel production. *Energy Conversion and Management*, 71, pp. 62-68.

Fox, M.A. and Dulay, M.T., 1993. Heterogeneous photocatalysis. *Chemical reviews*, 93, pp.341-357.

Geethakrishnan, T. and Palanisamy, P., 2006. Degenerate four-wave mixing experiments in methyl green dye-doped gelatin film. *Optik – International Journal for Light and Electron Optics*, 117, pp. 282-286.

Ghowsi, K., Ebrahimi, H.R., Kazemipour-Baravati, F. and Bagheri, H., 2014. Synthesize of ZnO/NPs and investigation of its effect in reduction of electrochemical charge transfer resistance; application of it for photodecomposition of calcon (CI 15705) dye in various media. *International Journal of Electrochemical Science*, 9, pp.1738-11746.

Gnanaprakasam, A., Sivakumar, V.M. and Thirumarimurugan, M., 2015. Influencing Parameters in the Photocatalytic Degradation of Organic Effluent via Nanometal Oxide Catalyst: A Review. *Indian Journal of Materials Science*, *2015*, pp. 1-16.

Goi, A., 2005. Advanced oxidation processes for water purification and soil remediation. Tallinn University of Technology Press.

Guo, X., Zhao, Q., Li, R., Pan, H., Guo, X., Yin, A. and Dai, W., 2010. Synthesis of ZnO nanoflowers and their wettabilities and photocatalytic properties. *Optics express*, 18, pp.18401-18406.

Gupta, A., Saurav, J.R. and Bhattacharya, 2015. Solar light based degradation of organic pollutants using ZnO nanobrushes for water filtration. *Royal Society of Chemistry*, 5, pp. 71472-71481.

Gupta, V.K., Jain, R., Mittal, A., Saleh, T.A., Nayak, A., Agarwal, S. and Sikarwar, S., 2012. Photo-catalytic degradation of toxic dye amaranth on TiO_2/UV in aqueous suspensions. *Materials Science and Engineering: C*, 32, pp. 12-17.

Gupta, V.K., Khamparia, S., Tyagi, I., Jaspal, D. and Malviya, A., 2015. Decolorization of mixture of dyes: A critical review. *Global Journal of Environmental Science and Management*, 1, pp. 71-94.

Gupta, V.K., Pathania, D., Singh, P., Rathore, B.S., 2014. Development of guar gum based cerium tungstate nanocomposite material for remediation of basic dye from water. Carbohydrate Polymers, 101, pp. 684-691.

Gutul, T., Rusu, E., Condur, N., Ursaki, V., Goncearenco, E. and Vlazan, P., 2014. Preparation of poly (N-vinylpyrrolidone)-stabilized ZnO colloid nanoparticles. *Beilstein journal of nanotechnology*, 5, pp. 402-406.

Hach, 2014. Water Analysis Handbook, 10th ed. US: Hach Company, USA.

Hadjltaief, H.B., Zina, M.B., Galvez, M.E. and Da Costa, P., 2016. Photocatalytic degradation of methyl green dye in aqueous solution over natural clay-supported ZnO–TiO_2 catalysts. *Journal of Photochemistry and Photobiology A: Chemistry*, 315, pp. 25-33.

Haque, M.M. and Muneer, M., 2007. TiO_2-mediated photocatalytic degradation of a textile dye derivative, bromothymol blue, in aqueous suspensions. *Dyes and Pigments*, *75*(2), pp.443-448.

Hayat, K., Gondal, M.A., Khaled, M.M. and Ahmed, S., 2010. Kinetic study of laser-induced photocatalytic degradation of dye (alizarin yellow) from wastewater using nanostructured ZnO. *Journal of Environmental Science and Health Part A*, 45, pp. 1413-1420.

Hendrix, Y., Lazaro, A., Yu, Q. and Brouwers, J., 2015. Titania-Silica Composites: A Review on the Photocatalytic Activity and Synthesis Methods. *World Journal of Nano Science and Engineering*, 5, p.161-168.

Hernández, S., Hidalgo, D., Sacco, A., Chiodoni, A., Lamberti, A., Cauda, V., Tresso, E. and Saracco, G., 2015. Comparison of photocatalytic and transport properties

of TiO$_2$ and ZnO nanostructures for solar-driven water splitting. *Physical Chemistry Chemical Physics*, 17, pp.7775-7786.

He, Y., Gao, J.F., Feng, F.Q., Liu, C., Peng, Y.Z. and Wang, S.Y., 2012. The comparative study on the rapid decolorization of azo, anthraquinone and triphenylmethane dyes by zero-valent iron. *Chemical Engineering Journal*, 179, pp. 8-18.

Hu, A., Liang, R., Zhang, X., Kurdi, S., Luong, D., Huang, H., Peng, P., Marzbanrad, E., Oakes, K.D., Zhou, Y. and Servos, M.R., 2013. Enhanced photocatalytic degradation of dyes by TiO$_2$ nanobelts with hierarchical structures. *Journal of Photochemistry and Photobiology A: Chemistry*, 256, pp. 7-15.

Huang, M., Xu, C., Wu, Z., Huang, Y., Lin, J. and Wu, J., 2008. Photocatalytic discolorization of methyl orange solution by Pt modified TiO$_2$ loaded on natural zeolite. *Dyes and Pigments*, 77, pp. 327-334.

Hussein, F.H., 2013. Chemical properties of treated textile dyeing wastewater. *Asian Journal of Chemistry*, 25, p.9393-9400.

Hu, X.L., Zhu, Y.J. and Wang, S.W., 2004. Sonochemical and microwave-assisted synthesis of linked single-crystalline ZnO rods. *Materials Chemistry and physics*, 88, pp. 421-426.

Ibhadon, A.O. and Fitzpatrick, P., 2013. Heterogeneous photocatalysis: recent advances and applications. *Catalysts*, 3, pp. 189-218.

Jia, W., Dang, S., Liu, H., Zhang, Z., Yu, C., Liu, X. and Xu, B., 2012. Evidence of the formation mechanism of ZnO in aqueous solution. *Materials Letters*, 82, pp. 99-101.

Jorfi, S., Barzegar, G., Ahmadi, M., Soltani, R.D.C., Takdastan, A., Saeedi, R. and Abtahi, M., 2016. Enhanced coagulation-photocatalytic treatment of Acid red 73 dye and real textile wastewater using UVA/synthesized MgO nanoparticles. *Journal of environmental management*, 177, pp. 111-118.

Joseph, A.I.J. and Thiripuranthagan, S., 2015. Metal doped titanate photo catalysts for the mineralization of congo red under visible irradiation. *RSC Advances*, 5, pp. 9792-9805.

Joshi, S.S., 2012. *Crystal Habit Modification Using Habit Modifiers*. INTECH Open Access Publisher.

Kaan, C.C., Aziz, A.A., Matheswaran, M., Saravanan, P. and Ibrahim, S., 2012. Heterogeneous Photocatalytic Oxidation an Effective Tool for Wastewater Treatment-A Review. INTECH Open Access Publisher.

Kalsi, P.S., 2007. *Spectroscopy of organic compounds*. New Age International, India.

Kamari, H.M., Al-Hada, N.M., Saion, E., Shaari, A.H., Talib, Z.A., Flaifel, M.H. and Ahmed, A.A.A., 2017. Calcined Solution-Based PVP Influence on ZnO Semiconductor Nanoparticle Properties. *Crystals*, 7, pp. 2-15.

Karami, H., Bigdeli, Z. and Matini, S., 2016. Pulsed Galvanostatic Synthesis of Zinc Oxide Nanostructures. *INTERNATIONAL JOURNAL OF ELECTROCHEMICAL SCIENCE*, 11, pp. 3095-3113.

Khan, R., Hassan, M.S., Uthirakumar, P., Yun, J.H., Khil, M.S. and Lee, I.H., 2015. Facile synthesis of ZnO nanoglobules and its photocatalytic activity in the degradation of methyl orange dye under UV irradiation. *Materials Letters*, 152, pp. 163-165.

Khan, R., Uthirakumar, P., Bae, K.B., Leem, S.J. and Lee, I.H., 2016. Localized surface plasmon enhanced photoluminescence of ZnO nanosheets by Au nanoparticles. *Materials Letters*, 163, pp. 8-11.

Khataee, A.R. and Kasiri, M.B., 2010. Photocatalytic degradation of organic dyes in the presence of nanostructured titanium dioxide: influence of the chemical structure of dyes. *Journal of Molecular Catalysis A: Chemical*, 328, pp. 8-26.

Khoshhesab, Z.M., Sarfaraz, M. and Houshyar, Z., 2012. Influence of urea on precipitation of zinc oxide nanostructures through chemical precipitation in ammonium hydrogencarbonate solution. Synth. React. Inorg. Met. Org. Nano Met. Chem. 42, 1363–1368.

Kołodziejczak-Radzimska, A., Jesionowski, T., Krysztafkiewicz, A., 2010. Obtaining zinc oxide from aqueous solutions of KOH and $Zn(CH_3COO)_2$. *Physicochemical Problem of Mineral Processing*, 44, pp 93–102.

Kołodziejczak-Radzimska, A., Markiewicz, E. and Jesionowski, T., 2012. Structural characterisation of ZnO particles obtained by the emulsion precipitation method. *Journal of Nanomaterials*, 2012, p.15-22.

Kołodziejczak-Radzimska, A. and Jesionowski, T., 2014. Zinc oxide—from synthesis to application: a review. *Materials*, 7, pp.2833-2881.

Kotelevtsev, S., Tonkopii, V. and H änninen, O., 2009. Biomonitoring of environmental pollution. *Physiology and Maintenance-Volume II: Enzymes: The Biological Catalysts of Life, Nutrition and Digestion*, 2, pp.139-148.

Kumar, K.M., Mandal, B.K., Naidu, E.A., Sinha, M., Kumar, K.S. and Reddy, P.S., 2013. Synthesis and characterisation of flower shaped Zinc Oxide nanostructures and its antimicrobial activity. *Spectrochimica Acta Part A: Molecular and Biomolecular Spectroscopy*, 104, pp. 171-174.

Kung, C.C., Lin, P.Y., Xue, Y., Akolkar, R., Dai, L., Yu, X. and Liu, C.C., 2014. Three dimensional graphene foam supported platinum–ruthenium bimetallic nanocatalysts for direct methanol and direct ethanol fuel cell applications. *Journal of Power Sources*, 256, pp. 329-335.

Lamia, M., Fatiha, D., Mohammed, B. and Ayada, D., 2016. Adsorption of methyl green onto Zeolite ZSM-5 (pyrr.) in aqueous solution. *Oriental Journal of Chemistry*, 32, pp. 171-180.

Lam, S.M., Sin, J.C., Abdullah, A.Z. and Mohamed, A.R., 2012. Degradation of wastewaters containing organic dyes photocatalysed by zinc oxide: a review. *Desalination and Water Treatment*, 41, pp.131-169.

Lam, S.M., Sin, J.C., Satoshi, I., Abdullah, A.Z. and Mohamed, A.R., 2014. Enhanced sunlight photocatalytic performance over Nb_2O_5/ZnO nanorod composites and the mechanism study. *Applied Catalysis A: General*, 471, pp. 126-135.

Lanje, A.S., Sharma, S.J., Ningthoujam, R.S., Ahn, J.S. and Pode, R.B., 2013. Low temperature dielectric studies of zinc oxide (ZnO) nanoparticles prepared by precipitation method. *Adv. Powder Technol*, 24, pp. 331-335.

Lee, A.H. and Nikraz, H., 2014. BOD: COD ratio as an indicator for pollutants leaching from landfill. *Journal of Clean Energy Technologies*, 2, pp. 263-266.

Lee, J.C., Park, S., Park, H.J., Lee, J.H., Kim, H.S. and Chung, Y.J., 2009. Photocatalytic degradation of TOC from aqueous phenol solution using solution combusted ZnO nanopowders. *Journal of electroceramics*, 22, pp. 110-113.

Likodimos, V., Han, C., Pelaez, M., Kontos, A.G., Liu, G., Zhu, D., Liao, S., de la Cruz, A.A., O'Shea, K., Dunlop, P.S. and Byrne, J.A., 2013. Anion-doped TiO_2 nanocatalysts for water purification under visible light. *Industrial & Engineering Chemistry Research*, 52, pp. 13957-13964.

Lin, J., Liu, X., Zhu, S., Liu, Y. and Chen, X., 2015. Anatase TiO_2 nanotube powder film with high crystallinity for enhanced photocatalytic performance. *Nanoscale Research Letters*, 10, pp.110-115.

Liu, S., Yang, J.H. and Choy, J.H., 2006. Microporous SiO_2 –TiO_2 nanosols pillared montmorillonite for photocatalytic decomposition of methyl orange. *Journal of Photochemistry and Photobiology A: Chemistry*, 179, pp. 75-80.

Liu, X., Cheng, H., Fu, F., Huang, W., Zuo, H., Yan, L. and Li, L., 2016. Fabrication of PbS quantum dots decorated ZnO nanorod arrays on Zn substrate and their visible light photocatalytic application. *Materials Letters*, 179, pp. 134-137.

Li, Y., Li, X., Li, J. and Yin, J., 2005. Photocatalytic degradation of methyl orange in a sparged tube reactor with TiO_2-coated activated carbon composites. *Catalysis Communications*, 6, pp. 650-655.

Ljubas, D., Smoljanić, G. and Juretić, H., 2015. Degradation of methyl orange and congo red dyes by using TiO_2 nanoparticles activated by the solar and the solar-like radiation. *Journal of environmental management*, 161, pp. 83-91.

Luo, J., Ma, S.Y., Sun, A.M., Cheng, L., Yang, G.J., Wang, T., Li, W.Q., Li, X.B., Mao, Y.Z. and Gz, D.J., 2014. Ethanol sensing enhancement by optimizing ZnO nanostructure: From 1D nanorods to 3D nanoflower.*Materials Letters*, 137, pp.17-20.

Lu, Y., Wang, L., Wang, D., Xie, T., Chen, L. and Lin, Y., 2011. A comparative study on plate-like and flower-like ZnO nanocrystals surface photovoltage property and photocatalytic activity. *Materials Chemistry and Physics*, 129, pp. 281-287.

Mahdizadeh, F. and Aber, S., 2015. Treatment of textile wastewater under visible LED lamps using CuO/ZnO nanoparticles immobilized on scoria rocks. *RSC Advances*, 5, pp. 75474-75482.

Mai, F.D., Chen, C.C., Chen, J.L. and Liu, S.C., 2008. Photodegradation of methyl green using visible irradiation in ZnO suspensions: determination of the reaction pathway and identification of intermediates by a high-performance liquid chromatography–photodiode array-electrospray ionization-mass spectrometry method. *Journal of Chromatography A*, 1189, pp. 355-365.

Mai, F., Lu, C., Wu, C., Huang, C., Chen, J. and Chen, C., 2008. Mechanisms of photocatalytic degradation of Victoria Blue R using nano-TiO_2. *Separation and Purification Technology*, 62, pp. 423-436.

Malik, A. and Grohmann, E. eds., 2011. *Environmental protection strategies for sustainable development*. Springer Science & Business Media.

Marchena, C.L., Lerici, L., Renzini, S., Pierella, L. and Pizzio, L., 2016. Synthesis and characterization of a novel tungstosilicic acid immobilized on zeolites catalyst for the photodegradation of methyl orange. *Applied Catalysis B: Environmental*, 188, pp. 23-30.

Mehmood, S., Rehman, M.A., Ismail, H., Mirza, B. and Bhatti, A.S., 2015. Significance of postgrowth processing of ZnO nanostructures on antibacterial activity against gram-positive and gram-negative bacteria. *International journal of nanomedicine*, 10, p. 4521.

Merck Millipore, 2016. Methyl Orange. [online] Available at: http://www.merckmillipore.com/MY/en/product/Methyl-orange-%28C.I.13025%29,MDA_CHEM-101322?ReferrerURL=https%3A%2F%2Fwww.google.com%2F [Accessed 28 Mar. 2017].

Miao, Y., Zhang, H., Yuan, S., Jiao, Z. and Zhu, X., 2016. Preparation of flower-like ZnO architectures assembled with nanosheets for enhanced photocatalytic activity. *Journal of colloid and interface science*, *462*, pp.9-18.

Milea, C.A., Bogatu, C. and Duta, A., 2011. The influence of parameters in silica sol-gel process. *Bulletin of TheTransilvania University of Brasov*, 4, p.53-60.

Milenova, K., Stambolova, I., Blaskov, V., Eliyas, A., Vassilev, S. and Shipochka, M., 2013. The effect of introducing copper dopant on the photocatalytic activity of ZnO nanoparticles. *Journal of Chemical Technology and Metallurgy*, 48, pp. 259-264.

Muhd Julkapli, N., Bagheri, S. and Bee Abd Hamid, S., 2014. Recent advances in heterogeneous photocatalytic decolorization of synthetic dyes. *The Scientific World Journal*, *2014*.

Muruganandham, M. and Wu, J.J., 2008. Synthesis, characterization and catalytic activity of easily recyclable zinc oxide nanobundles. *Applied Catalysis B: Environmental*, 80, pp. 32-41.

Moezzi, A., McDonagh, A.M. and Cortie, M.B., 2012. Zinc oxide particles: Synthesis, properties and applications. *Chemical Engineering Journal*, 185, pp. 1-22.

Morkoç, H. and Özgür, Ü., 2008. Zinc oxide: fundamentals, materials and device technology. John Wiley & Sons.

Nakata, K. and Fujishima, A., 2012. TiO_2 photocatalysis: design and applications. *Journal of Photochemistry and Photobiology C: Photochemistry Reviews*, 13, pp.169-189.

Naseri, M.G., Saion, E. and Zadeh, N.K., 2013. The amazing effects and role of PVP on the crystallinity, phase composition and morphology of nickel ferrite nanoparticles prepared by thermal treatment method. *International Nano Letters*, 3, pp. 19-26.

Natarajan, K., Natarajan, T.S., Bajaj, H.C. and Tayade, R. J., 2011. Photocatalytic reactor based on $UV-LED/TiO_2$ coated quartz tube for degradation of dyes. *Chemical Engineering Journal*, 178, pp. 40-49.

National Electrical Manufacturers Association, 2012. NEMA statement on compact fluorescent lamps and ultraviolet emissions. [Online] Available at: <http://www.nema.org/news/Pages/NEMA-Statement-on-Compact-Fluorescent-Lamps-and-Ultraviolet-Emissions.aspx> [Accessed 14 June 2016].

Nawi, M.A., Jawad, A.H., Sabar, S. and Ngah, W.W., 2011. Photocatalytic-oxidation of solid state chitosan by immobilized bilayer assembly of TiO_2–chitosan under a compact household fluorescent lamp irradiation. *Carbohydrate Polymers*, 83, pp. 1146-1152.

Nekouei, S., Nekouei, F., Tyagi, I., Agarwal, S. and Gupta, V.K., 2016. Mixed cloud point/solid phase extraction of lead (II) and cadmium (II) in water samples using modified-ZnO nanopowders. *Process Safety and Environmental Protection*, 99, pp. 175-185.

Nielsen, S.S. ed., 2010. *Food analysis*. New York, NY, USA:: Springer.

Nor, N.M., Hadibarata, T., Zubir, M.M.F.A., Lazim, Z.M., Adnan, L.A. and Fulazzaky, M.A., 2015. Mechanism of triphenylmethane Cresol Red degradation by Trichoderma harzianum M06. *Bioprocess and biosystems engineering*, 38, pp. 2167-2175.

Ong, S.T., Keng, P.S., Lee, W.N., Ha, S.T. and Hung, Y.T., 2011. Dye waste treatment. *Water*, 3, pp. 157-176.

Pajootan, E., Arami, M. and Mahmoodi, N.M., 2012. Binary system dye removal by electrocoagulation from synthetic and real colored wastewaters. *Journal of the Taiwan Institute of Chemical Engineers*, 43, pp. 282-290.

Patrocinio, A.O.T., Schneider, J., Franca, M.D., Santos, L.M., Caixeta, B.P., Machado, A.E.H. and Bahnemann, D.W., 2015. Charge carrier dynamics and photocatalytic behavior of TiO_2 nanopowders submitted to hydrothermal or conventional heat treatment. *RSC Advances*, 5, pp. 70536-70545.

Pare, B., Jonnalagadda, S.B., Tomar, H., Singh, P. and Bhagwat, V.W., 2008. ZnO assisted photocatalytic degradation of acridine orange in aqueous solution using visible irradiation. *Desalination*, 232, pp. 80-90.

Parida, K.M. and Sahu, N., 2008. Visible light induced photocatalytic activity of rare earth titania nanocomposites. *Journal of Molecular Catalysis A: Chemical*, 287, pp.151-158.

Pelaez, M., Nolan, N.T., Pillai, S.C., Seery, M.K., Falaras, P., Kontos, A.G., Dunlop, P.S., Hamilton, J.W., Byrne, J.A., O'shea, K. and Entezari, M.H., 2012. A review on the visible light active titanium dioxide photocatalysts for environmental applications. *Applied Catalysis B: Environmental*, 125, pp. 331-349.

Peng, C., Guo, J., Yang, W., Shi, C., Liu, M., Zheng, Y., Xu, J., Chen, P., Huang, T. and Yang, Y., 2016. Synthesis of three-dimensional flower-like hierarchical ZnO nanostructure and its enhanced acetone gas sensing properties. *Journal of Alloys and Compounds*, 654, pp. 371-378.

Pereira, L. and Alves, M., 2012. Dyes—environmental impact and remediation. In *Environmental protection strategies for sustainable development*, pp. 111-162. Springer Netherlands.

Phuruangrat, A., Thongtem, S. and Thongtem, T., 2016. Ultrasonic-assisted synthesis and photocatalytic performance of ZnO nanoplates and microflowers. *Materials & Design*.

Pingmuang, K., Wetchakun, N., Kangwansupamonkon, W., Ounnunkad, K., Inceesungvorn, B. and Phanichphant, S., 2013. Photocatalytic Mineralization of Organic Acids over Visible-Light-Driven $Au/BiVO_4$ Photocatalyst. *International Journal of Photoenergy*, 2013, pp. 1-7.

Popli, S. and Patel, U.D., 2015. Destruction of azo dyes by anaerobic–aerobic sequential biological treatment: a review. *International Journal of Environmental Science and Technology*, 12, pp.405-420.

Pournuroz, Z., Khosravi, M., Giahi, M. and Sohrabi, M., 2015. Compare Removal of Reactive Red 195 and Blue 19 by Nano TiO2-ZnO. *Oriental Journal of Chemistry*, 31, pp.1711-1715.

Qi, G., Zhao, S. and Yuan, Z., 2013. From function-guided assembly of a lotus leaf-like ZnO nanostructure to a formaldehyde gas-sensing application. *Sensors and Actuators B: Chemical*, 184, pp. 143-149.

Rai, P., Jo, J.N., Lee, I.H. and Yu, Y.T., 2010. Fabrication of 3D rotor-like ZnO nanostructure from 1D ZnO nanorods and their morphology dependent photoluminescence property. *Solid State Sciences*, 12, pp. 1703-1710.

Ram, C., Pareek, R.K. and Singh, V., 2012. Photocatalytic degradation of textile dye by using titanium dioxide nanocatalyst. *International Journal of Theoretical & Applied Sciences*, 4, pp. 82-88.

Rao, A.N. and Venkatarangaiah, V.T., 2014. The effect of cathode materials on indirect electrochemical oxidation of methyl orange, malachite green and methylene blue. *Portugaliae Electrochimica Acta*, 32, pp. 213-231.

Reddy, P.M.K., Sk, M. and Ch, S., 2014. Mineralization of aqueous organic pollutants using a catalytic plasma reactor. *Indian Journal of Chemistry: A*, 53, pp. 499-503.

Ribeiro, A.R., Nunes, O.C., Pereira, M.F. and Silva, A.M., 2015. An overview on the advanced oxidation processes applied for the treatment of water pollutants defined in the recently launched Directive 2013/39/EU. *Environment international*, 75, pp.33-51.

Robbins, R., 2015. Scanning Electron Microscope Operation Zeiss Supra-40. [Online] Available at: < https://www.utdallas.edu/~rar011300/SEM/Scanning%20Electron%20Microscope%20Operation.pdf> [Accessed 14 June 2016].

Safa, S., Azimirad, R., Hejazi, R. and Rabbani, M., 2014. ZnO hierarchical nanostructures as a powerful photocatalyst for the degradation of p-Nitrophenol. *Chinese Journal of Physics*, 52, pp.1612-1624.

Safa, S., Azimirad, R., Mohammadi, K., Hejazi, R. and Khayatian, A., 2015. Investigation of ethanol vapor sensing properties of ZnO flower-like nanostructures. *Measurement*, 73, pp. 588-595.

Saggioro, E.M., Oliveira, A.S., Pavesi, T., Maia, C.G., Ferreira, L.F.V. and Moreira, J.C., 2011. Use of titanium dioxide photocatalysis on the remediation of model textile wastewaters containing azo dyes. *Molecules*, 16, pp. 10370-10386.

Sanroman, M.A., Pazos, M., Ricart, M.T. and Cameselle, C., 2004. Electrochemical decolourisation of structurally different dyes. *Chemosphere*, 57, pp. 233-239.

Saquib, M., Tariq, M.A., Faisal, M. and Muneer, M., 2008. Photocatalytic degradation of two selected dye derivatives in aqueous suspensions of titanium dioxide. *Desalination*, 219, pp. 301-311.

Saratale, R.G., Saratale, G.D., Chang, J.S. and Govindwar, S.P., 2011. Bacterial decolorization and degradation of azo dyes: a review. *Journal of the Taiwan Institute of Chemical Engineers*, 42, pp.138-157.

Saravanan, R., Karthikeyan, S., Gupta, V.K., Sekaran, G., Narayanan, V. and Stephen, A., 2013. Enhanced photocatalytic activity of ZnO/CuO nanocomposite for the degradation of textile dye on visible light illumination. *Materials Science and Engineering: C*, 33, pp. 91-98.

Satyanarayana, T., Johri, B.N. and Prakash, A. eds., 2012. *Microorganisms in environmental management: microbes and environment*. Springer Science & Business Media.

Shah, M., 2014. Effective treatment systems for azo dye degradation: a joint venture between physico-chemical & microbiological process. *International Journal of Environmental Bioremediation & Biodegradation*, 2, pp. 231-242.

Shahmiri, M., Ibrahim, N.A., Shayesteh, F., Asim, N. and Motallebi, N., 2013. Preparation of PVP-coated copper oxide nanosheets as antibacterial and antifungal agents. *Journal of Materials Research*, 28, pp. 3109-3118.

Shanthi, M. and Kuzhalosai, V., 2012. Photocatalytic degradation of an azo dye, Acid Red 27, in aqueous solution using nano ZnO. *Indian Journal of Chemistry*, 51, pp. 428-434.

Sharma, S.K. ed., 2015. *Green chemistry for dyes removal from waste water: research trends and applications*. John Wiley & Sons.

Sharma, S., Ruparelia, J.P. and Patel, M.L., 2011, December. A general review on Advanced Oxidation Processes for waste water treatment. In *Nirma University International Conference, Ahmedabad, Gujarat*.

Sin, J.C. and Lam, S.M., 2016. Hydrothermal synthesis of europium-doped flower-like ZnO hierarchical structures with enhanced sunlight photocatalytic degradation of phenol. *Materials Letters*, 182, pp. 223-226.

Sin, J.C., Lam, S.M., Lee, K.T. and Mohamed, A.R., 2013. Fabrication of erbium-doped spherical-like ZnO hierarchical nanostructures with enhanced visible light-driven photocatalytic activity. *Materials Letters*, 91, pp. 1-4.

Sobana, N. and Swaminathan, M., 2007. The effect of operational parameters on the photocatalytic degradation of acid red 18 by ZnO. *Separation and Purification Technology*, 56, pp. 101-107.

Souza, R.P., Freitas, T.K., Domingues, F.S., Pezoti, O., Ambrosio, E., Ferrari-Lima, A.M. and Garcia, J.C., 2016. Photocatalytic activity of TiO_2, ZnO and Nb_2O_5 applied to degradation of textile wastewater. *Journal of Photochemistry and Photobiology A: Chemistry*, 329, pp. 9-17.

Stanković, A., Veselinović, L., Škapin, S.D., Marković, S. and Usković, D., 2011. Controlled mechanochemically assisted synthesis of ZnO nanopowders in the presence of oxalic acid. *Journal of materials science*, 46, pp. 3716-3724.

Sun, J., Liu, N., Zhai, S., Xiao, Z., An, Q. and Huang, D., 2014. Gold-titania/protonated zeolite nanocomposite photocatalysts for methyl orange degradation under ultraviolet and visible irradiation. *Materials Science in Semiconductor Processing*, 25, pp. 286-293.

Suresh, S. and Sundaramoorthy, S. ed., 2014. *Green chemical engineering: An introduction to catalysis, kinetics and chemical processes*. CRC Press.

Su, Y., Deng, L., Zhang, N., Wang, X. and Zhu, X., 2009. Photocatalytic degradation of CI Acid Blue 80 in aqueous suspensions of titanium dioxide under sunlight. *Reaction Kinetics and Catalysis Letters*, 98, pp. 227-240.

Tariq, M.A., Faisal, M., Saquib, M. and Muneer, M., 2008. Heterogeneous photocatalytic degradation of an anthraquinone and a triphenylmethane dye derivative in aqueous suspensions of semiconductor. *Dyes and Pigments*, 76, pp. 358-365.

Teo, T.W. and Khoh, R.L. eds., 2014. *Teaching Science in Culturally Relevant Ways: Ideas from Singapore Teachers*. World Scientific.

Tiwari, D., Lalhriatpuia, C., Lee, S.M. and Kong, S.H., 2015. Efficient application of nano-TiO_2 thin films in the photocatalytic removal of Alizarin Yellow from aqueous solutions. *Applied Surface Sciences*, 353, pp. 275-283.

Tomei, M.C., Pascual, J.S. and Angelucci, D.M., 2016. Analyzing performance of real textile wastewater bio-decolourization under different reaction environments. *Journal of Cleaner Production*, 129, pp.468-477.

Udom, I., 2014. Investigation of Enhanced Titanium and Zinc Oxide Semiconductors for the Photodegradation of Aqueous Organic Compounds.

Umar, A., Chauhan, M.S., Chauhan, S., Kumar, R., Kumar, G., Al-Sayari, S.A., Hwang, S.W. and Al-Hajry, A., 2011. Large-scale synthesis of ZnO balls made of fluffy thin nanosheets by simple solution process: structural, optical and photocatalytic properties. *Journal of colloid and interface science*, 363, pp. 521-528.

Umar, M. and Aziz, H.A., 2013. Photocatalytic degradation of organic pollutants in water. INTECH Open Access Publisher.

Valente, J.S., Tzompantzi, F. and Prince, J., 2011. Highly efficient photocatalytic elimination of phenol and chlorinated phenols by CeO_2/MgAl layered double hydroxides. *Applied Catalysis B: Environmental*, 102, pp. 276-285.

Vaseem, M., Umar, A. and Hahn, Y.B., 2010. ZnO nanoparticles: growth, properties, and applications. *Metal Oxide Nanostructures and Their Applications*, 5, pp. 1-36.

Vijayabalan, A., Selvam, K., Velmurugan, R. and Swaminathan, M., 2009. Photocatalytic activity of surface fluorinated TiO_2-P25 in the degradation of Reactive Orange 4. *Journal of Hazardous Materials*, 172, pp. 914-921.

Wahab, R., Kim, Y.S. and Shin, H.S., 2011. Fabrication, characterization and growth mechanism of heterostructured zinc oxide nanostructures via solution method. *Current Applied Physics*, 11, pp. 334-340.

Wang, F., Ho, J.H., Jiang, Y. and Amal, R., 2015. Tuning phase composition of TiO_2 by Sn^{4+} doping for efficient photocatalytic hydrogen generation. *ACS applied materials & interfaces*, 7, pp. 23941-23948.

Wang, Q., Hui, J., Li, J., Cai, Y., Yin, S., Wang, F. and Su, B., 2013. Photodegradation of methyl orange with PANI-modified BiOCl photocatalyst under visible light irradiation. *Applied Surface Science*, 283, pp. 577-583.

Wang, R., Higgins, D.C., Hoque, M.A., Lee, D., Hassan, F. and Chen, Z., 2013. Controlled growth of platinum nanowire arrays on sulfur doped graphene as high performance electrocatalyst. *Scientific reports*, *3*.

Wang, Y., Zhang, C., Bi, S. and Luo, G., 2010. Preparation of ZnO nanoparticles using the direct precipitation method in a membrane dispersion micro-structured reactor. *Powder Technol*. 202, pp. 130-136.

Wang, Z., Huang, K., Xue, M. and Liu, Z., 2011. Textile dyeing wastewater treatment, pp. 91-116. INTECH Open Access Publisher.

Wijannarong, S., Aroonsrimorakot, S., Thavipoke, P., Sangjan, S., 2013. Removal of Reactive Dyes from Textile Dyeing Industrial Effluent by Ozonation Process. APCBEE Procedia, 5, pp. 279-282.

Wong, Y.C., Ranjini, K.N. and Wan-Nurdiyana, W.A., 2014. Removal of Congo Red and Acid Yellow 36 Dye Using Orange Peel and Rice Husk as Absorbent. *Oriental Journal Of Chemistry*, 30, pp. 529-539.

Xie, J. and Wu, Q., 2010. One-pot synthesis of ZnO/Ag nanospheres with enhanced photocatalytic activity. *Materials Letters*, 64, pp.389-392.

Xu, H.Y., Wu, L.C., Zhao, H., Jin, L.G. and Qi, S.Y., 2015. Synergic effect between adsorption and photocatalysis of metal-free g-C_3N_4 derived from different precursors. *Public Library of Science One*, 10, pp. 1-20.

Yan, L., Deng, B., Shen, C., Long, C., Deng, Q. and Tao, C., 2015. Selenium speciation using capillary electrophoresis coupled with modified electrothermal atomic absorption spectrometry after selective extraction with 5-sulfosalicylic acid functionalized magnetic nanoparticles. *Journal of Chromatography A*, 1395, pp. 173-179.

Yang, G., Yan, Z., Xiao, T. and Yang, B., 2013. Low-temperature synthesis of alkalis doped TiO_2 photocatalysts and their photocatalytic performance for degradation of methyl orange. *Journal of Alloys and Compounds*, 580, pp.15-22.

Yang, J., Jia, H., Lv, X. and Wang, Y., 2016. Facile preparation of urchin-like ZnO nanostructures and their photocatalytic performance. *Ceramics International*, 42, pp. 12409-12413.

Yang, L.Y., Dong, S.Y., Sun, J.H., Feng, J.L., Wu, Q.H. and Sun, S.P., 2010. Microwave-assisted preparation, characterization and photocatalytic properties of a dumbbell-shaped ZnO photocatalyst. *Journal of hazardous materials*, 179, pp.438-443.

Yang, Y., Zhang, Z., Yan, J., Liu, Q., Zhang, F. and Li, W., 2015. Study on Field Emission Characteristics of Ti-based Chrysanthemum-like Nano-ZnO Cathode by Electrophoresis Deposition. *Rare Metal Materials and Engineering*, 44, pp. 2711-2715.

Yathisha, R.O., Nayaka, Y.A. and Vidyasagar, C.C., 2016. Microwave combustion synthesis of hexagonal prism shaped ZnO nanoparticles and effect of Cr on structural, optical and electrical properties of ZnO nanoparticles. *Materials Chemistry and Physics*, 181, pp. 167-175.

Zengin, G., Ozgunay, H., Ayan, E.M. and Mutlu, M.M., 2012. Determination of dyestuffs remaining in dyeing processes of vegetable-tanned leathers and their removal using shavings. *Polish Journal of Environmental Studies*, 21, pp. 499-508.

Zhang, D., Wu, J., Zhou, B., Hong, Y., Li, S. and Wen, W., 2013. Efficient photocatalytic activity with carbon-doped SiO_2 nanoparticles. *Nanoscale*, 5, pp.6167-6172.

Zhang, H.D., Long, Y.Z., Li, Z.J. and Sun, B., 2014. Fabrication of comb-like ZnO nanostructures for room-temperature CO gas sensing application.*Vacuum*, 101, pp.113-117.

Zhang, H., Yang, D., Ji, Y., Ma, X., Xu, J. and Que, D., 2004. Low temperature synthesis of flowerlike ZnO nanostructures by cetyltrimethylammonium bromide-assisted hydrothermal process. *The Journal of Physical Chemistry B*, 108, pp. 3955-3958.

Zhang, L., Lv, F., Zhang, W., Li, R., Zhong, H., Zhao, Y., Zhang, Y. and Wang, X., 2009. Photo degradation of methyl orange by attapulgite–SnO_2–TiO_2 nanocomposites. *Journal of Hazardous materials*, 171, pp. 294-300.

Zhang, X., Qin, J., Xue, Y., Yu, P., Zhang, B., Wang, L. and Liu, R., 2014. Effect of aspect ratio and surface defects on the photocatalytic activity of ZnO nanorods. *Scientific reports*, *4*.

Zhang, Y., Ram, M.K., Stefanakos, E.K. and Goswami, D.Y., 2012. Synthesis, characterization, and applications of ZnO nanowires. *Journal of Nanomaterials*, 2012, p.20-44.

Zhou, Q., Wen, J.Z., Zhao, P. and Anderson, W.A., 2017. Synthesis of Vertically-Aligned Zinc Oxide Nanowires and Their Application as a Photocatalyst. *Nanomaterials*, 7, pp. 9-21.

Zhou, Y., Lu, S.X. and Xu, W.G., 2009. Photocatalytic activity of Nd-doped ZnO for the degradation of CI Reactive Blue 4 in aqueous suspension. *Environmental progress & sustainable energy*, 28, pp.226-233.

Zhu, H., Jiang, R., Xiao, L., Liu, L., Cao, C. and Zeng, G., 2013. CdS nanocrystals/TiO$_2$/crosslinked chitosan composite: Facile preparation, characterization and adsorption-photocatalytic properties. *Applied Surface Science*, 273, pp.661-669.

Zucca, P., Rescigno, A., Pintus, M., Rinaldi, A.C. and Sanjust, E., 2012. Degradation of textile dyes using immobilized lignin peroxidase-like metalloporphines under mild experimental conditions. *Chemistry Central Journal*, 6, pp. 1-8.

Zyoud, A., Zu'bi, A., Helal, M.H., Park, D., Campet, G. and Hilal, H.S., 2015. Optimizing photo-mineralization of aqueous methyl orange by nano-ZnO catalyst under simulated natural conditions. *Journal of Environmental Health Science and Engineering*, 13, pp. 46-55.

APPENDICES
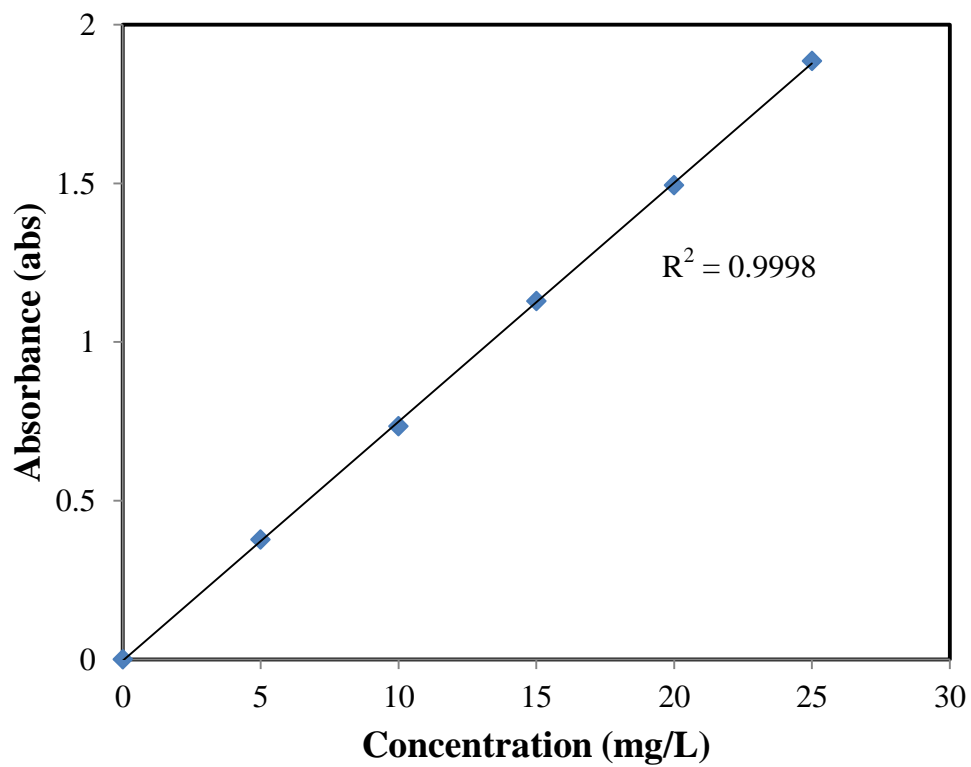
Appendix A1: MO Calibration Curve.
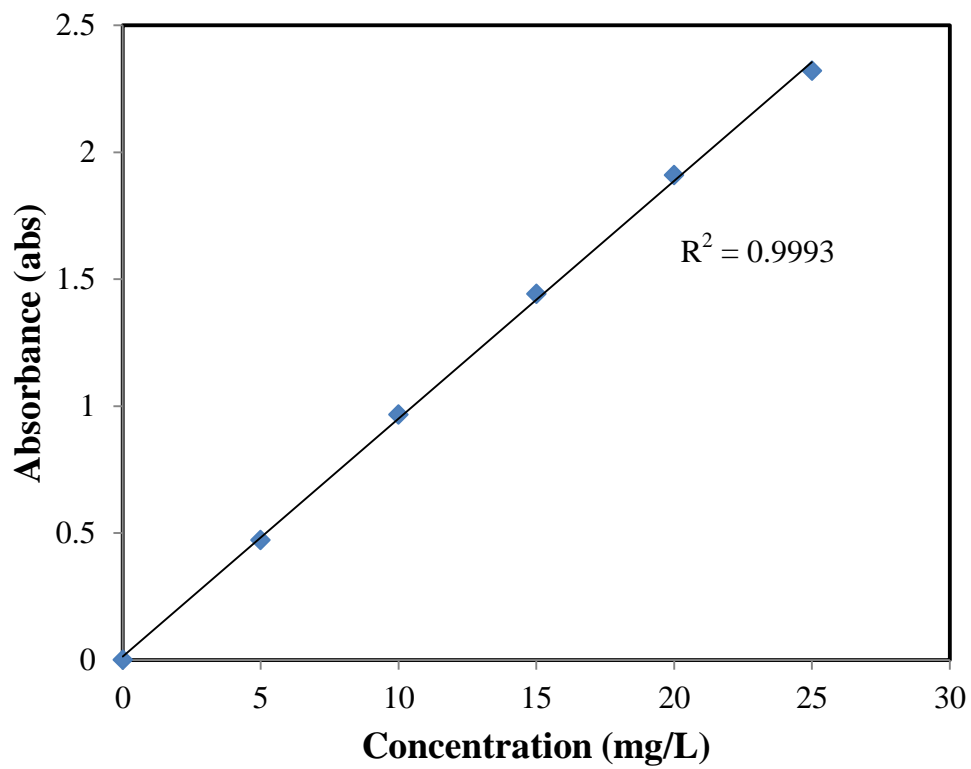
Appendix A2: MG Calibration Curve

PUBLICATION

Lam, S.M., Kee, M.W. and Sin, J.C., 2017. Synthesis of flower-like ZnO micro/nanostructures for enhanced photodegradation of dye mixtures (methyl orange and methyl green) and real textile wastewater. *Applied Surface Science* (Submitted).